CalVal Jason

Jason-1 validation and cross calibration activities

Contract No 60453/00 - lot2.C

Reference : CLS.DOS/NT/09-006

Nomenclature : SALP-RP-MA-EA-21631-CLS

Issue : 1rev 1

Date : September 8, 2009

SALP Service Altimetrie & Localisation Precise

CLS Collecte Localisation Satellites

cnes Centre National d'Études Spatiales

CLS - 8-10 Rue Hermès - Parc Technologique du Canal - 31520 Ramonville St-Agne - FRANCE
Telephone 33 5 61 39 47 00 / Fax 33 5 61 75 10 14

Chronology Issues :		
Issue :	Date :	Reason for change :
1.0	05/01/2009	Created
1.1	14/08/2009	Revision, taking into account remarks from N. Picot

People involved in this issue :		
Written by :	L. Commien S. Philipps M. Ablain	CLS CLS CLS
Checked by :	DT/AQM	CLS
Approved by :	JP. Dumont	CLS
Application authorized by :		

Index sheet :	
Context	
Keywords	Jason-1, Calval, orbits, reprocessing
hyperlink	

Distribution :		
Company	Means of distribution	Names
CLS/DOS	G. DIBARBOURE	1 electonic copy
	J. DORANDEU	1 electonic copy
	V. ROSMORDUC	1 electonic copy
	P. ESCUDIER	1 electonic copy
DOC/CLS	DOCUMENTATION	1 electonic copy
CNES	T. GUINLE	1 CD
CNES	P. BOUBE	1 CD
CNES	D. CHERMAIN	1 CD
CNES	E. BRONNER	1 electonic copy
CNES	J. LAMBIN	1 electonic copy
CNES	A. LOMBARD	1 electonic copy
CNES	N. PICOT	1 electonic copy

List of tables and figures :

List of Tables

List of Figures

List of items to be defined or to be confirmed :

Applicable documents / reference documents :

Contents

1. Introduction

This document presents the synthesis report concerning validation activities of Jason-1 GDRs under SALP contract (N° 60453/00 Lot2.C) supported by CNES at the CLS Space Oceanography Division. It is divided into two parts: CAL/VAL Jason-1 activities - Jason-1 / T/P cross-calibration.

Since the beginning of the mission, Jason-1 data have been analyzed and monitored in order to assess the quality of Jason-1 GDR products (AVISO and PODAAC User handbook, [56]) for oceanographic applications. This report is basically concerned with long-term monitoring of the Jason-1 altimeter system, from all GDR products available to date, that is for almost 7 years of data (cycles 1 to 253). This includes careful monitoring of all altimeter and radiometer parameters, performance assessment, geophysical evaluation and cross-calibration with T/P measurements. Moreover, a specific study is presented in this document, about the on-going GDR-C reprocessing and especially about the new orbit version and JMR processing and its impact on mean sea level calculation.
This work is routinely performed at CLS and in this frame, besides continuous analyzes in terms of altimeter data quality, Jason-1 GDR Quality Assessment Reports (e.g. Ablain et al. 2008 [4]) are produced and associated to data dissemination. Even if only low order statistics are mainly presented here, other analyzes including histograms, plots and maps are continuously produced and used in the quality assessment process. The work performed in terms of data quality assessment also includes cross-calibration analyzes mainly with the T/P mission until November 2005 (end of the T/P mission). Even if T/P mission is finished, cross-calibration analyzes are useful for the reprocessing activities in order to study the sea state bias or the SSH bias for instance.
Indeed, it is now well recognized that the usefulness of any altimeter data only makes sense in a multi-mission context, given the growing importance of scientific needs and applications, particularly for operational oceanography. One major objective of the Jason-1 mission is to continue the T/P high precision altimetry and to allow combination with other missions (ENVISAT, GFO). This kind of comparisons between different altimeter missions flying together provides a large number of estimations and consequently efficient long term monitoring of instrument measurements. Of course, other sources of comparisons are also needed, using independent datasets (e.g. Queffeulou et al. 2004 [59], Ray and Beckley 2003 [62], Arnault et al. 2004 [8], Provost et al. 2004 [57]). [74] and [75] show comparisons between altimeter data and in-situ data (respectively tide gauge measurements and T/S profilers).

2. Processing status

2.1. GDR and CAL/VAL Processing

Jason-1 GDRs, in version "b" from cycle 1 to 232 and in version "c" from cycle 233 to 253 (till 28/11/2008), are used in this report. Since cycle 233, Jason-1 products are produced by CMA ground processing software in version "c" (see section 2.3.). From June 2008 to present, Jason-1 GDR products are being reprocessed. Currently, cycles 151 to 232 have been reprocessed and certified, except for a few cycles (see section 7.2.). The purpose of this document is to report the major features of the data quality from the Jason-1 mission. Moreover, the document is associated with comparison results from T/P GDRs. All these cycle reports are available on AVISO website: http://www.jason.oceanobs.com. In addition to these reports, several meeting (CAVE, OSTST) have been performed to inform the Jason-1 GDR's users about the main results and the studies in progress.

2.2. CAL/VAL status

2.2.1. Missing measurements

This section presents a summary of major satellite events that occurred from cycle 1 to 253. Table 1 gives a status about the number of missing passes (or partly missing) for GDRs version "b" and the associated events for each cycle.
Gyro calibration, Star Tracker unavailability and ground processing issues were the main events which produced missing data from cycle 1 to 64 (2002 and 2003).
During year 2004 (cycle 65 to 109), 2 safe hold mode incidents have produced 15 days of missing data due to a wheel anomaly. As result of this incident, only 3 wheels have been available but this has had no impact on scientific applications.
During year 2005 (110-146), most of incidents are due to SEU. The altimeter was reinitializied automatically without C-band. Few passes have only been impacted each time, and they are rejected because of the lack of C-band data, and therefore lack of bifrequency ionospheric correction.
During year 2006 (cycles 147 - 183) Jason-1 experienced a safe hold mode (cycle 177 to 179) producing 17 days of missing data due to mass memory error. In addition 2 altimeter SEU occurred. It also happened that small data gaps occur (less than a minute duration).
During 2007 (cycles 183 to 214) Jason-1 had experienced several altimeter SEU. In 2008 (cycles 215 to 253), there were two major events : the altimeter switch-off in may, due to the close encounter with drifting Topex/Poseidon, and a safehold mode in August.

Jason-1 Cycles	Number of Missing passes	Number of partly missing passes	Events
001	5	7	Science telemetry unavailability
002	16	0	On board Doris anomaly
.../...			

Jason-1 Cycles	Number of Missing passes	Number of partly missing passes	Events
003	0	2	Gyro-calibration
004	2	5	Gyro-calibration and Science telemetry unavailability
006	1	4	Altimeter echo data unavailability
007	0	2	Science telemetry unavailability
008	2	5	Ground processing issue
009	3	4	Poseidon-2 altimeter SEU and Gyro-calibration
010	0	2	Gyro-calibration
015	0	1	Ground processing issue
019	0	1	Ground processing issue
021	0	1	Star tracker unavailability
023	0	1	Ground processing issue
026	0	2	Gyro-calibration
027	0	2	Gyro-calibration
031	0	1	Star tracker unavailability
038	0	4	Ground processing issue
039	0	1	Gyro-calibration
042	5	2	Poseidon-2 altimeter SEU
045	0	3	Gyro-calibration
046	0	1	Poseidon-2 altimeter SEU
048	0	1	Gyro-calibration
062	0	1	Ground processing issue
064	0	2	Exceptional calibrations
075	4	0	Poseidon-2 altimeter SEU
077	69	0	Safe hold mode (15/02/04 to 21/02/04)
078	82	0	Safe hold mode (15/02/04 to 21/02/04)

.../...

Jason-1 Cycles	Number of Missing passes	Number of partly missing passes	Events
080	0	1	Calibration over ocean
082	54	1	Failure in module 3 of PLTM2
087	0	1	Calibration over ocean
091	2	4	DORIS instrument switch to redundancy and altimeter incident (no C band information)
094	0	1	Altimeter incident or star tracker unavailability
099	0	1	Altimeter incident or star tracker unavailability
101	0	1	Altimeter incident or star tracker unavailability
102	1	0	Altimeter SEU (no C band information)
103	0	2	Altimeter SEU (no C band information)
104	0	1	No data between 21:29:18 and 21:30:07 on November 8th pass 189
106	3	2	Altimeter SEU (no C band information)
108	0	2	Altimeter SEU (no C band information)
114	3	1	Altimeter SEU (no C band information)
115	0	4	2 altimeter SEU incidents (C band) and altimeter initialization procedure.
118	6	2	Altimeter SEU (no C band information)
131	0	7	TRSR2 "elephant packets" anomaly
132	0	1	Altimeter SEU (no C band information)
			.../...

Jason-1 Cycles	Number of Missing passes	Number of partly missing passes	Events
133	0	2	Altimeter SEU (no C band information)
136	104	2	Altimeter SEU (no C band information), Platform incident (20/09/05 to 28/09/05)
137	91	2	Platform incident (20/09/05 to 28/09/05)
161	0	5	TRSR elephant packets
165	0	1	(planned) Poseidon calibration (board filter)
173	0	3	Altimeter SEU (no C band information)
177	141	1	Safehold mode (30/10/2006 to 16/11/2006)
178	254	0	Safehold mode (30/10/2006 to 16/11/2006)
179	45	1	Safehold mode (30/10/2006 to 16/11/2006)
181	5	2	Altimeter SEU
185	0	3	calibration over ocean
191	0	2	Altimeter SEU
192	0	1	calibration over ocean
198	1	1	Altimeter SEU
200	0	1	calibration over ocean
206	0	3	Altimeter SEU
219	2	0	Missing telemetry
222	0	2	calibrations over ocean
231	0	1	erroneous command sent by JTCCS
233	142	2	altimeter switch off (TP/J1 close encounter)
234	0	1	calibration

.../...

Jason-1 Cycles	Number of Missing passes	Number of partly missing passes	Events
242	84	1	safehold mode
243	254	0	safehold mode
254	1	1	Altimeter SEU

Table 1: *M*issing pass status

2.2.2. Edited measurements

Table 2 indicates the cycles which have a larger amount of removed data due to editing criteria (see section 3.2.1.). Most of the occurrences correspond to dual-ionospheric correction at default value (altimeter SEU) or missing radiometer wet troposphere correction (following safehold modes). Notice that since cycle 78, the satellite operates with only 3 wheels: the maneuver impact (burn maneuver, yaw transition) is greater than before on the attitude control. Consequently, some measurements could be edited due to higher mispointing values when a maneuver occurs, until improvements in ground retracking algorithm have been set up and applied in the GDR "b" release, and improvements on Star Tracker behavior have been performed in 2006. Therefore only few measurements were edited by mispointing criterion.

Jason-1 Cycles	Comments
001	Passes 252 to 254 are edited due to radiometer wet troposphere correction at default value.
006	Pass 56 (in the Pacific ocean) is partly edited due to the bad quality of data. Indeed, the altimetric parameters values are out of the thresholds.
008	All the altimetric parameters are edited for 10% of pass 252 due to the bad quality of all the altimetric parameters as a result of a Star Tracker incident leading to a quite high off nadir angle. Half of pass 252 edited by radiometer wet troposphere correction at default value.
009	Passes 004 and 005 partly edited by dual-ionospheric correction at default value (no c-band information).
019	Most of pass 010 is edited by radiometer wet troposphere correction at default value. Passes 19 to 21 are edited due to datation anomaly.
021	Small part of pass 210 is edited after checking the square of the mispointing angle criterion.
069	Passes 209 to 211 are edited due to the radiometer wet troposphere correction at default value. This is linked to the safe hold mode on cycle 69 : the JMR has been set on 2 hours after the altimeter.
.../...	

Jason-1 Cycles	Comments
078	Passes 83 to 85 are edited due to the radiometer wet troposphere correction at default value. This is linked to the safe hold mode on cycle 88 : the JMR has been set on 2 hours after the altimeter.
091	Passes 126, 127 and partly 130 are edited by dual-ionospheric correction at default value (no c-band information).
102	Passes 187, 188 and partly 189 are edited by dual-ionospheric correction at default value (no c-band information).
103	Passes 29 to 31 are edited by dual-ionospheric correction at default value (no c-band information).
108	Passes 16 and 17, as well as part of passes 15 and 18 are edited by dual-ionospheric correction at default value (no c-band information).
115	Passes 19 to 21 and 29 to 31 are edited by dual-ionospheric correction at default value (no c-band information).
133	Pass 13 is partly edited due to dual-ionospheric correction at default value (no c-band information).
137	Passes 92, 93 and partly 94 are edited by radiometer wet tropospheric correction, since the radiometer was later switched on than the other instruments.
173	As the altimeter is only restarted during pass 68, the dual-frequency ionospheric correction is partially missing for passes 65 and 68 and fully for passes 66 and 67.
175	Pass 9 is partly edited by mispointing criterion out of threshold (probably aberrant quaternion).
179	As radiometer was only switch on later, passes 046 to 058, as well as part of pass 059 are edited by radiometer wet troposphere correction at default values.
181	Pass 247 is partly edited by dual-frequency ionosphere at default value (no C-band information).
198	Pass 073 is partly edited by dual-frequency ionosphere at default value (no C-band information).
212	Pass 187 is entirely edited: one half by altimetric parameters at default value, other half by apparent squared mispointing values out of thresholds. Pass 186 is partly edited by apparent squared mispointing values out of thresholds.
220	Pass 189 is partly edited by altimetric parameters at default value.
.../...	

Jason-1 Cycles	Comments
224	Passes 30 and 163 are partly edited by altimetric parameters at default value. Just before and after these parts, they are edited by outbounded apparent squared mispointing values.

Table 2: *E*dited measurement status

2.3. Jason-1 product version "b" and "c"

2.3.1. Models and Standards History

Three versions of the Jason-1 Interim Geophysical Data Records (IGDRs) and Geophysical Data Records (GDRs) have been generated to date. These three versions are identified by the version numbers "a", "b" and "c" in the name of the data products. For example, version "a" GDRs are named "JA1_GDR_2Pa" and version "b" GDRs are named "JA1_GDR_2Pb". Both versions adopt an identical data record format as described in Jason-1 User Handbook and differ only in the models and standards that they adopt. Version "a" I/GDRs were the first version released soon after launch. Version "b" I/GDRs were first implemented operationally from the start of cycle 140 for the IGDRs and cycle 136 for the GDRs. Reprocessing to generate version "b" GDRs for cycles 1-135 were performed in 2006 and 2007 in order to generate a consistent data set. Version "c" I/GDRs were first operationally implemented from mid cycle 237 for the IGDRs and cycle 233 for the GDRs. The GDRs production was suspended after cycle 232 before the start of the version "c" production, because questions about the POE standards were raised. The GDRs production started again for cycle 240, and the previous cycles were then processed and broadcasted in version "c" as well. Table 3 below summarizes the models and standards that are adopted in these three versions of the Jason I/GDRs. More details on some of these models are provided in Jason-1 User Handbook document ([56]).

Model	Product Version "a"	Product Version "b"	Product Version "c"
Orbit	JGM3 Gravity Field DORIS tracking data for IGDRs DORIS+SLR tracking data for GDRs	EIGEN-CG03C Gravity Field DORIS tracking data for IGDRs DORIS+SLR+GPS tracking data for GDRs	EIGEN-GL04S with time-varying gravity DORIS tracking data for IGDRs DORIS+SLR+GPS tracking data for GDRs with increased weight of D/L
Altimeter Retracking	MLE3 + 1st order Brown model (mispointing estimated separately)	MLE4 + 2nd order Brown model : MLE4 simultaneously retrieves the 4 parameters that can be inverted from the altimeter waveforms: epoch, SWH, Sigma0 and mispointing angle. This algorithm is more robust for large off-nadir angles (up to 0.8°).	Identical to version "b"
.../...			

Model	Product Version "a"	Product Version "b"	Product Version "c"
Altimeter Instrument Corrections	Consistent with MLE3 retracking algorithm.	Consistent with MLE4 retracking algorithm.	Identical to version "b". A new correction is available in the product to account for the apparent datation bias (field 28). Users are advised to add this correction to the Ku-band altimeter range, as it is not a component of the net instrument correction that has already been applied to the provided Ku-band range
Jason Microwave Radiometer Parameters	Using calibration parameters derived from cycles 1-30.	Using calibration parameters derived from cycles 1-115.	Using calibration parameters derived from cycles 1-227
Dry Troposphere Range Correction	From ECMWF atmospheric pressures.	From ECMWF atmospheric pressures and model for S1 and S2 atmospheric tides.	From ECMWF atmospheric pressures and model for S1 and S2 atmospheric tides. Uses new ECMWF delivery to correct for spurious oscillation effects.
Wet Troposphere Range Correction from Model	From ECMWF model	From ECMWF model.	Identical to version "b"
Back up model for Ku-band ionospheric range correction.	Derived from DORIS measurements.	Derived from DORIS measurements.	Derived from JPL's Global Ionosphere Model (GIM) maps
Sea State Bias Model	Empirical model derived from cycles 19-30 of version "a" data.	Empirical model derived from cycles 11-100 of MLE3 altimeter data with version "b" geophysical models.	Empirical model derived from cycles 11-100 of MLE4 altimeter data with version "c" geophysical models"
Mean Sea Surface Model	GSFC00.1	CLS01	Identical to version "b"

.../...

Model	Product Version "a"	Product Version "b"	Product Version "c"
Along Track Mean Sea Surface Model	None (set to default)	None (set to default)	None (set to default)
Geoid	EGM96	EGM96	Identical to version "b"
Bathymetry Model	DTM2000.1	DTM2000.1	Identical to version "b"
Mean Dynamic Topography	None (was a spare)	None (was a spare)	Rio 2005 solution
Inverse Barometer Correction	Computed from ECMWF atmospheric pressures	Computed from ECMWF atmospheric pressures after removing model for S1 and S2 atmospheric tides.	Identical to Version "b" but using new ECMWF delivery to correct for spurious oscillation effects
Non-tidal High-frequency De-aliasing Correction	None (set to default)	Mog2D ocean model on GDRs, none (set to default) on IGDRs. Ocean model forced by ECMWF atmospheric pressures after removing model for S1 and S2 atmospheric tides.	High resolution Mog2D model for both IGDR and GDR products
Tide Solution 1	GOT99	GOT00.2 + S1 ocean tide . S1 load tide ignored.	Identical to version "b"
Tide Solution 2	FES99	FES2004 + S1 and M4 ocean tides. S1 and M4 load tides ignored.	FES2004 + S1 and M4 ocean tides. S1, K2 and loading tides have been updated
Equilibrium long-period ocean tide model.	From Cartwright and Taylor tidal potential. Identical to version "b"	From Cartwright and Taylor tidal potential.	
Non-equilibrium long-period ocean tide model.	None (set to default)	Mm, Mf, Mtm, and Msqm from FES2004.	Identical to version "b"
Solid Earth Tide Model	From Cartwright and Taylor tidal potential.	From Cartwright and Taylor tidal potential.	Identical to version "b"

.../...

Model	Product Version "a"	Product Version "b"	Product Version "c"
Pole Tide Model	Equilibrium model	Equilibrium model.	Identical to version "b"
Wind Speed from Model	ECMWF model	ECMWF model	Identical to version "b"
Altimeter Wind Speed	Table derived from TOPEX/POSEIDON data.	Table derived from version "a" Jason-1 GDR data.	Identical to version "b"
Rain Flag	Derived from TOPEX/POSEIDON data.	Derived from version "a" Jason-1 GDRs.	Derived from version "b" Jason-1 GDRs using the AGC instead of sigma naught values
Ice Flag	Climatology table	Climatology table	New flag based on the comparison of the model wet tropospheric correction and of a radiometer bi frequency wet tropospheric correction (derived from 23.8 GHz and 34.0 GHz), accounting for a backup solution based on climatologic estimates of the latitudinal boundary of the ice shelf, and from altimeter wind speed.

Table 3: *M*odels and standards adopted for the Jason-1 product version "a", "b", and "c"

2.3.2. Impact of product versions

The main changes between GDRs version "a" and "b" were the new orbit, the retracking of the wave forms with MLE4 algorithm, and new geophysical corrections. This had not only an impact on editing procedure, but also on crossover performances. For version "c", the main changes are the new orbit, new JMR calibration and new sea state bias. In the following sections these issues are briefly addressed. For further information concerning reprocessing in version "b", please refer to [55] or [6]. Concerning reprocessing in version "c", please refer to [18] or section 7.1..

2.3.2.1. Editing procedure

For GDR version "c" the same editing criteria and thresholds like in GDR version "b" should be used. Since GDR version "b" the MLE4 retracking algorithm is used. It is based on a second-

order altimeter echo model and is more robust for large off-nadir angles (up to 0.8 degrees). For product version "a" (CMA version 6.3), the maximum threshold on square off-nadir angle proposed in Jason-1 User Handbook document was set to 0.16 deg^2. Since GDR version "b", this threshold is too restrictive and has to be set to 0.64 deg^2.

However, this editing criteria had the side effect of removing some bad measurements impacted by rain cells, sigma0 blooms or ice. With the new threshold (0.64 deg^2), these measurements are not rejected any more even though the estimated SSH is not accurate for such waveforms.
Therefore 2 new criteria have to be added to check for data quality:

- Standard deviation on Ku sigma0 $\leq$ 1 dB
- Number measurements of Ku sigma0 $\geq$ 10

The Jason-1 User Handbook suggests the following editing criteria for the version "a" GDRs:

- -0.2 deg^2 $\leq$ square of off-nadir angle from waveforms (off_nadir_angle_ku_wvf) $\leq$ 0.16 deg^2
- sigma0_rms_ku $<$ 0.22 dB (optional criterion)

Since the version "b" GDRs these two edit criteria should be replaced by:

- -0.2 deg^2 $\leq$ square of off-nadir angle from waveforms (off_nadir_angle_ku_wvf) $\leq$ 0.64 deg^2
- and sigma0_rms_ku $\leq$ 1.0 dB
- and sig0_numval_ku $\geq$ 10

With these new criteria, the editing gives similar results for both product versions. Most of anomalous SSH measurements are rejected. Please note that some of them are still not detected, in particular close to sea ice.

2.3.2.2. General impact of version "c"

For further information on the impact of version "c" on GDR and IGDR products, please refer to Part 7.2., where a detailed description of the orbit and JMR impact on the whole dataset, and a status of current reprocessing performances are given.

3. Data coverage and edited measurements

3.1. Missing measurements

3.1.1. Over ocean

Determination of missing measurements relative to the theoretically expected orbit ground pattern is used to detect missing telemetry in Jason-1 datasets due to altimetry events for instance. This procedure is applied cycle per cycle and leads to results plotted on the left figure 1. It represents the percentage of missing measurements relative to the theory, when limited to ocean surfaces. The mean value is about 3.7% but this figure is not significant due to several events where the measurements are missing. All these events are described on table 1.
On figure 1 on the right, the percentage of missing measurements is plotted without taking into account the cycles where instrumental events or other anomalies occurred. Moreover shallow waters and high latitudes have been removed. This allows us to detect small data gaps in open ocean. The mean value is about 0.03%. This weak percentage of missing measurements is mainly explained by the rain cells, ice sea or sigma0 blooms. These sea states can disturb significantly the Ku band waveform shape leading to a non significant measure.
Another reason for these small data gaps in open ocean, are datation gaps, which occur occasionally.

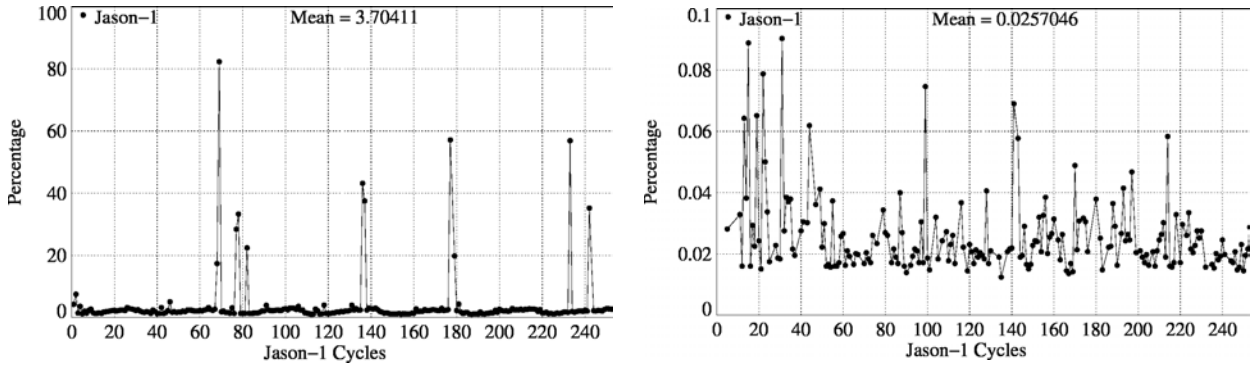

Figure 1: *Cycle per cycle percentage of missing measurements over ocean*

3.1.2. Over land and ocean

Figure 2 shows the percentage of missing measurements for Jason-1 and T/P (all surfaces) computed with respect to a theoretical possible number of measurements. Due to differences between tracker algorithms, the number of data is greater for T/P (excepted when T/P experienced problems, especially since the tape recorders were no longer in service (T/P cycle 444, Jason-1 cycle 101)) than for Jason-1. Differences appear on land surfaces as shown in figure 3.

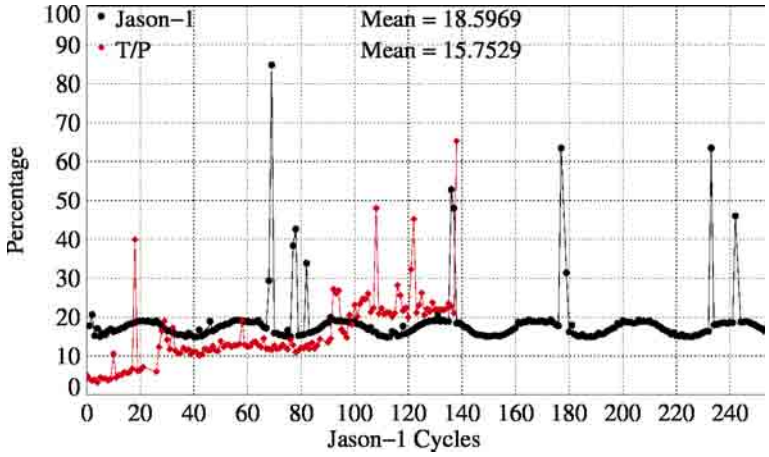

Figure 2: *Percentage of missing measurements over ocean and land for J1 and T/P*

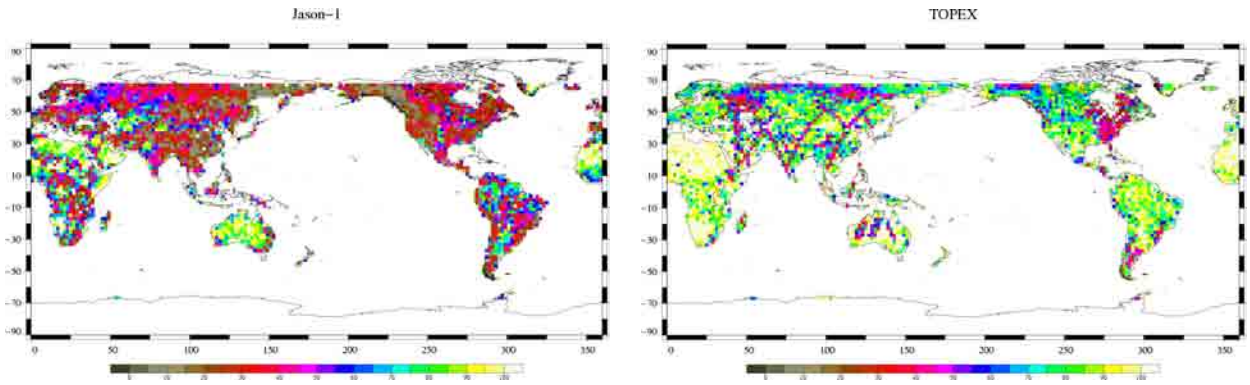

Figure 3: *Map of percentage of available measurements over land for Jason-1 on cycle 61 (left) and for TOPEX on cycle 404 (right)*

3.2. Edited measurements

3.2.1. Editing criteria definition

Editing criteria are used to select valid measurements over ocean. The editing process is divided into 4 parts. First, only measurements over ocean and lakes are kept (see section 3.2.2.). Second, the quality criteria concern the flags which are described in section 3.2.3., section 3.2.4. and 3.2.5.. Then, threshold criteria are applied on altimeter, radiometer and geophysical parameters and are described in the table 4. Moreover, a spline criterion is applied to remove the remaining spurious data. These criteria defined for the GDR products "b" and "c" are also defined in AVISO and PODAAC User handbook. For each criterion, the cycle per cycle percentage of edited measurements has been monitored. This allows detection of anomalies in the number of removed data, which could come from instrumental, geophysical or algorithmic changes.

Parameter	Min thresholds	Max thresholds	mean edited
Sea surface height	$-130\,m$	$100\,m$	0.76%
Sea level anomaly	$-10\,m$	$10.0\,m$	1.34%
Number measurements of range	10	*Not applicable*	1.09%
Standard deviation of range	$0\,m$	$0.2\,m$	1.28%
Square off-nadir angle	$-0.2\,deg^2$	$0.64\,deg^2$	0.49%
Dry troposphere correction	$-2.5\,m$	$-1.9\,m$	0.00%
Inverted barometer correction	$-2.0\,m$	$2.0\,m$	0.00%
JMR wet troposphere correction	$-0.5m$	$-0.001\,m$	0.13%
Ionosphere correction	$-0.4\,m$	$0.04\,m$	1.08%
Significant waveheight	$0.0\,m$	$11.0\,m$	0.55%
Sea State Bias	$-0.5\,m$	$0.0\,m$	0.88%
Number measurements of Ku-band Sigma0	10	*Not applicable*	1.09%
Standard deviation of Ku-band Sigma0	$0\,dB$	$1.0\,dB$	1.63%
Ku-band Sigma0 [1]	$7.0\,dB$	$30.0\,dB$	0.51%
Ocean tide	$-5.0\,m$	$5.0\,m$	0.04%
Equilibrium tide	$-0.5\,m$	$0.5\,m$	0.00%
Earth tide	$-1.0\,m$	$1.0\,m$	0.00%
.../...			

Parameter	Min thresholds	Max thresholds	mean edited
Pole tide	$-15.0\,m$	$15.0\,m$	0.00%
Altimeter wind speed	$0\,m.s^{-1}$	$30.0\,m.s^{-1}$	0.91%
All together	-	-	2.93%

Table 4: *E*diting criteria

3.2.2. Selection of measurements over ocean and lakes

In order to remove data over land, a land-water mask is used. Only measurements over ocean or lakes are kept. Indeed, this allows us to keep more data near the coasts and then detecting potential anomalies in these areas. Furthermore, there is no impact on global performance estimations since the most significant results are derived from analyzes in deep ocean areas. Figure 4 (left) shows the cycle per cycle percentage of measurements eliminated by this selection. It shows a seasonal signal. This is due to the varying number of measurements available in the GDRs, which varies not only over ocean, but also over land. After removing the annual signal, there is no trend noticeable Figure 4 (right).

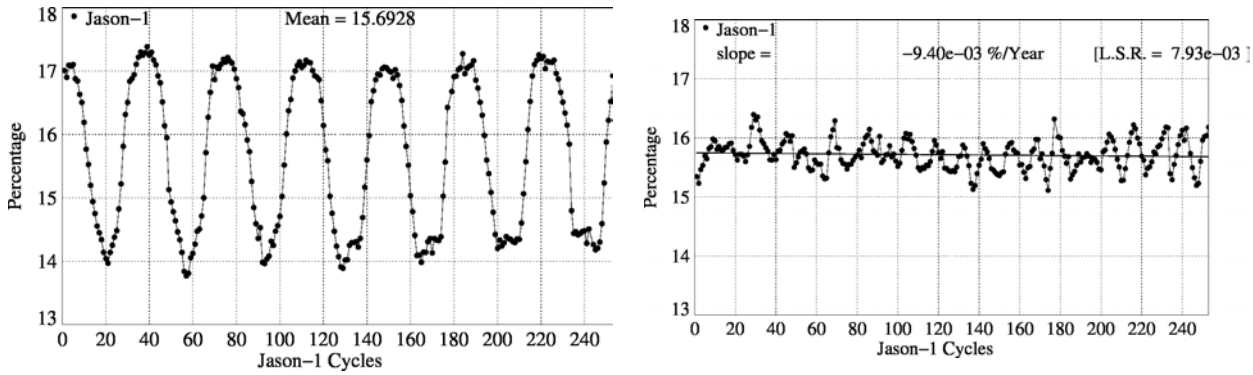

Figure 4: *Cycle per cycle percentage of eliminated measurements during selection of ocean/lake measurements (left). Trend of eliminated measurements after removing annual signal (right).*

[1]The thresholds used for the Ku-band Sigma0 are the same than for T/P, but the sigma0 bias between Jason-1 and T/P (about 2.4 dB) is applied.

3.2.3. Flagging quality criteria: Ice flag

The ice flag is used to remove the sea ice data. Figure 5 shows the cycle per cycle percentage of measurements edited by this criterion. No anomalous trend is detected (figure 5 right) but an annual cycle is visible. Indeed, the maximum number of points over ice is reached during the northern fall. As Jason-1 takes measurements between 66° north and south, it does not detect thawing of sea ice (due to global warming), which takes place especially in northern hemisphere beyond 66°N. The ice flag edited measurements are plotted in Figure 6 for one cycle of GDR "b". It shows that the ice flag was not perfectly tuned especially in the northern hemisphere, for instance the Hudson Bay is divided into 2 parts (figure 6, left). By using an empirical ice flag similar to the one used for ERS satellite (which involves the difference between dual-frequency radiometer wet troposphere and model wet troposphere), the detection of ice is improved. This empirical ice flag is now implemented in GDRs version c (see section 3.2.4.).

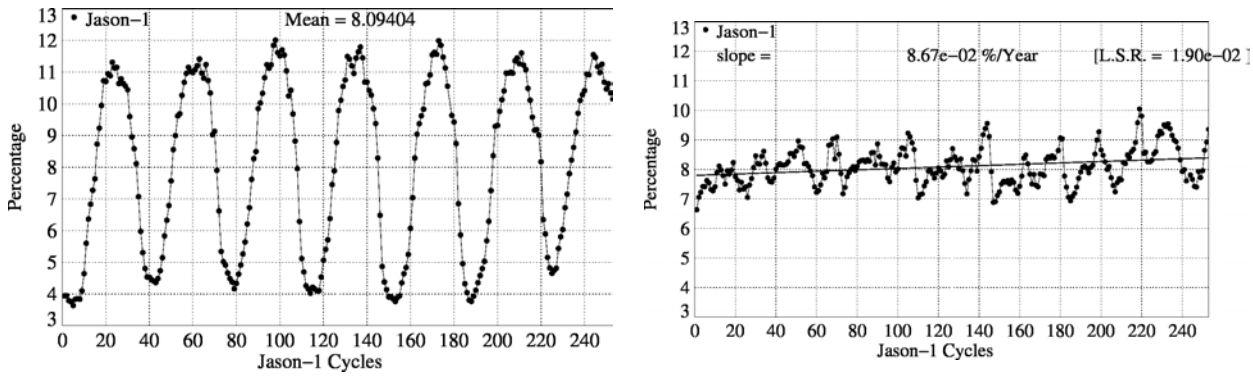

Figure 5: *Cycle per cycle percentage of edited measurements by ice flag criterion (left), after subtracting annual signal (right).*

3.2.4. Flagging quality criteria: Ice flag with ERS method

The ice flag of ERS uses the difference between the dual-frequency radiometer wet troposphere and the ECMWF model wet troposphere correction. This difference is small over ocean, but important over ice. In [29] this method was adapted for Jason-1. The dual-frequency wet troposphere is calculated by

$$\text{Tropo\_bifr} = -0.01 * (142.932 - 56.2442 * LOG(280 - TEMP\_BRI\_C2) + 28.5724 * LOG(280 - TEMP\_BRI\_C3))$$

Ice is detected when for latitudes higher than 50° the following 2 conditions are fullfilled:

- Number of elementary measurements ≤ 10
- $abs(dual frequency\ wet\ troposphere - ECMWF\ model\ wet\ troposphere) \geq 10cm$

This criteria works fine, and detects ice in the entire Hudson Bay. Nevertheless ice cover can also be found south of 50°N as for example in the northern part of Caspian sea, in the Aral Sea or in the La Perouse strait (north of Japon). Therefore the ERS ice flag should be extended to a latitude of 40°N within a coast distance of 500 km (to avoid erroneous ice detection in open sea). Figure 6 (right) shows ice detected on cycle 185 using the extended ERS ice flag. It shows that ice is detected in the entire Hudson Bay, as well as in the Aral sea and in the northern part of the Caspian Sea.
This ice flag is an empirical method, which certainly does also have erroneous ice detection or ice which is not detected, but statistically it works better than the ice flag featured in version "b". Therefore, it was implemented in version "c".

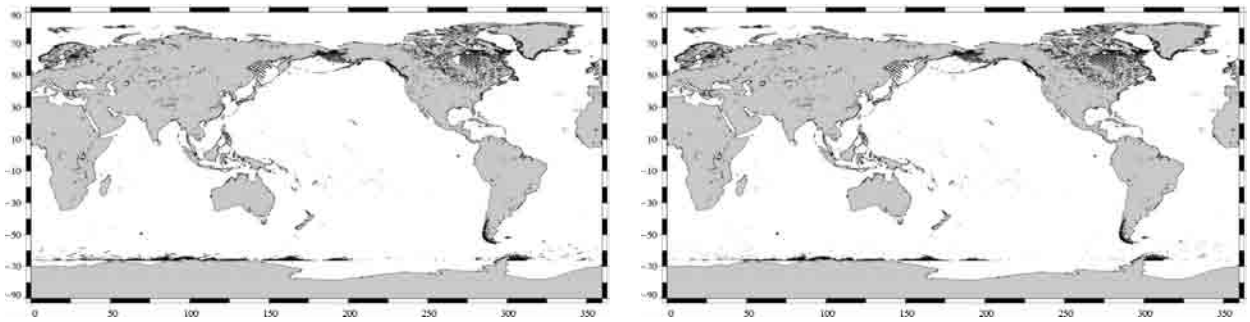

Figure 6: *Map of edited measurements by ice flag criterion on cycle 185 (left) and map of measurements, which would be edited when using ice flag criterion of type ERS on cycle 185 (right).*

3.2.5. Flagging quality criteria: Rain flag

The rain flag is not used for data selection since it is quite restrictive. It is thus recommended not to be used by users. The rain flag has changed in version "c", making it even more restrictive. The percentage of rain edited measurements is plotted in figure 7 over cycles 196 to 216 (covering 7 months in 2007) and from cycles 233 to 253 (same period in 2008). It shows that measurements are especially edited near coasts, but also in the equatorial zone and open ocean. The rain flag seems to be too strict, using it would lead to editing 7.6% of additional measurements.

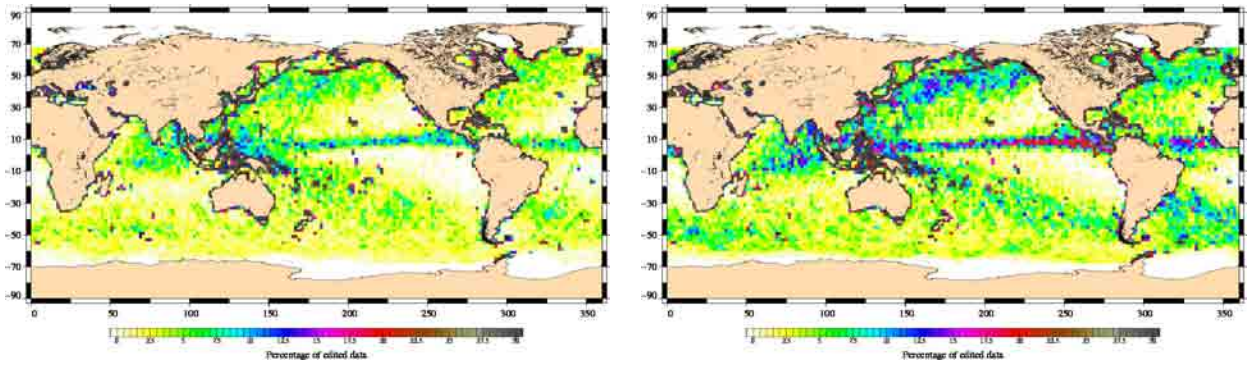

Figure 7: *Map of percentage of edited measurements by rain flag criterion over an 7-month period; left: cycles 196 to 216 (GDR-B); right: cycles 233 to 253 (GDR-C).*

3.2.6. Threshold criteria: Global

Instrumental parameters have also been analyzed from comparison with thresholds, after selecting only ocean/lake measurements and applied flagging quality criteria (ice flag). Note that no measurements are edited by threshold criteria on the following corrections : dry troposphere correction, inverted barometer correction, equilibrium tide, earth and pole tide, which are all model corrections.

The percentage of measurements edited using each criterion has been monitored on a cycle per cycle basis (figure 8). The mean percentage of edited measurements is about 2.9%. An annual cycle is visible due to the seasonal sea ice coverage in the northern hemisphere. Indeed most of northern hemisphere coasts are without ice during northern hemisphere summer. Consequently some of these coastal measurements are edited by the thresholds criteria in summer instead of the ice flag in winter. This seasonal effect visible in the statistics is not balanced by the southern hemisphere coasts due to the shore distribution between both hemispheres.
Note that for some cycles, especially cycles 69 and 179, the percentage of edited measurements is higher than usual. This is mostly due to the lack of radiometer wet troposphere correction, see section 3.2.11..

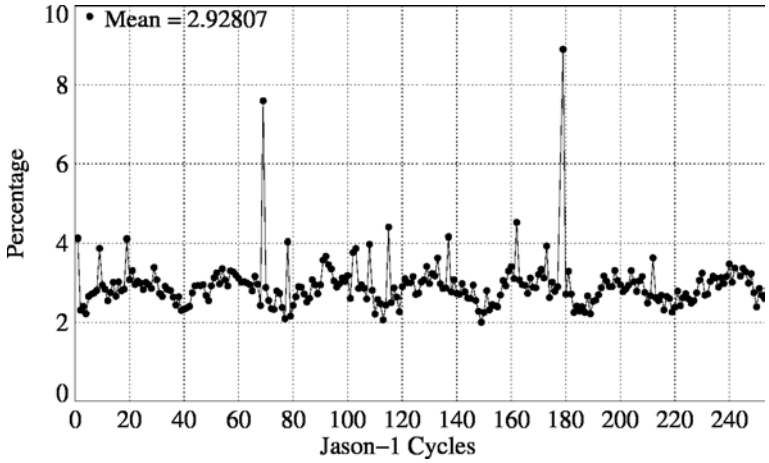

Figure 8: *Cycle per cycle percentage of edited measurements by threshold criteria*

3.2.7. Threshold criteria: 20-Hz measurements number

The percentage of edited measurements because of a too low number of 20-Hz measurements is represented on left side of figure 9. Neither a trend nor any anomaly has been detected, except for cycle 212.
Indeed during this cycle, about half of a pass had all altimetric parameters set at default values, due to off-pointing of the satellite, avoiding the retrieval of altimetric parameters.

The map of measurements edited by the 20-Hz measurements number criterion is plotted on the right panel of figure 9 and shows correlation with heavy rain, wet areas as well as coastal regions. Indeed the waveforms are distorted by rain cells, which makes them often unexploitable for SSH calculation. In consequence edited measurements due to several altimetric criteria are often correlated with wet areas.

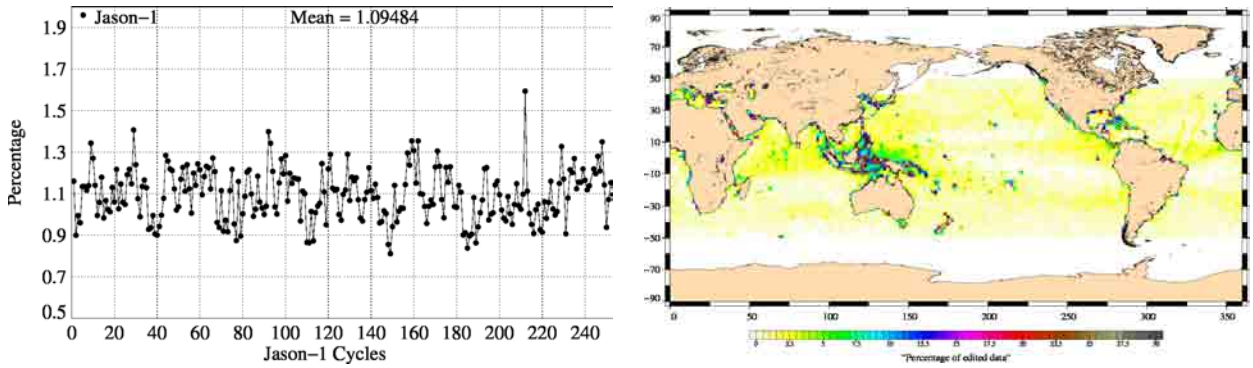

Figure 9: *Cycle per cycle percentage of edited measurements by 20-Hz measurements number criterion (left). Right: Map of percentage of edited measurements by 20-Hz measurements number criterion over an one-year period (cycles 217 to 253).*

3.2.8. Threshold criteria: 20-Hz measurements standard deviation

The percentage of edited measurements due to 20-Hz measurements standard deviation criterion is shown in figure 10. The observed annual signal (left) is linked to the seasonal variability associated with ice coverage. After removing the annual signal (figure 10 right), no trend is visible.

Figure 11 shows a map of measurements edited by the 20-Hz measurements standard deviation criterion. As in section 3.2.7., edited measurements are mainly correlated with wet areas.

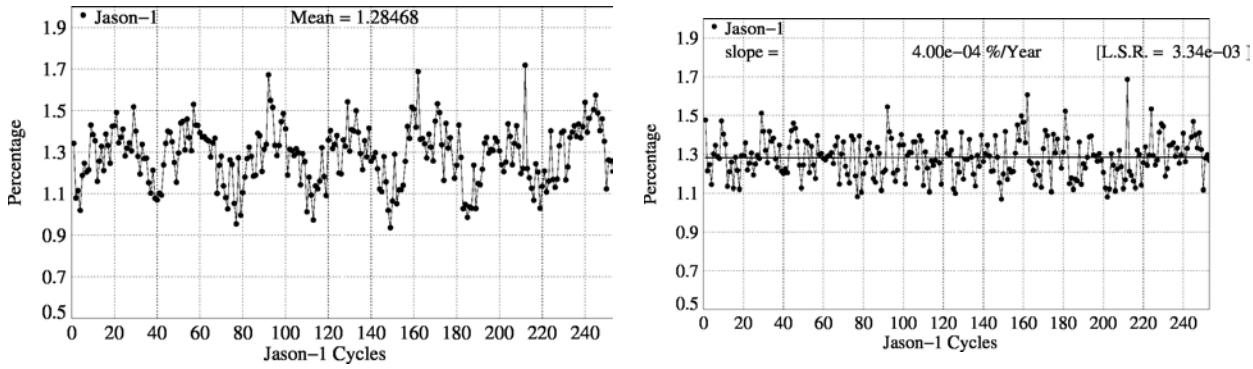

Figure 10: *Cycle per cycle percentage of edited measurements by 20-Hz measurements standard deviation criterion (left); after removing annual signal (right).*

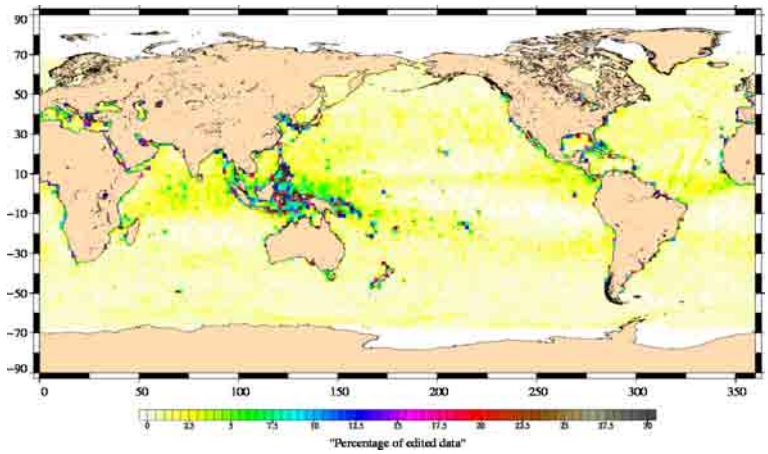

Figure 11: *Map of percentage of edited measurements by 20-Hz measurements standard deviation criterion over an one-year period (cycles 217 to 253).*

3.2.9. Threshold criteria: Significant wave height

The percentage of edited measurements due to significant wave height criterion is represented in figure 12. It is about 0.55%. No drift has been detected over the Jason-1 period. The peaks visible for cycles 212 and 224 are due to a portion of a pass at default values. The effect is barely visible on the global rejected measurements figure 8 for cycle 212, and unseen for cycle 224, because of the weak impact of the SWH criterion with regard to the global rejection criteria. Figure 12 (right part) shows that measurements edited by SWH criterion are especially found near coasts in the equatorial regions.

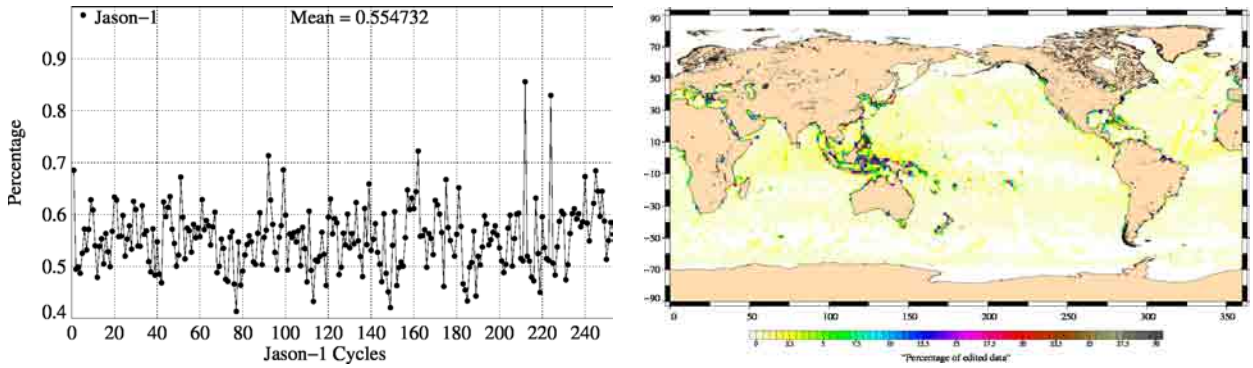

Figure 12: *Cycle per cycle percentage of edited measurements by SWH criterion (left). Right: Map of percentage of edited measurements by SWH criterion over an one-year period (cycles 217 to 253).*

3.2.10. Backscatter coefficient

The percentage of edited measurements due to backscatter coefficient criterion is represented in figure 13. It is about 0.51% and shows no drift. The peaks visible for cycles 212 and 224 are due to a portion of a pass at default values. The right part of figure 13 shows that measurements edited by backscatter coefficient criterion are especially found near coasts in the equatorial regions.

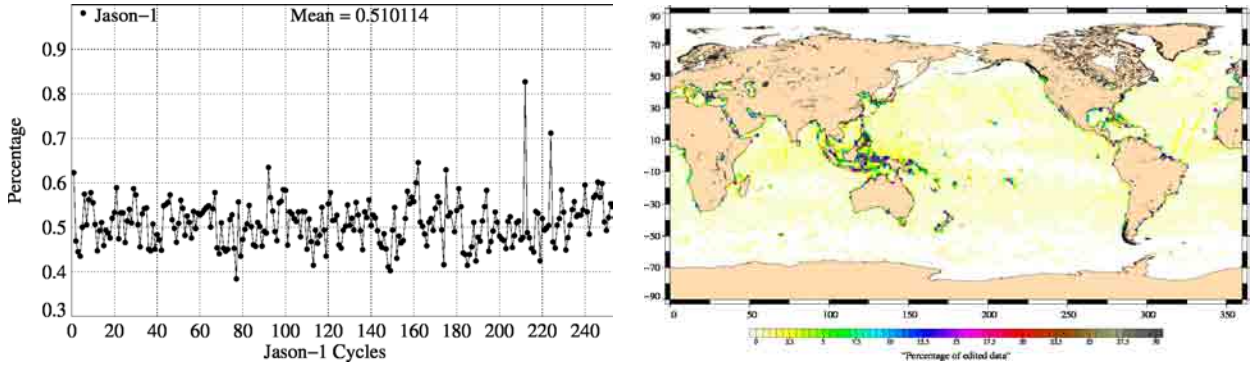

Figure 13: *Cycle per cycle percentage of edited measurements by Sigma0 criterion (left). Right: Map of percentage of edited measurements by Sigma0 criterion over an one-year period (cycles 217 to 253).*

3.2.11. Radiometer wet troposphere correction

The percentage of edited measurements due to radiometer wet troposphere correction criterion is represented in figure 14. It is about 0.13%. When removing cycles which experienced problems, percentage of edited measurements drops to 0.07%. The figure shows irregular oscillations which are not correlated to annual cycle. At the end of the shown period, percentage of edited measurements decreases (due to a decrease of default values). This might be related to use of new CMA version 9.0 (since cycle 198). The map 14 shows that only few measurements are edited by radiometer wet troposphere correction criterion.

Notice that for some cycles the percentage of edited measurements is higher than usual. This is often linked to the Jason safe hold mode on some of these cycles (69, 78, 137, and 179): the radiometer has been set on 2 hours later than the altimeter. As a result, the radiometer wet troposphere correction has been set to default value during this period and these measurements have been edited.
For cycle 1 radiometer wet troposphere correction is missing for passes, which were absent in GDR "a" product version. Concerning cycles 8 and 19, radiometer wet troposphere correction is missing for a portion of a pass, for which it was present in GDR "a" product version.

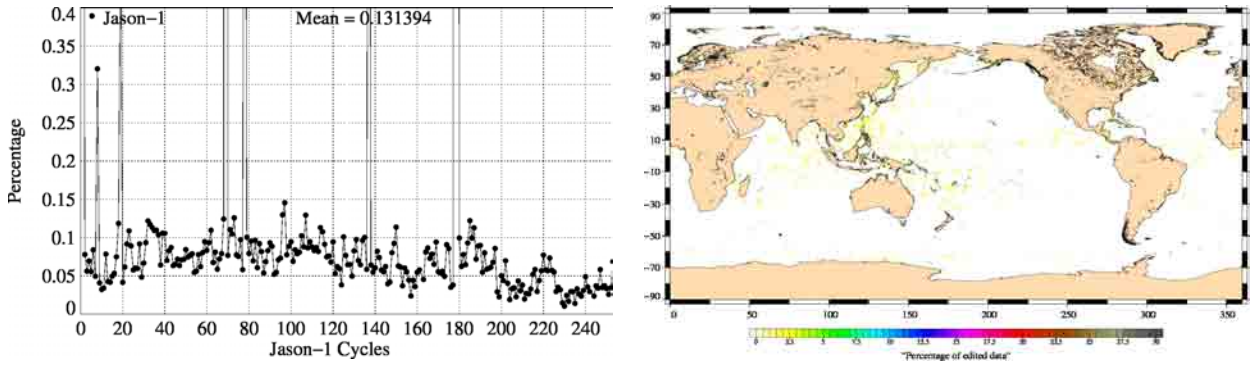

Figure 14: *Cycle per cycle percentage of edited measurements by radiometer wet troposphere criterion (left). Map of percentage of edited measurements by radiometer wet troposphere criterion over an one-year period (cycles 217 to 253).*

3.2.12. Dual frequency ionosphere correction

The percentage of edited measurements due to dual frequency ionosphere correction criterion is represented in figure 15. It is about 1.08% and shows no drift. The map 15 shows that measurements edited by dual frequency ionosphere correction are mostly found in equatorial regions.
Notice that for cycles 9, 91, 102, 103, 108, 115, 133, 173, 181, 198, and 212 the percentage of edited measurements is higher than usual. This is almost always linked to an altimeter SEU (C band) occurred on these cycles. The dual frequency ionosphere correction has been set to default value during this period and these measurements have been edited. Only the peak for cycle 212 is not due to an altimeter SEU (see section 3.2.7.).

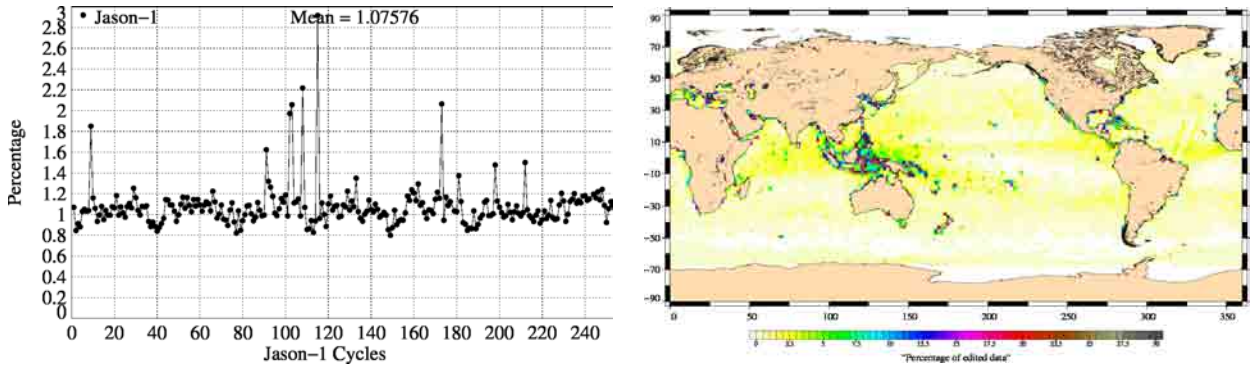

Figure 15: *Cycle per cycle percentage of edited measurements by dual frequency ionosphere criterion (left). Map of percentage of edited measurements by dual frequency ionosphere criterion over an one-year period (cycles 217 to 253).*

3.2.13. Square off-nadir angle

The percentage of edited measurements due to square off-nadir angle criterion is represented in figure 16. It is about 0.48% and shows no drift. The peaks in cycles 212 and 224 are due to very high mispointing caused by low star tracker availability and gyro wheels behavior. This even avoided retrieval of altimetric parameters for a portion of a pass. The map 16 shows that edited measurements are mostly found in coastal regions.

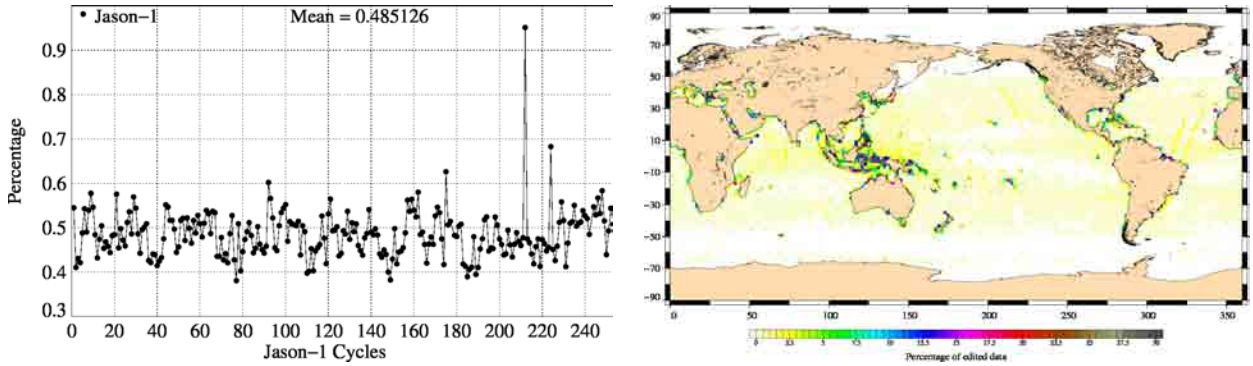

Figure 16: *Cycle per cycle percentage of edited measurements by square off-nadir angle criterion (left). Right: Map of percentage of edited measurements by square off-nadir angle criterion over an one-year period (cycles 217 to 253).*

3.2.14. Sea state bias correction

The percentage of edited measurements due to sea state bias correction criterion is represented in figure 17. The percentage of edited measurements is about 0.88% and shows no drift. An annual cycle is visible, which is highly correlated to the percentage of edited measurements by wind speed criterion, as sea state bias is computed with significant wave height and wind speed. Note that, since the GDRs have been computed in version c, the percentage of measurements edited by the SSB criterion has decreased to 0.5%, due to the change of SSB calculation for GDRs version "c". Indeed this difference is explained by the processing of wave and wind speed measurements which fall out of fringes of the SSB look-up table. This processing is different between Cal/Val chain (which updated Venice SSB during GDR "b" period) and CMA chain (which produces SSB during GDR "c" period).

The map 17 shows that edited measurements are mostly found in equatorial regions near coasts.

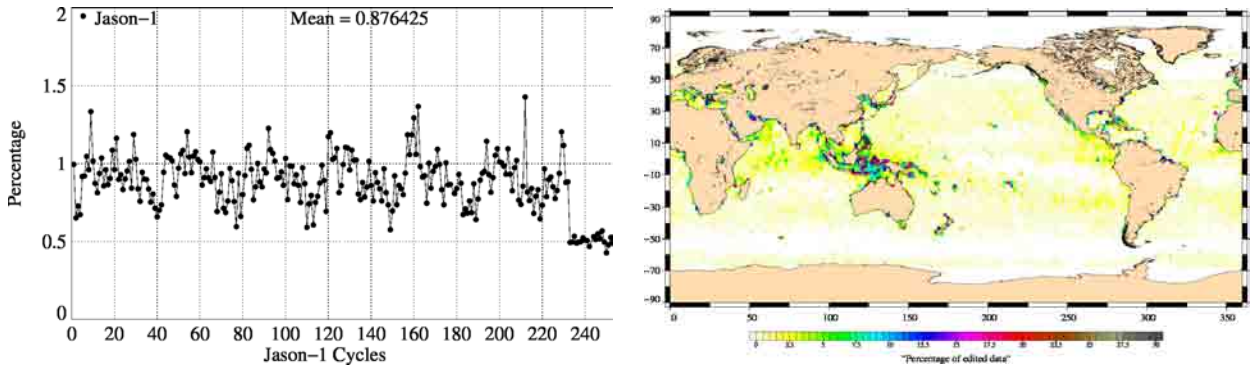

Figure 17: *Cycle per cycle percentage of edited measurements by sea state bias criterion (left). Right: Map of percentage of edited measurements by sea state bias criterion over an one-year period (cycles 217 to 253).*

3.2.15. Altimeter wind speed

The percentage of edited measurements due to altimeter wind speed criterion is represented in figure 18. It is about 0.91% and shows no drift. The measurements are edited, because they have default values. This is the case when sigma0 itself is at default value, or when it shows very high values (higher than 25 dB), which occur during sigma bloom and also over sea ice. The annual cycle is probably due to sea ice, which was not detected by the ice flag.

The map 18 showing percentage of measurements edited by altimeter wind speed criterion is highly correlated with the map 17.

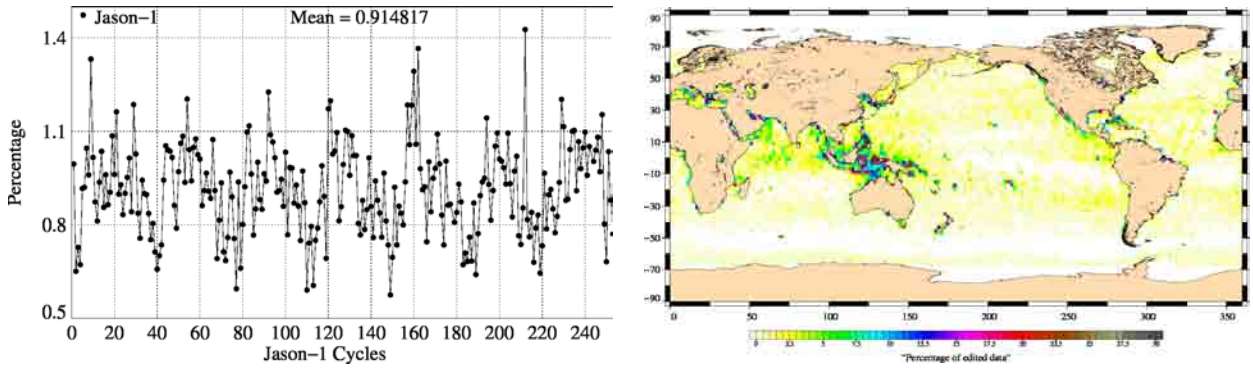

Figure 18: *Cycle per cycle percentage of edited measurements by altimeter wind speed criterion (left). Right: Map of percentage of edited measurements by altimeter wind speed criterion over an one-year period (cycles 217 to 253).*

3.2.16. Ocean tide correction

The percentage of edited measurements due to ocean tide correction criterion is represented in figure 19. It is about 0.04% and shows no drift. The ocean tide correction is a model output, there should therefore be no edited measurements. Indeed there are no measurements edited in open ocean areas, but only very few near coasts or in lakes or rivers (see map 19). These measurements are mostly at default values.

Some of these lakes are in high latitudes and therefore periodically covered by ice. This explains the annual signal visible in figure 19. A slight increase in edited measurements is visible since GDRs version "c". This is related to the new ice flag, which edits slightly less measurements than the previously. Some of these measurements are now edited by ocean tide correction criterion.

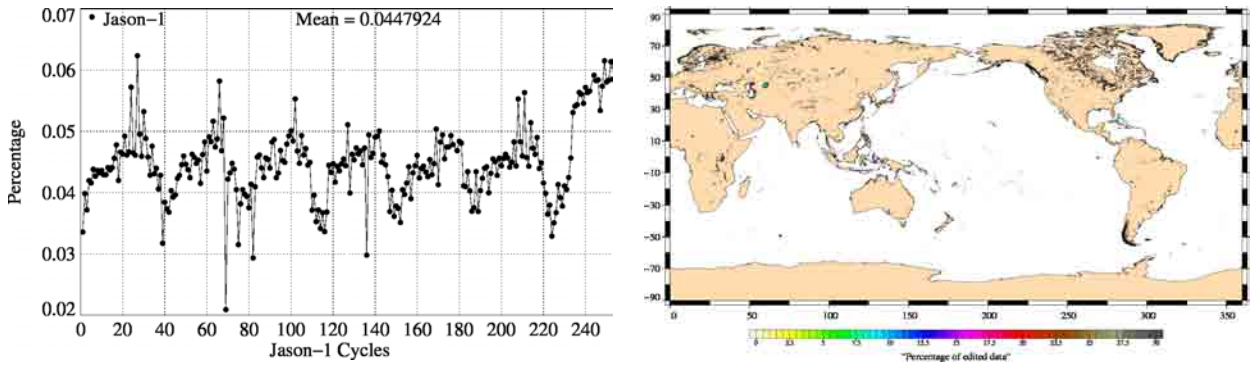

Figure 19: *Cycle per cycle percentage of edited measurements by ocean tide criterion (left). Right: Map of percentage of edited measurements by ocean tide criterion over an one-year period (cycles 217 to 253).*

3.2.17. Sea surface height

The percentage of edited measurements due to sea surface height criterion is represented in figure 20. It is about 0.75% and shows no drift. There is however an annual signal visible. For the peak in cycle 212 see section 3.2.13..

The measurements edited by sea surface height criterion are mostly found near coasts in equatorial regions (see map 20)

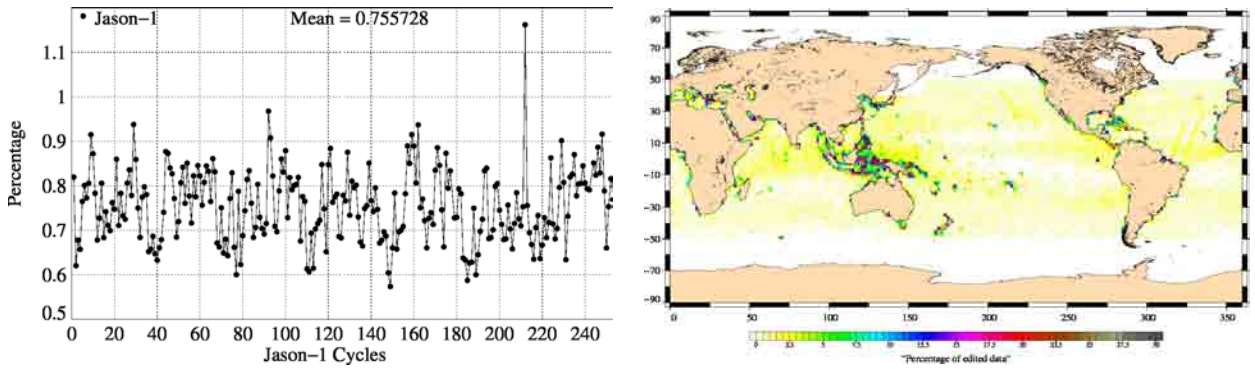

Figure 20: *Cycle per cycle percentage of edited measurements by sea surface height criterion (left). Right: Map of percentage of edited measurements by sea surface height criterion over an one-year period (cycles 217 to 253).*

3.2.18. Sea level anomaly

The percentage of edited measurements due to sea level anomaly criterion is represented in figure 21. It is about 1.34% and shows no drift. The graph is quite similar to the one in figure 8 (showing the percentage of measurements edited by all the threshold criteria), as the SLA clip contains many of the parameters used for editing.
Whereas the map in figure 21 allows us to plot the measurements edited due to sea level anomaly out of thresholds (after applying all other threshold criteria). These are only very few measurements.

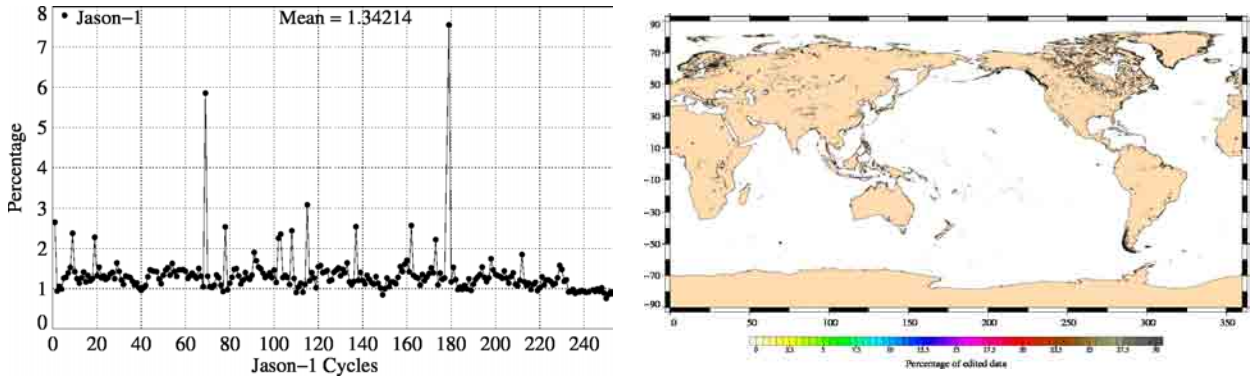

Figure 21: *Cycle per cycle percentage of edited measurements by sea level anomaly criterion (left). Right: Map of percentage of edited measurements by sea level anomaly criterion (after applying all other threshold criteria) over an one-year period (cycles 217 to 253).*

4. Monitoring of altimeter and radiometer parameters

4.1. Methodology

Both mean and standard deviation of the main parameters of Jason-1 have been monitored since the beginning of the mission. Moreover, a comparison with T/P parameters has been performed: it allows us to monitor the bias between the parameters of the 2 missions. The comparison is done till the end of scientific mission of T/P, which occurred during Jason-1 cycle 138. Two different methods have been used to compute the bias:

- During the verification phase, Jason-1 and T/P are on the same ground track and are spaced out about 1 minute apart. The mean of the T/P Jason-1 differences can be computed using a point by point repeat track analysis.
- From cycle Jason-1 22 (Cycle T/P 365), the 15th of August 2002, a maneuver sequence was conducted over 30 days to move T/P to the new Tandem Mission orbit : Furtheron T/P was located one half the TP/Jason-1 track spacing to the West of Jason-1. Geographical variations are then too strong to directly compare Jason-1 and T/P parameters on a point by point basis. Therefore cycle per cycle differences have been carried out to monitor Jason-1 and T/P differences, but data gaps on both satellites have been taken into account.

4.2. 20 Hz Measurements

The monitoring of the number and the standard deviation of 20 Hz elementary range measurements used to derive 1 Hz data is presented here. These two parameters are computed during the altimeter ground processing. Before a regression is performed to derive the 1 Hz range from 20 Hz data, a MQE criterion is used to select valid 20 Hz measurements. This first step of selection thus consists in verifying that the 20 Hz waveforms can be effectively approximated by a Brown echo model (Brown, 1977 [9]) (Thibaut et al. 2002 [69]). Through an iterative regression process, elementary ranges too far from the regression line are discarded until convergence is reached. Thus, monitoring the number of 20 Hz range measurements and the standard deviation computed among them is likely to reveal changes at instrumental level.

4.2.1. 20 Hz measurements number in Ku-Band and C-Band

Figure 22 shows the cycle per cycle mean of 20-Hz measurements number in Ku-Band (on the left) and C-Band (on the right). Apart from a very weak seasonal signal, no trend neither any anomaly has been detected.

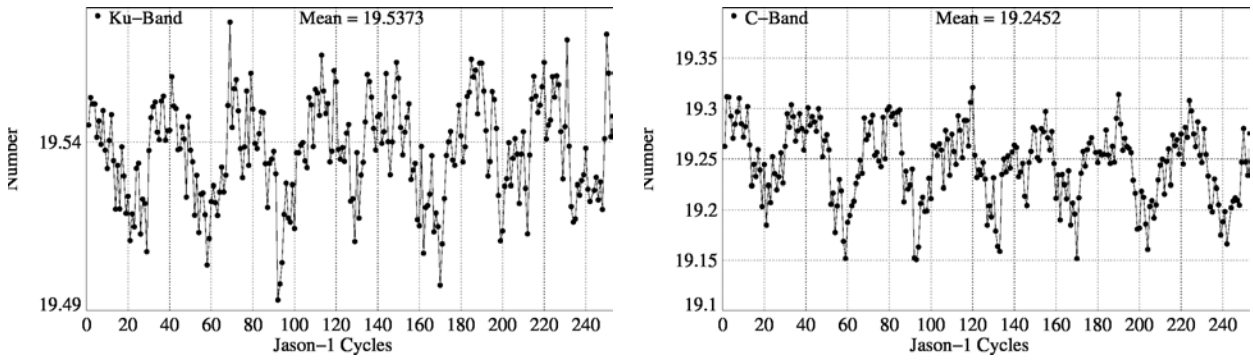

Figure 22: *Cycle per cycle mean of 20-Hz measurements number in Ku-Band (left) and C-Band (right)*

4.2.2. 20 Hz measurements standard deviation in Ku-Band and C-Band

Figure 23 shows the cycle per cycle standard deviation of the 20 Hz measurements in Ku-Band (on the left) and C-Band (on the right). Apart from a weak seasonal signal, neither trend nor any anomaly has been detected. Values of C-Band standard deviation of the 20 Hz measurements are higher than those of Ku-Band, as integration is done over less waveforms, leading to increased noise.

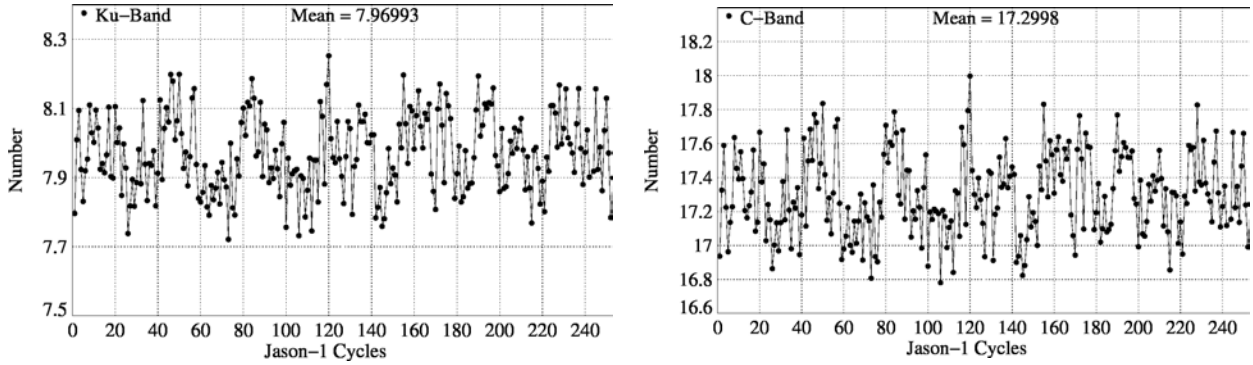

Figure 23: *Cycle per cycle mean of 20-Hz measurements standard deviation in Ku-Band (left) and C-Band (right)*

4.3. Off-Nadir Angle from waveforms

The off-nadir angle is estimated from the waveform shape during the altimeter processing. The square of the off-nadir angle, averaged in a one-cycle basis, has been plotted in figure 24. The mean values are slightly positive. This mean value is not significant in terms of actual platform mispointing. In fact squared attitude is what is retrieved from waveforms, not attitude. During the first half of the mission off-nadir angles are low and quite stable, except for cycle 69 related to a platform safehold mode. During the second half of the mission (since approximately cycle 100), off-nadir angle has very strong values. There are periods where the combination of low Beta angles and Sun glint or Moon in field of view significantly reduces the tracking performance of both star trackers, especially during fixed-yaw. When the off-nadir angle is larger than the 0.2 degree specification, errors may be introduced in the altimeter parameters if not taken into account in the ground processing (Vincent et al., 2003). Thus, an improvement of the retracking algorithm was made since GDR version "b" (section 2.3.), to correct for estimations of altimeter parameters for mispointing angle errors up to 0.8 deg. (Amarouche et al. 2004 [7]).

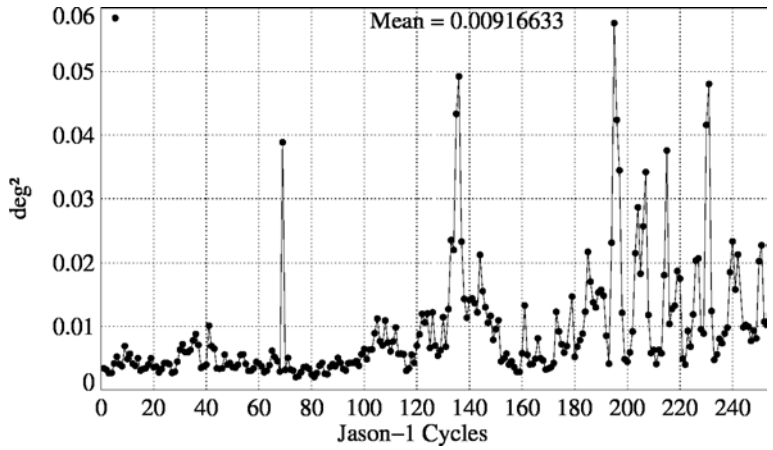

Figure 24: *Cycle mean of the square of the off-nadir angle deduced from waveforms (deg^2)*

During year 2008, the satellite has experienced several severe mispointing cases, although the mispointing values remained within the threshold editing criteria (-0.2 to $0.64 deg^2$). This feature has been repeatedly pointed out, especially after maneuvers. Neither specific geographic pattern nor ascending/descending tracks systematisms are observed. The high mispointing values are related to low star tracker availability and gyro wheels behavior. Figure 25 shows the square of the off-nadir angle for cycle 215, an extreme example of the high mispointing values observed.

Without getting out of bounds, along-track jumps may be observed, with mispointing values raising from 0 to $0.6 deg^2$ within a few seconds. An instance has been plotted on Figure 26, from cycle 249 track 116 and the corresponding Jason-2 track (cycle 11). Such jumps are not detected by editing criteria.

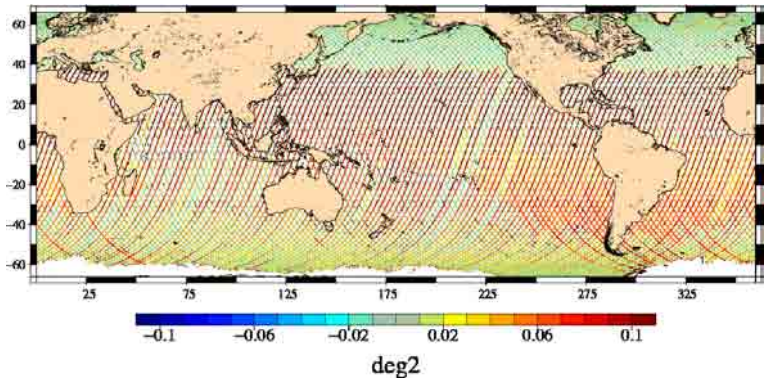

Figure 25: *Square of the off-nadir angle deduced from waveforms (deg^2) for cycle 215*

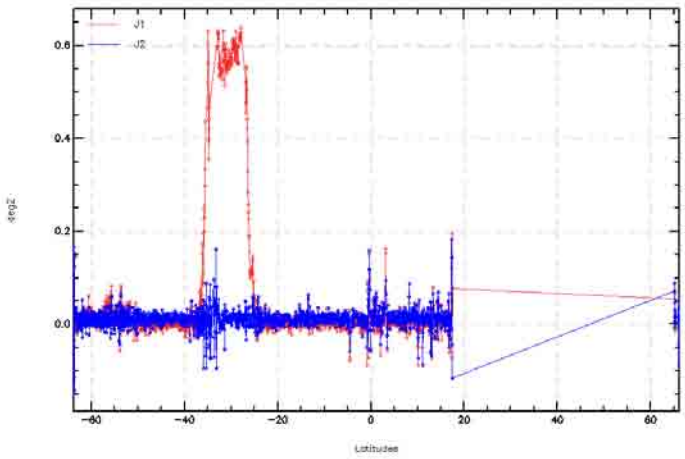

Figure 26: *Square of the off-nadir angle deduced from waveforms (deg^2) for cycle 249/track 116*

4.4. Significant wave height

4.4.1. Ku-band SWH

Jason-1 and T/P Ku SWH are compared in terms of global statistics in figure 27: cycle means and standard deviations of both missions are presented in a cycle basis, as well as mean differences between T/P and Jason-1. Global variations of the SWH statistics are the same on the two missions. A weak annual signal is visible. Jason-1 SWH shows a very small drift of 5 mm/yr. The (TOPEX - Jason-1) SWH bias is about 8.2 cm. This value remains almost steady at the 1 cm level throughout the Jason-1 mission (showing only a weak drift of 1.2 mm/yr), even if some variability is observed for particular cycles. The estimation of the (Poseidon-1 - Poseidon-2) SWH difference is about 15.0 cm for Poseidon cycle 18 not plotted here.
The standard deviation of Ku-band SWH shows an annual signal for both Jason-1 and T/P data.

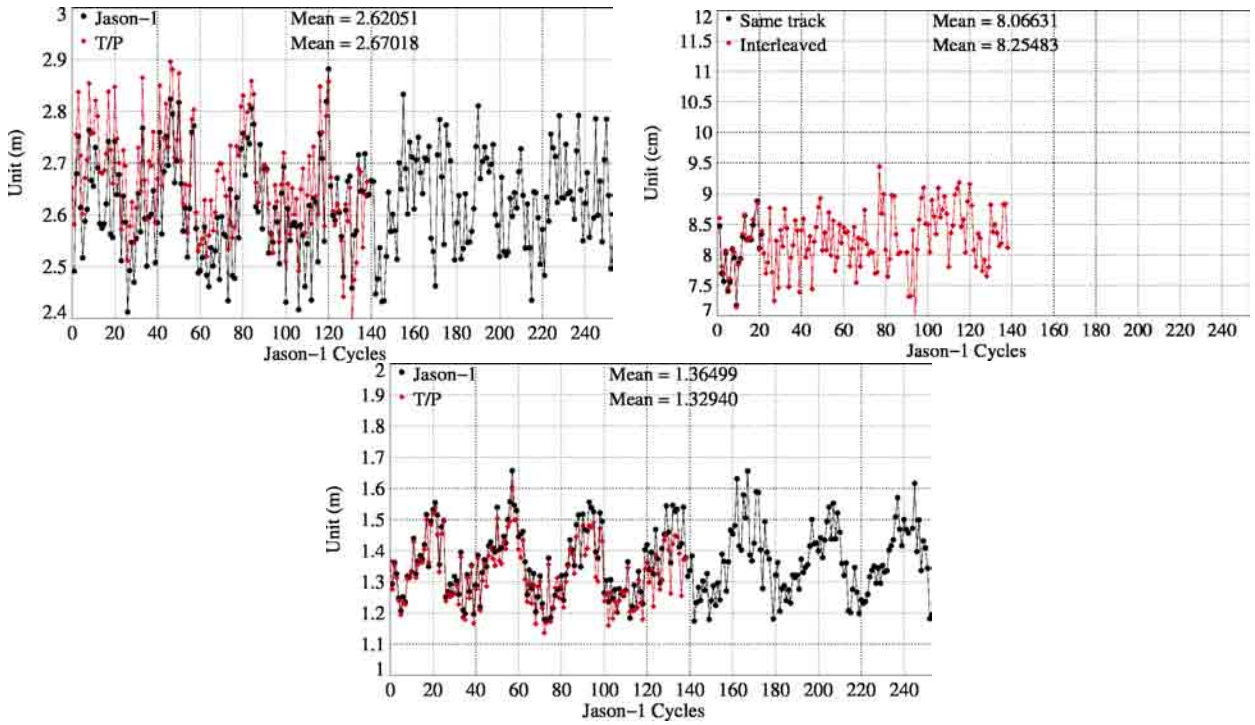

Figure 27: *Cycle per cycle mean (left), T/P−Jason mean differences (right), and standard deviation (bottom) of Ku-band SWH*

4.4.2. C-band SWH

Figure 28 shows global statistics of Jason-1 and T/P C-band SWH. The cycle per cycle mean of both missions shows a small annual signal (figure 28 top left). Jason-1 and T/P values are quite similar. After removing annual signal, Jason-1 data show a very small drift of 4.8 mm/yr. The (TOPEX - Jason-1) C-band SWH mean bias is about 10 cm (figure 28 top right). There is a drift of -4 mm/yr visible. Standard deviation of C-band SWH are quite similar on both missions showing an annual signal.

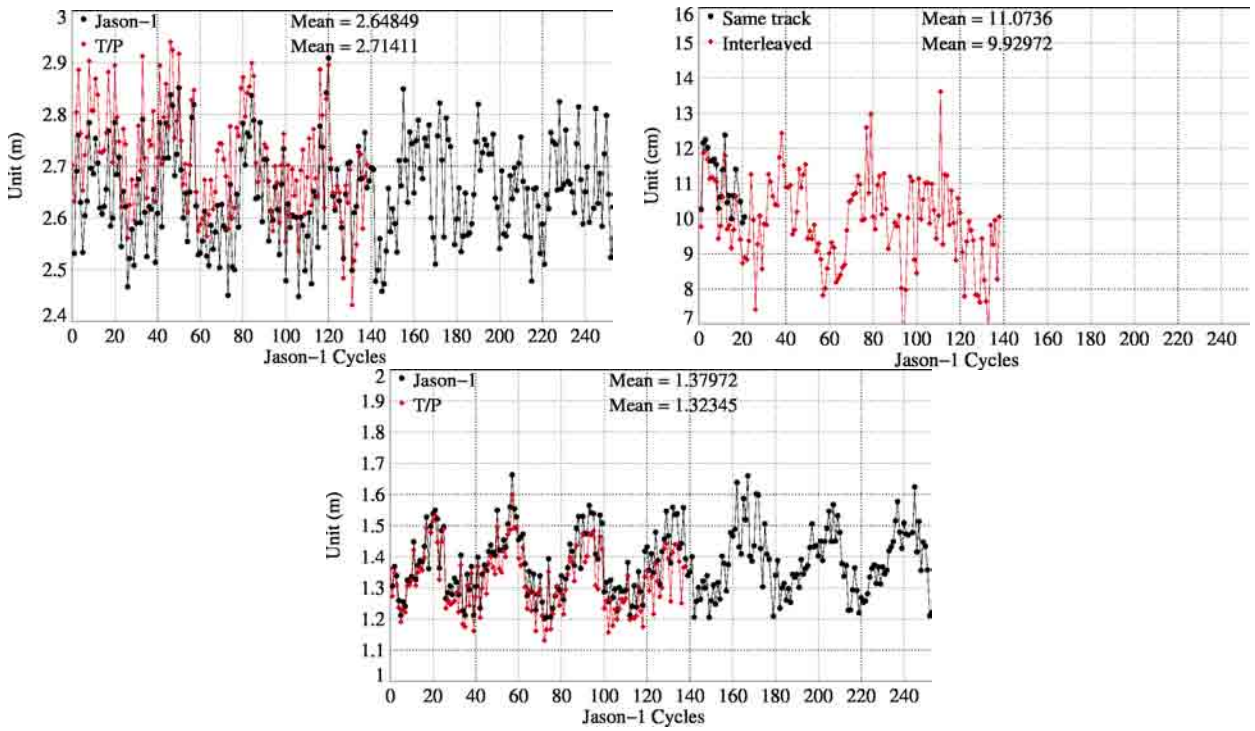

Figure 28: *Cycle per cycle mean (left), T/P−Jason mean differences (right), and standard deviation (bottom) of C-band SWH*

4.5. Backscatter coefficient

4.5.1. Ku-band Sigma0

The cycle per cycle mean (figure 29: top panel on the left) for Jason-1 (black curve) Ku-band sigma0 is coherent with the TOPEX mean (red curve). In order to compare both parameters and keep a significant dynamic scale, TOPEX Ku-Sigma0 is biased by a 2.26 dB value to align TOPEX with the Jason-1 uncalibrated Sigma0. The bias between the two corrections (figure 29: top panel on the right) is quite stable about -2.5 dB. A small trend close to -0.02 dB/yr has been detected for Jason-1 and was analyzed in the 2007 annual report.
Besides, the absolute bias is higher than usual from T/P cycle 433 to 437 (J1 cycles 90 to 94) by 0.1 dB : this is due to the TOPEX Sigma0. Indeed, the satellite attitude was impacted by a pitch wheel event linked to the T/P safe-hold mode occurred on cycle T/P 430 (see electronic communication : T/P Daily Status (26/07/2004)). This anomaly has probably biased the TOPEX sigma0 during this period. Jason-1 and T/P curves on bottom panel, showing the standard deviation differences, are very similar .

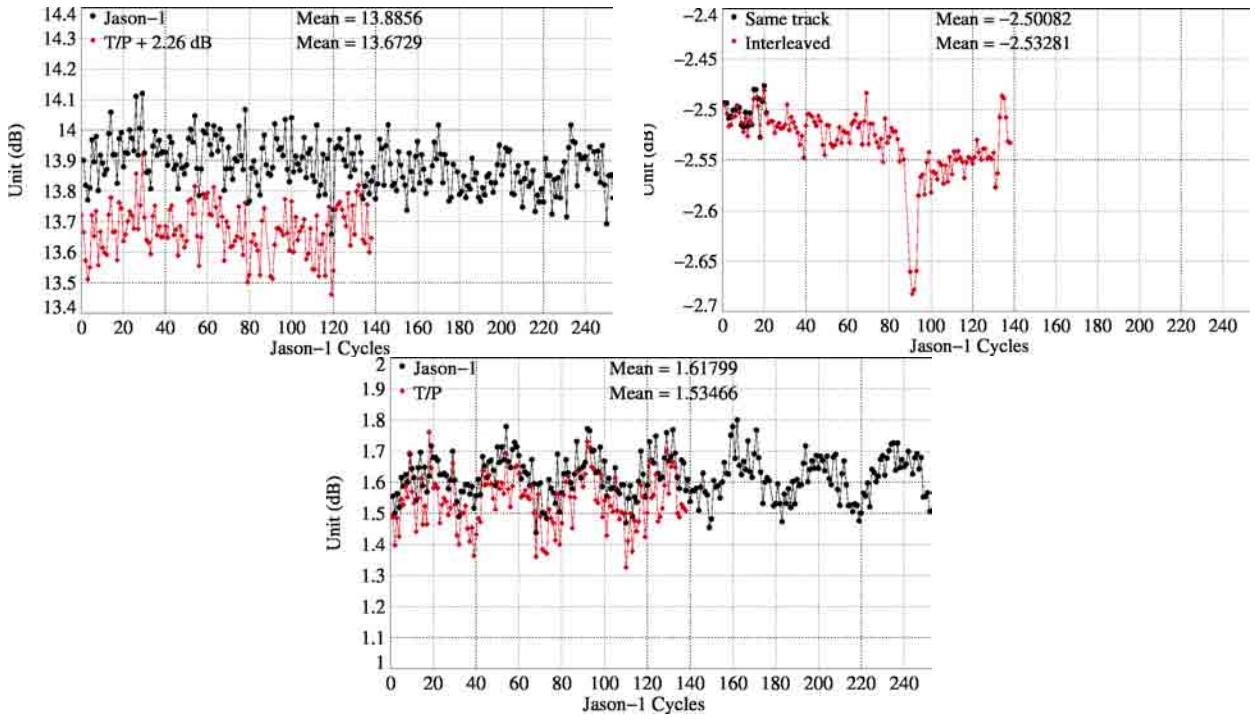

Figure 29: *Cycle per cycle mean (left), T/P−Jason mean differences (right), and standard deviation (bottom) of Ku-band SIGMA0*

4.5.2. C-band Sigma0

The cycle per cycle mean (figure 30: top panel on the left) for Jason-1 (black curve) Ku-band sigma0 is coherent with the TOPEX mean (red curve). The bias between the two corrections (figure 30: top panel on the right) decreases from -0.6 dB to -0.8 dB. This is due to the T/P C-band Sigma0 (Ablain et al. 2004 [3]).
Note that the Jason C-band Sigma0 is biased by a -0.26 dB value to align it on TOPEX in the science processing software. Standard deviation of C-band sigma0 (figure 30: bottom) has similar values for both missions and shows an annual signal.

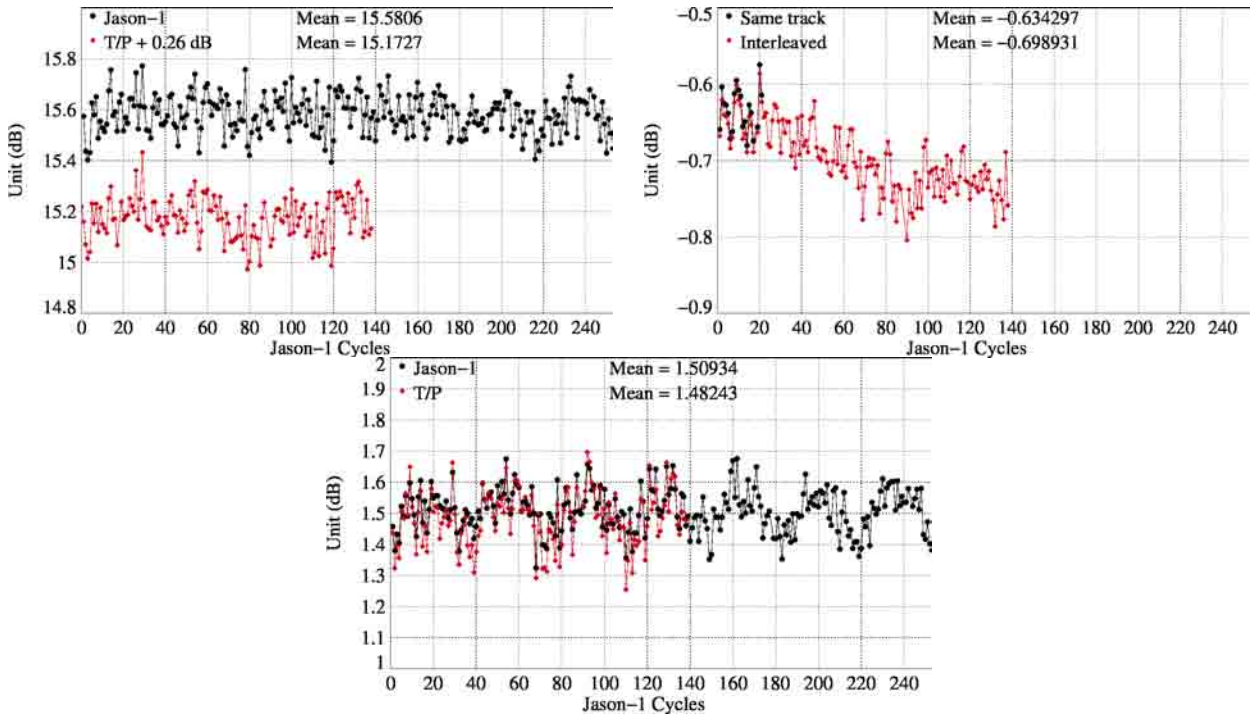

Figure 30: *Cycle per cycle mean (left), T/P−Jason mean differences (right), and standard deviation (bottom) of C-band SIGMA0*

4.6. Dual-frequency ionosphere correction

The dual frequency ionosphere corrections derived from the TOPEX and Jason-1 altimeters have been monitored and compared in the same way (figure 31). The mean difference between TOPEX and Jason-1 estimates is about 0 mm, with cycle to cycle variations lower than 2 mm. There is nevertheless a small visible drift of 0.3 mm/yr. Both corrections are very similar and vary according to the solar activity. Note that, as for TOPEX (Le Traon et al. 1994 [45]), it is recommended to filter the Jason-1 dual frequency ionosphere correction before using it as a SSH geophysical correction (Chambers et al. 2002 [14]). A low-pass filter has thus been used to remove the noise of the correction in all SSH results presented in the following sections.

Figure 32 shows differences between Jason-1 dual-frequency ionosphere correction and DORIS ionosphere correction. In fact, mean differences have been computed according to several local time intervals of 4 hours and afterwards averages for each year have been computed.
Differences between Jason-1 and DORIS ionosphere corrections are quite high (especially for local hours of 10 a.m. to 6 p.m., reaching 1.5 cm of difference) during the beginning of the Jason-1 mission. This is probably correlated with the higher solar activity in the beginning of the mission (during 2002). In the following, solar activity (and therefore difference between Jason-1 and DORIS ionosphere) decreases.

In version "c" product, the DORIS ionospheric correction is no longer available. It has been replaced by the GIM ionospheric correction (model), which displays better metrics than the DORIS' one.

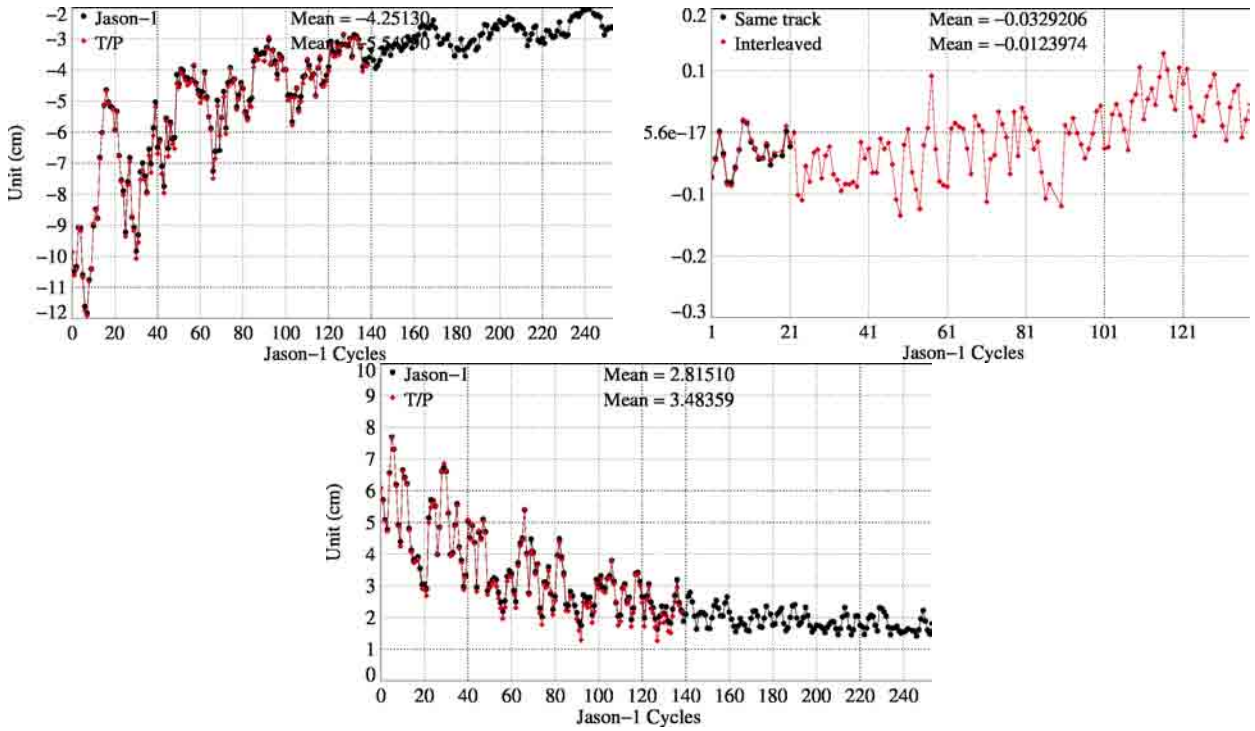

Figure 31: *Cycle per cycle mean (left), T/P−Jason mean differences (right), and standard deviation (bottom) of dual frequency ionosphere correction*

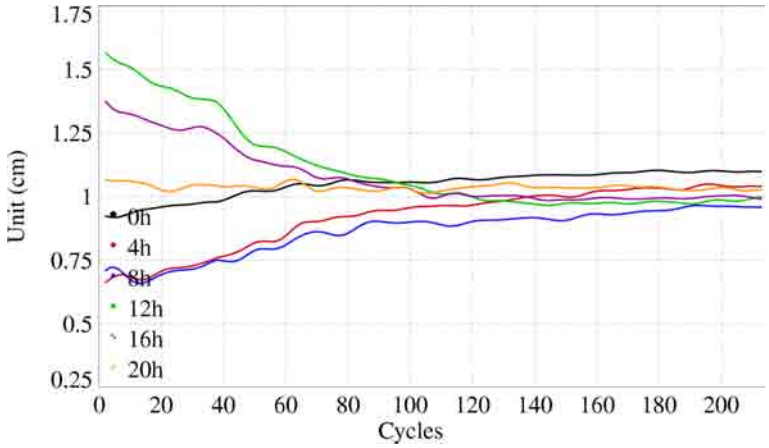

Figure 32: *Difference between DORIS and Jason-1 ionospheric correction in function of local time*

4.7. JMR Wet troposphere correction

4.7.1. Comparison with the ECMWF model

The JMR correction provided in the GDR "b" contains several anomalies, as reported in the 2007 Jason-1 annual report. These anomalies were brought out using a comparison with the ECMWF model (see http://www.ecmwf.int/products/data/operational_system/evolution/evolution_2008.html).

As in version "a", a drift from cycle 27 to cycle 32 due to instrumental changes (see Obligis et al.,2004 [51]) was visible, although it has been softened in version "b". In version "c", JMR has been recalibrated. The effect of this change is a bias about 3mm (see 7.2.3.). The ECMWF model is continually improved. This is visible on the standard deviation of wet troposphere correction difference (between radiometer and ECMWF model) which is shown on figure 33, right panel. At the beginning of 2003 standard deviation decreases from 1.7 cm to 1.4 cm. This corresponds to a model evolution. In the following, it continues to decrease.

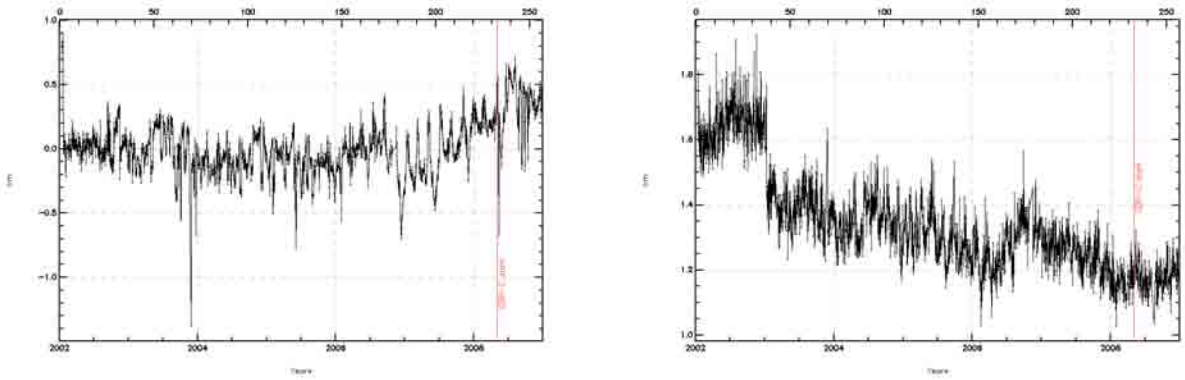

Figure 33: *Daily mean (left) and standard deviation (right) of radiometer and ECMWF model wet troposphere correction differences for Jason-1 using radiometer correction of GDR version "b" (before red line) and GDR version "c" (after red line).*

However, in 2007 and 2008, since two ECMWF model evolutions, the slope of the JMR-model differences tends to increase and an annual cycle has appeared. In [53], Picard suggest that the model evolutions do not render some features observed by radiometer (MWR, the ENVISAT radiometer, experiments the same patterns as JMR), and that there may be sensitivity issues on the 18 and 34 GHz channels.

4.7.2. Radiometer behavior after altimeter switch-off

In 2008, the altimeter was not working during two periods:

- During cycle 233, the Poseidon-2 altimeter was switched off, to ensure the satellite preservation during the Jason-1/Topex-Poseidon close encounter;

- Cycles 242 and 243 were partly or totally missing because of a safehold mode due to a problem on wheel 3.

These events have been followed by unusual behaviors of the radiometer correction relatively to the model correction. After the close encounter, the mean differences between JMR and ECMWF dropped, at the end of cycle 233 and beginning of cycle 234, then oscillated till reaching a value slightly lower than before the switch off (figure 34 left).

After the safehold mode (cycles 242-243), the difference between JMR and model started to oscillate, until it stabilized at cycle 250 (figure 34 right).

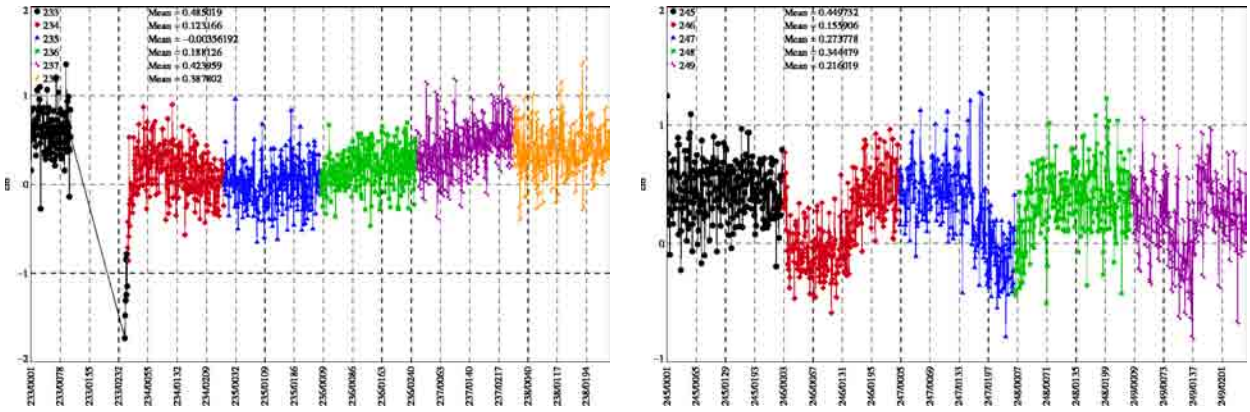

Figure 34: *Pass by pass mean of radiometer and ECMWF model wet troposphere correction differences for Jason-1 using radiometer correction of GDR version "c" (red): after J1/TP close encounter (left) and after safehold mode (right).*

5. Crossover analysis

Crossover differences are systematically analyzed to estimate data quality and the Sea Surface Height (SSH) performances. Furthermore, T/P crossover performances (as long as they were available) have been monitored in order to compare both performances. SSH crossover differences are computed on a one cycle basis, with a maximum time lag of 10 days, in order to reduce the impact of ocean variability which is a source of error in the performance estimation. The main SSH calculation for Jason-1 and T/P are defined below. For TOPEX, Jason-1 standards have been used for the tidal and atmospheric corrections.

$$SSH = Orbit - Altimeter\ Range - \sum_{i=1}^{n} Correction_i$$

with $Jason-1\ Orbit = POE\ CNES\ orbit$ and

$$\begin{aligned}
\sum_{i=1}^{n} Correction_i \;=\;& Dry\ troposphere\ correction : new\ S1\ and S2\ atmospheric\ tides\ applied \\
&+ Combined\ atmospheric\ correction :\ MOG2D\ and\ inverse\ barometer \\
&+ Radiometer\ wet\ troposphere\ correction \\
&+ Filtered\ dual\ frequency\ ionospheric\ correction \\
&+ Non\ parametric\ sea\ state\ bias\ correction \\
&+ Geocentric\ ocean\ tide\ height,\ GOT\ 2000 :\ S1\ atmospheric\ tide\ is\ applied \\
&+ Solid\ earth\ tide\ height \\
&+ Geocentric\ pole\ tide\ height
\end{aligned}$$

Note that for TOPEX data, a non-parametric sea state bias has been updated over TOPEX B period according to the collinear method (Gaspard et al., October 2002, [34]). For Poseidon-1 data, non-parametric SSB is not yet available.

5.1. Mean crossover differences

The mean of crossover differences represents the average of SSH differences between ascending and descending passes. It should not be significantly different from zero. More importantly, special care is given to the geographical homogeneity of the mean differences at crossovers. The map of the Jason-1 crossover differences averaged over the whole period of available GDR (cycle 1 to 253) has been plotted in figure 35 (on the left). It is quite homogeneous. Note that this map is partly computed with GDR version "c" (for cycle 233 to 253). A small bias between northern and southern hemisphere is observable. This is a result of an apparent altimeter datation bias, which related to Doppler velocity translates in the observed hemispheric bias ([6]). In GDR version "c" products, a new empirically correction, called pseudo_datation_bias_corr_ku is available, which will correct for this behaviour.

The cycle mean of Jason-1 and T/P SSH crossover differences is plotted for the whole Jason-1 period in figure 35 (right). Slightly larger variations are observed for Jason-1 than for TOPEX in the first cycles. However, some correlation between the two curves can be deduced from this figure. That shows that consistent signals impact the two systems.

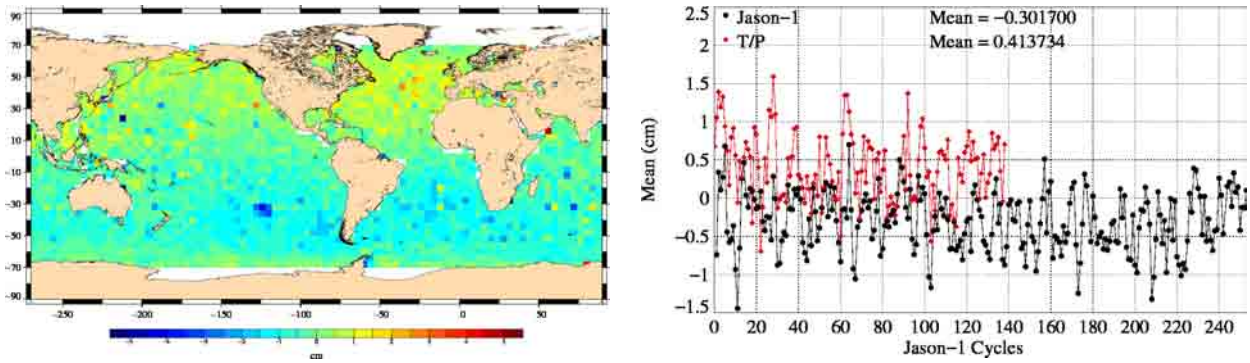

Figure 35: *Map of mean crossovers for Jason cycle 1 to 253(GDR version "b" until cycle 232, then version "c", left) and cycle per cycle mean crossovers (right)*

When separating the GDR version "b" part (cycles 1-232) from version "c" part (233-253), it is worth noting that the north/south inconsistency can no longer be seen (figure 36). The mean differences at crossovers, however, do not seem more geographically consistent. With only 21 cycles in version "c" (figure 36, right), it is hard to predict if a geographical pattern will emerge, and the average map will be more significant when more cycles are available.

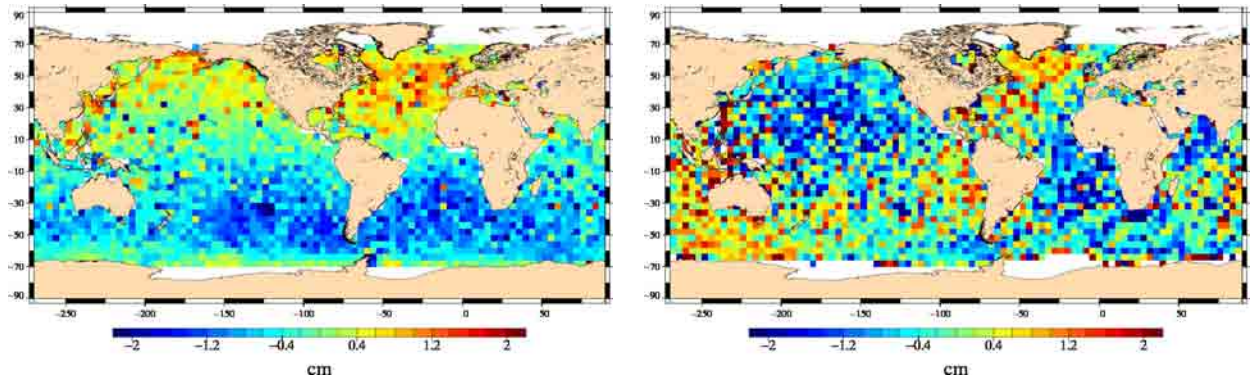

Figure 36: *Map of mean crossovers for Jason cycle 1 to 232 (GDR version "b", left) and 233 to 253 (version "c", right)*

5.2. Standard deviation of crossover differences

The cycle per cycle standard deviation of crossover differences are plotted in figure 37 (on the left) according to different crossover selections. 3 selections are applied:

- Black curve: no selection is applied. The mean value is 6.47 cm. It shows an annual signal linked to the sea ice variations in the Northern Hemisphere.
- Red curve: shallow waters have been removed (bathy$\leq -1000m$). The previous annual signal has been removed by this selection even though a signal probably due to seasonal ocean variations remains.
- Blue curve: the last selection allows monitoring the Jason-1 system performance. Indeed, areas with shallow waters (1000 m), of high ocean variability ($\geq 20cm$) and of high latitudes ($\geq abs(50)$ degrees) have been removed. The standard deviation then provides reliable estimates of the altimeter system performances. In that case, no trend is observed in the standard deviation of Jason-1 SSH crossovers: good performances are obtained, with a standard deviation value of about 5.2 cm all along the mission.

The map of standard deviation of crossover differences overall the Jason-1 period, in figure 37 (on the right) shows usual results with high variability areas linked to ocean variability.

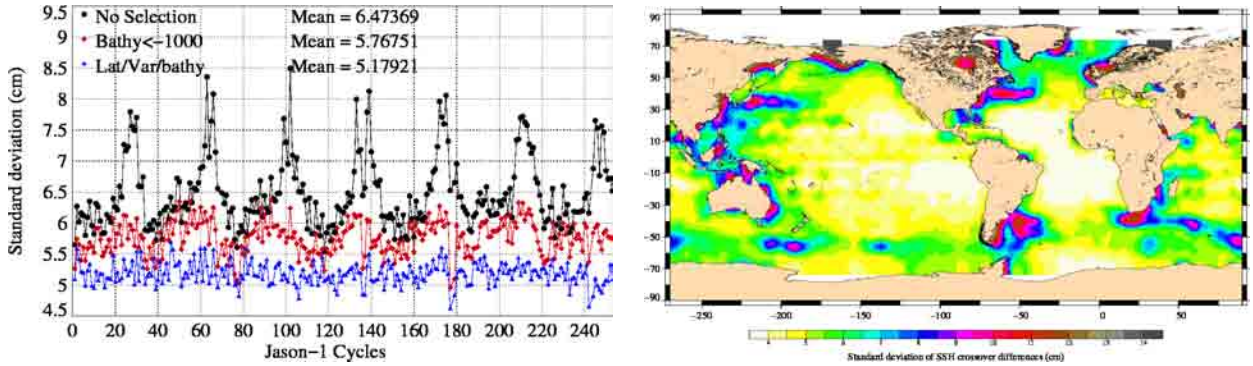

Figure 37: *Cycle per cycle standard deviation crossovers with different selections and map of Jason-1 standard deviation crossovers*

6. Along-track analysis

This analysis is used to compute Sea Level Anomalies (SLA) variability and thus to estimate data quality; it is used to determine the SSH bias between Jason-1 and T/P and the trend in the Mean Sea Level (MSL).

6.1. Along-track performances

6.1.1. Along-track performances on sea level anomaly

Along track analyzes are also used to assess the altimeter system performances, by computing Sea Level Anomalies (SLA). The SLA variance gives an estimate of the errors of the system, even though the ocean variability fully contributes in this case. A comparison between Jason-1 and T/P has been performed computing the variance of SLA relative to the CLS01 MSS. This allows global and direct calculations.
The SLA standard deviation is plotted in figure 38 for Jason-1 (GDRs version "b" from cycles 1 to 232, "c" from cycle 233 onward) and T/P. It exhibits similar and good performances for both satellites. However, during the verification phase, the variability is slightly higher for Jason-1 but from cycle 26 onward the performances are very similar. A significant signal is observed from cycle 25 to 35. It is due to the 2002-2003 "El Niño" (McPhaden, 2003, [54]). The SLA rise at the end of the series is also remarkable. It may be due to the 2007-2008 "La Niña" episode. A short investigation is presented in the following section.

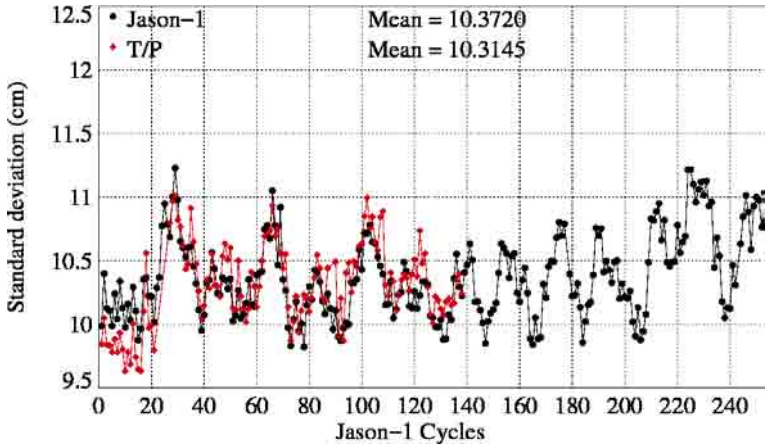

Figure 38: *Cycle per cycle SLA standard deviation*

6.1.2. SLA rise during ENSO events

The El Niño-Southern Oscillation (ENSO) consists of alternative warm and cold anomalies in the tropical Pacific, which has dramatic impacts on global climate and ocean circulation. Two ENSO events occurred during the Jason-1 data availability: a warm event (El Niño) in 2002-2003

and a cold event (La Niña), beginning at the end of 2007 and persisting till mid 2008. Figure 39 shows the SLA standard deviation for Jason-1 from cycle 1 to 253, with selections on bathymetry, latitude and oceanic variability, for the North, South and tropical Pacific. The 2002-2003 event mainly impacted the North Pacific. On the contrary, the latest La Niña event makes the SLA standard deviation increase rapidly. The Pacific is the only contributor to the rise of global SLA standard deviation in 2007-2008 in the tropical area. Similar results were found using ENVISAT and GFO data, confirming the climatic feature, and not an anomaly of Jason-1 data.

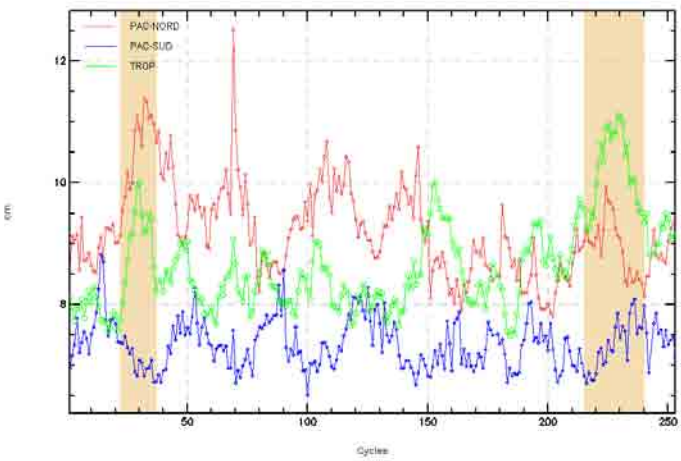

Figure 39: *Cycle per cycle SLA standard deviation with selections (abs(Latitude)* ≤ 50*, Bathy* $\leq -1000m$*, oceanic variability* $\leq 20cm$*)*

6.2. Jason-1 Mean sea level

6.2.1. Sea surface height estimation

Estimation of the mean sea level trend is important for climate change studies. MSL estimation from Jason-1 and T/P are plotted in figure 40 (on the left), after reduction of the relative bias between the two time series.
Several error sources can influence MSL evolution, one of them is the choice of wet troposphere correction. On the one hand ECMWF model wet troposphere correction might be influenced by model evolutions, on the other hand radiometer wet troposphere correction is influenced by yaw mode transitions or thermal instabilities after altimeter switch-off (see section 4.7.1.). Therefore MSL calculated with radiometer correction (black curve) and with model correction (blue curve) are shown in figure 40. Note that a 1 cm shift has been introduced in order to distinguish the two curves. The results are obtained after area weighting (Dorandeu and Le Traon 1999 [22]). The figure shows good agreement between the two missions and demonstrates that the Jason-1 mission ensures continuous precise MSL monitoring as it was done for more than a decade by the T/P mission. On both missions, seasonal signals are observed, because the inverse barometer correction has been applied in the SSH computation (Dorandeu and Le Traon 1999 [22]). Moreover, 60-day signals are also detected on Jason-1 and T/P series, with nearly the same amplitude. A source of error could be from the largest tidal constituents at twice-daily periods which alias at periods close to 60 days for Jason-1 and T/P (Marshall et al. 1995 [48]). Orbit errors in T/P altimeter series used to compute the tide solutions could also have contaminated these models (Luthcke et al. 2003 [47]). Using JMR or model wet troposphere correction has only a slight impact on the slope of about 0.1 mm/year.

On figure 40 (right panel), annual, semi-annual, and 60-days signals have been adjusted. This allows to decrease the adjustment formal error for both satellites. The global MSL slope is lower for Jason-1 (2.44 mm/yr) than for T/P (2.67 mm/yr), but for Jason-1, the shown time period is more than two years longer than for T/P. Also, the MSL slope of Jason-1 shows a flattening at the end of 2006 and during 2007 (between cycles 183 and 219). Calibration with In-situ data (see section 8.5.1. and more detailed in annual reports [74] and [75]) shows no drift of altimetric MSL. Therefore this flattening might be due to "La Niña" active during this period.

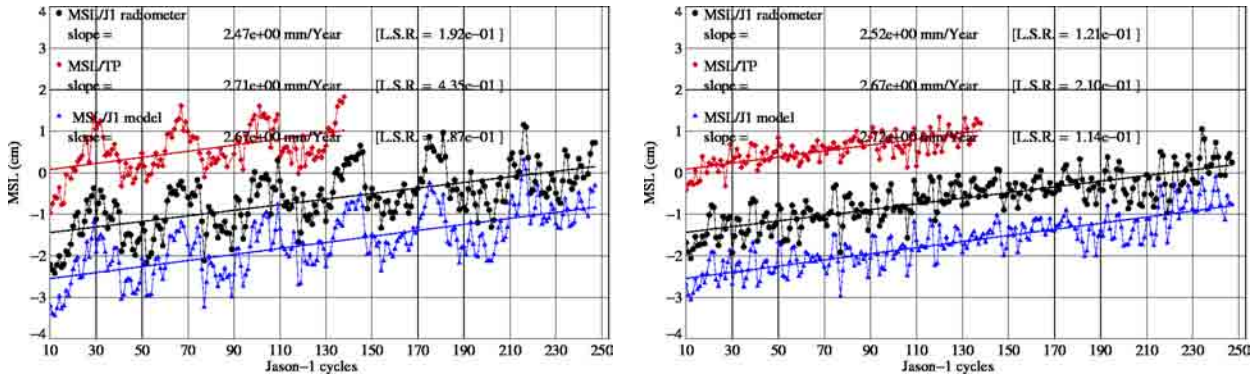

Figure 40: *Jason-1 and T/P mean sea level (on the left) with annual, semi-annual and 60-days adjustment (on the right)*

The shown MSL trends were computed using as well ascending and descending passes, but when computing Jason-1 MSL slope separately for ascending and descending passes, differences are noticed. Figure 41 shows SLA slopes using Jason-1 GDRs (with ECMWF model wet troposphere correction) and T/P MGDRs.
Jason-1 SLA slopes are quite different:

- 2.37 mm/yr using descending passes
- 2.99 mm/yr using ascending passes

This represents a difference of 0.62 mm/yr. For Envisat data, difference of SLA slope between ascending and descending passes is even greater as stated in [31] and the Envisat 2008 report, reaching a 2.26mm/yr slope difference between odd and even tracks. SLA slopes using T/P data are far more homogeneous when separating ascending and descending passes.

- 3.26 mm/yr using descending passes
- 3.11 mm/yr using ascending passes

There is no explanation up to now, for this behavior of Jason-1 data. Since ascending and descending passes cover the same geographical regions, there is no reason why SLA slope should rise differently. A study using several orbit solutions showed, that use of different orbits has an impact on difference of SLA slope noticed between ascending and descending passes. Nevertheless the difference between SLA using ascending or descending passes, is especially visible for 2007. The latest GSFC orbit has been made available and investigation will be led in 2009 to check if this feature is visible with other orbits.

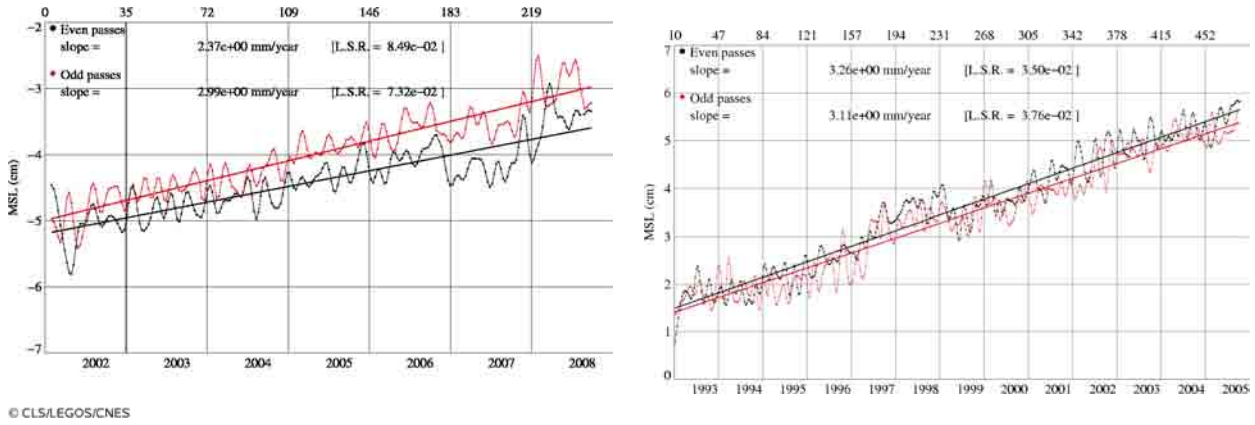

Figure 41: *J1 (left) and T/P (right) SLA slopes using only ascending (odd) or descending (even) passes.*

6.2.2. SSH bias between Jason-1 and T/P

6.2.2.1. Temporal evolution of SSH bias between Jason-1 and T/P

The ECMWF wet troposphere correction is also used in figure 42 which represents the temporal evolution of the SSH bias between T/P and Jason-1. This prevents from errors due to radiometer biases, as the model correction is the same for the two missions. The impact of all geophysical corrections and the particular effect of the SSB correction are also displayed in the figure. Among all geophysical corrections, the greater impact on the T/P to Jason-1 SSH bias estimation is produced by the SSB correction, since results differ by more than 1 cm when applying or not this correction. This is already a great improvement, since difference was 6 cm when using Jason-1 GDRs version "a". Notice that present results have been obtained using a dedicated TOPEX Side B SSB estimation (S. Labroue et al. 2002), since TOPEX side A and side B SSB models are different (e.g. Chambers et al. 2003). Apart from higher variability for Jason-1 cycle 18 (Poseidon-1 was switched on for T/P cycle 361), the T/P to Jason-1 SSH bias nearly remains constant through the Jason-1 mission period.

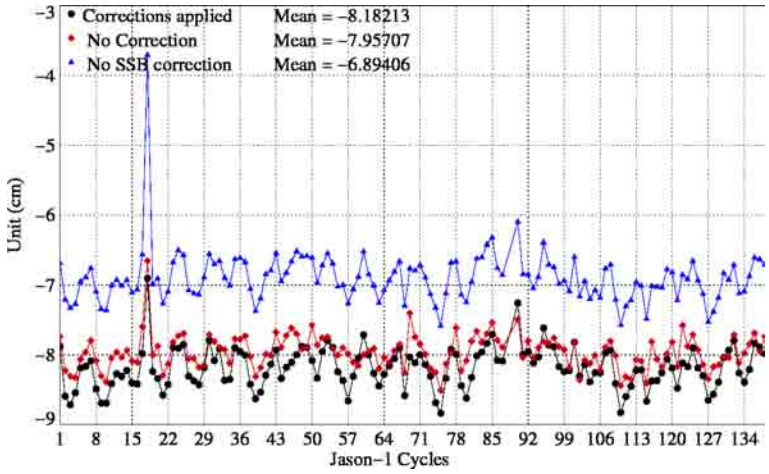

Figure 42: *Cycle per cycle mean of (T/P−Jason-1) SSH differences*

6.2.2.2. Spatial distribution of SSH bias between Jason-1 and T/P

Jason-1 and T/P have not been on the same track from cycle 21 onward. Consequently, the SSH differences can not be obtained directly as a result of the ocean variability. Thus, the map of the SSH differences between Jason-1 and T/P is obtained at the Jason-T/P crossovers in figure 43. The figure was generated using Jason-1 GDR version "b" (cycle 1 to 138) with an orbit based on EIGEN-CG03C gravity field, whereas T/P still contains an orbit based on JGM3 gravity field. Large structures of negative and positive differences up to an amplitude of 2 cm are visible. These are due to residual orbit errors on T/P mission.
These large differences are also visible, when looking on the verification phase of Jason-1 (cycles 1 to 21) (figure 44, left panel). Both satellites (T/P and Jason-1) were on the same ground track, which makes direct measurement comparison possible. For OSTST meetings in 2006 and 2007 retracked TOPEX cycles of the Jason-1 verification phase were already available. They contained also on orbit based on GRACE gravity model. This reduces the differences, as visible on figure 44 (right panel). The data of both missions are much more homogeneous, when looking at global maps. Indeed, when separating ascending and descending passes during computing T/P - Jason-1 SLA differences, large hemispheric biases appear (see figure 45).

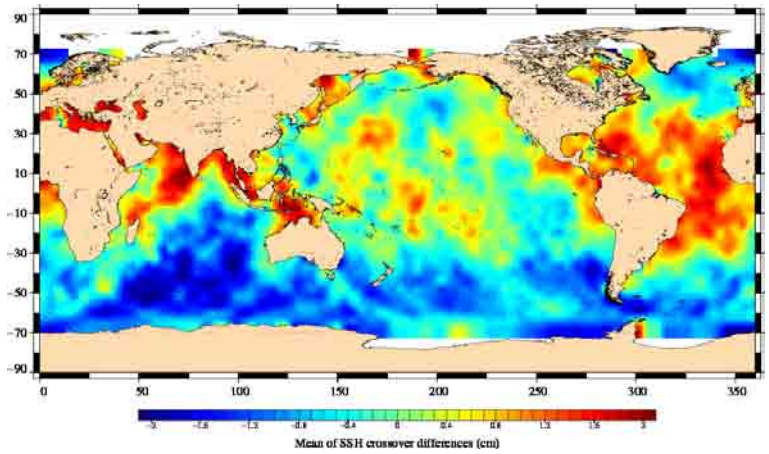

Figure 43: *Map of (T/P−Jason-1) SSH differences for Jason-1 GDR version "b" period.*

Finally new SSB corrections have been computed on cycles 1-21 for TOPEX using RGDR, with the collinear method. For J1 the Venice SSB was used ([42]). These new TOPEX and J1 SSB models are now much closer than before. When applying them in the SLA calculation in addition to the new orbits and the new ranges (Figure 46), the discrepancies between J1 and T/P are reduced. However, an East/West patch (< 1cm) remains, but it is not correlated with SWH. The origin of this signal is explained by CNES and GSFC orbit, used respectively for J1 and TOPEX. Indeed, using GSFC orbit for Jason-1 similar to those used in RGDR TOPEX data, allows to remove this East/West signal (see [5]).

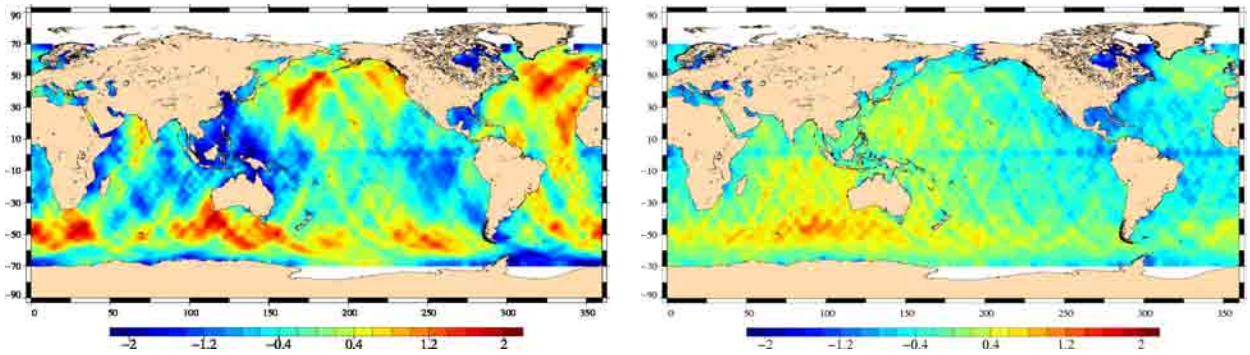

Figure 44: *Map of (T/P−Jason-1) SSH differences for Jason-1 cycles 1 - 21, using orbit of MGDR (left) and GSFC orbit based on GRACE gravity model (right) for T/P.*

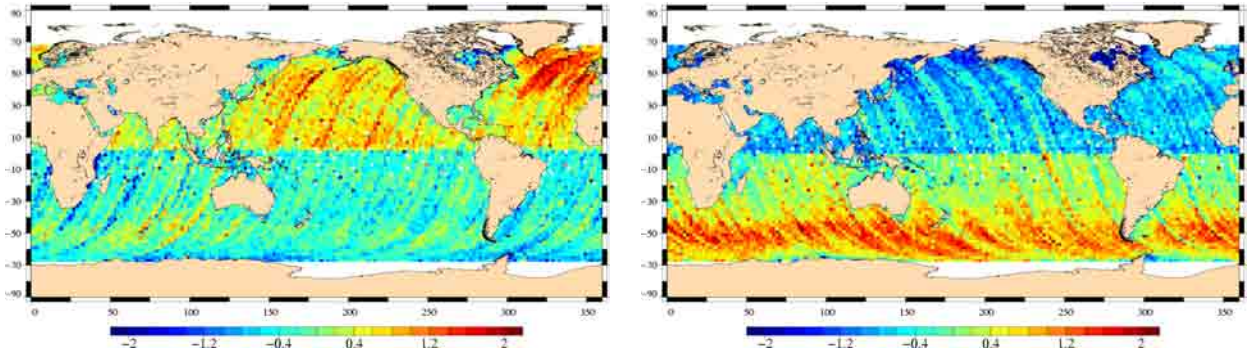

Figure 45: *Map of (T/P−Jason-1) SSH differences separating ascending and descending passes for cycles 1 - 21, using orbit based on GRACE gravity model for T/P.*

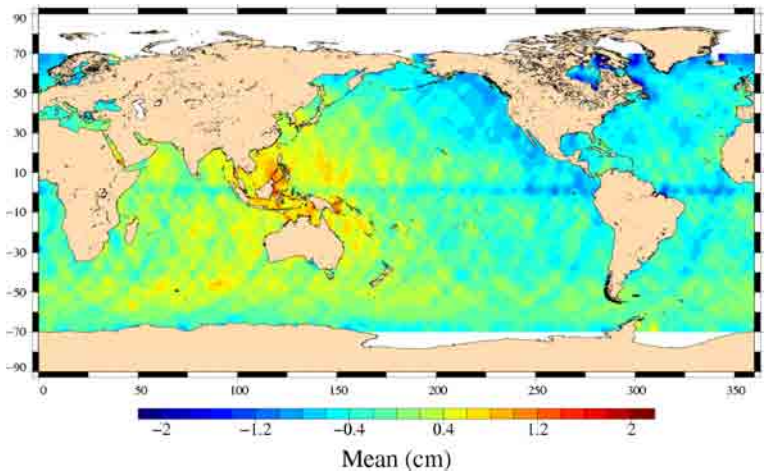

Figure 46: *Map of (T/P−Jason-1) SSH differences for Jason-1 cycles 1 - 21, using GSFC orbit based on GRACE gravity model for T/P, as well as recomputed Sea State Bias.*

6.2.2.3. Hemispheric SSH bias between Jason-1 and T/P

In order to further investigate hemispheric (T/P−Jason-1) SSH biases, its temporal evolution is presented in figure 47. It shows hemispheric differences between T/P and Jason-1, when separating northern and southern hemisphere. From the northern hemisphere to the southern hemisphere the (T/P−Jason-1) SSH bias estimates can thus differ by up to 2 cm. These hemispheric differences seem consistent from one cycle to another. These differences are mainly due to the orbit. The use of GDRs version "b" has already considerably lowered the difference between northern and southern hemisphere during cycles 50 to 70. Using orbits with ITRF 2005 reference system for both Jason-1 and T/P will probably further reduce these hemispheric differences.

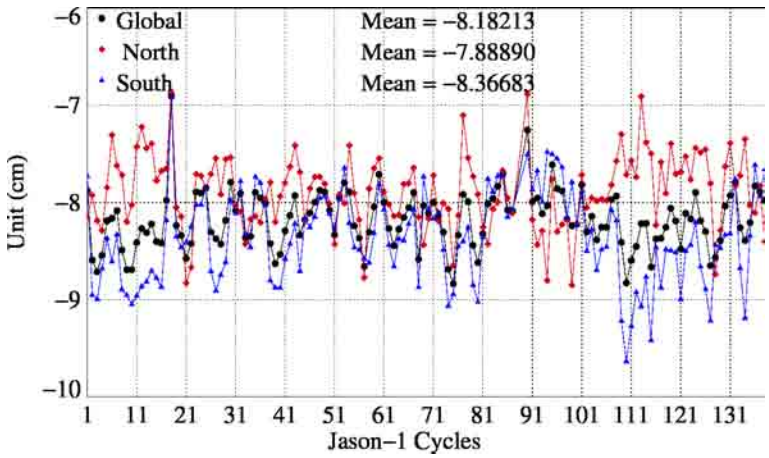

Figure 47: *Cycle per cycle mean of (T/P−Jason-1) SSH differences by hemisphere*

6.3. Sea level seasonal variations

From Sea Level Anomalies computed relative to the Mean Sea Surface CLS 2001 (Hernandez et al, 2001), the surface topography seasonal variations have been mapped from figure 48 to 54 for the overall Jason-1 data set. Major oceanic signals are showed clearly by these maps: it allow us to assess the data quality for oceanographic applications. The most important changes are observed in the equatorial band with the development of an El Niño in 2002-2003. The event peaked in the fourth quarter of 2002, and declined early in 2003. Conditions indicate an event of moderate intensity that is significantly weaker than the strong 1997-1998 El Niño (McPhaden,2003, [54]). End of 2007, a La Niña event is visible in Eastern Pacific on figure 53. It lasted till the mid 2008 (see [73]).

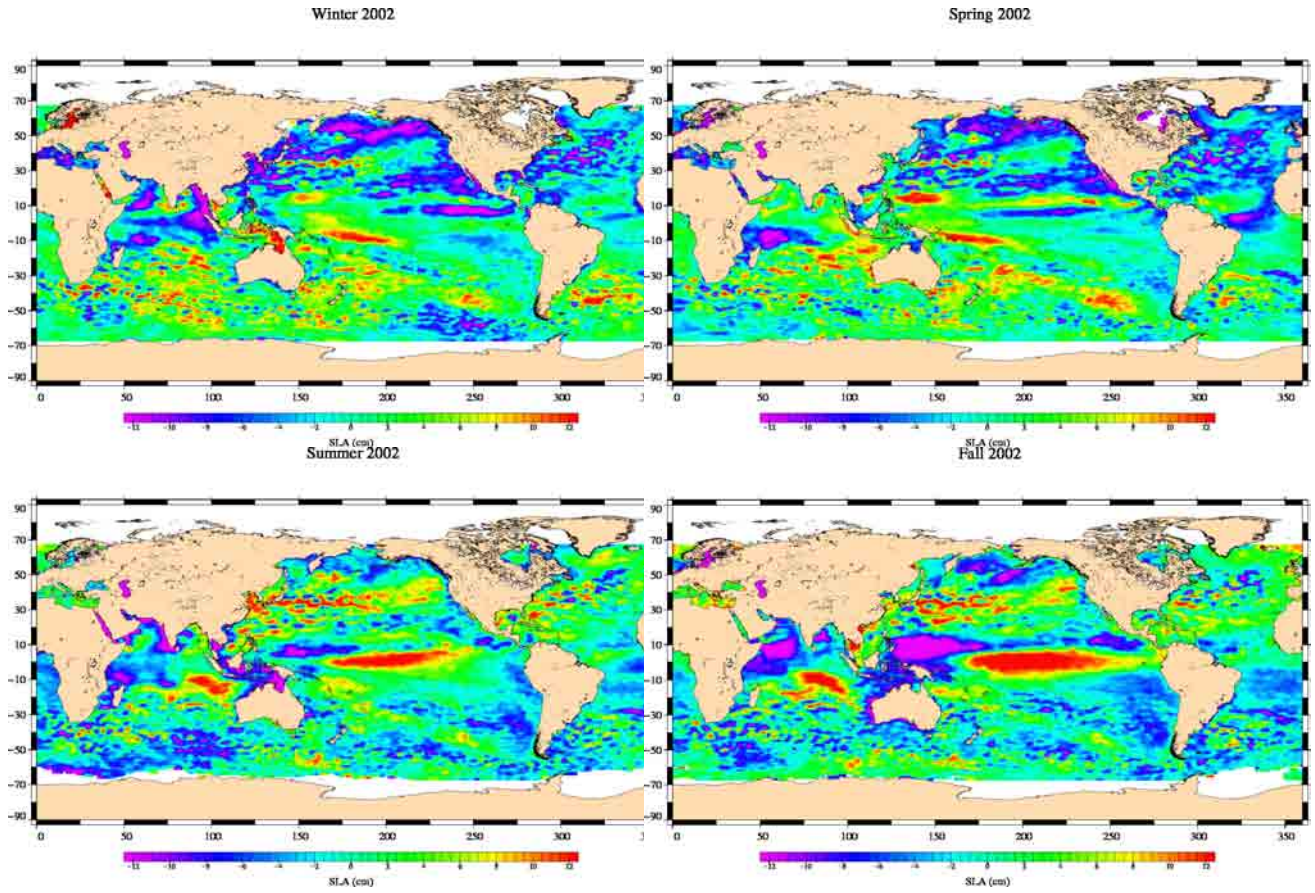

Figure 48: *Seasonal variations of Jason SLA (cm) for year 2002 relative to a MSS CLS 2001*

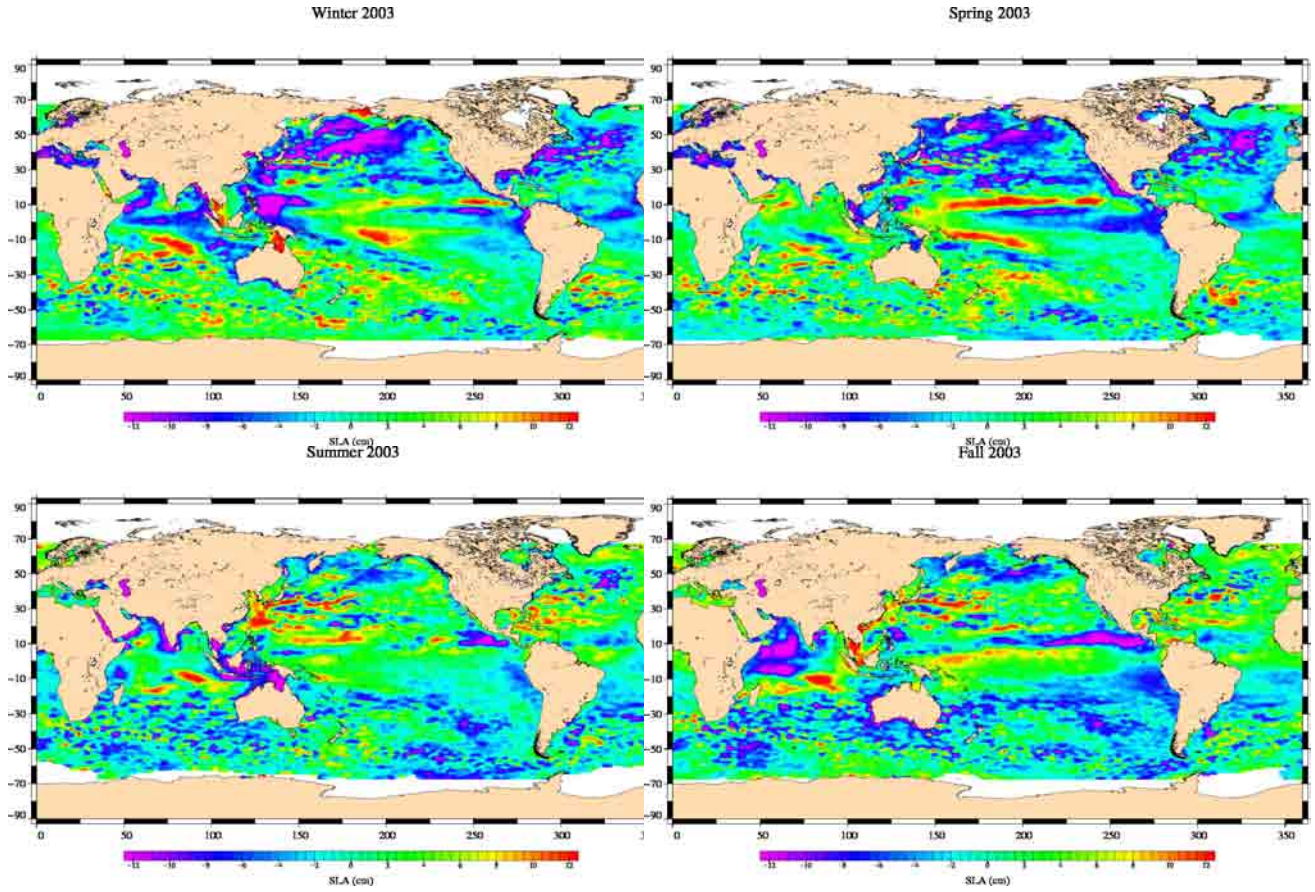

Figure 49: *Seasonal variations of Jason SLA (cm) for year 2003 relative to a MSS CLS 2001*

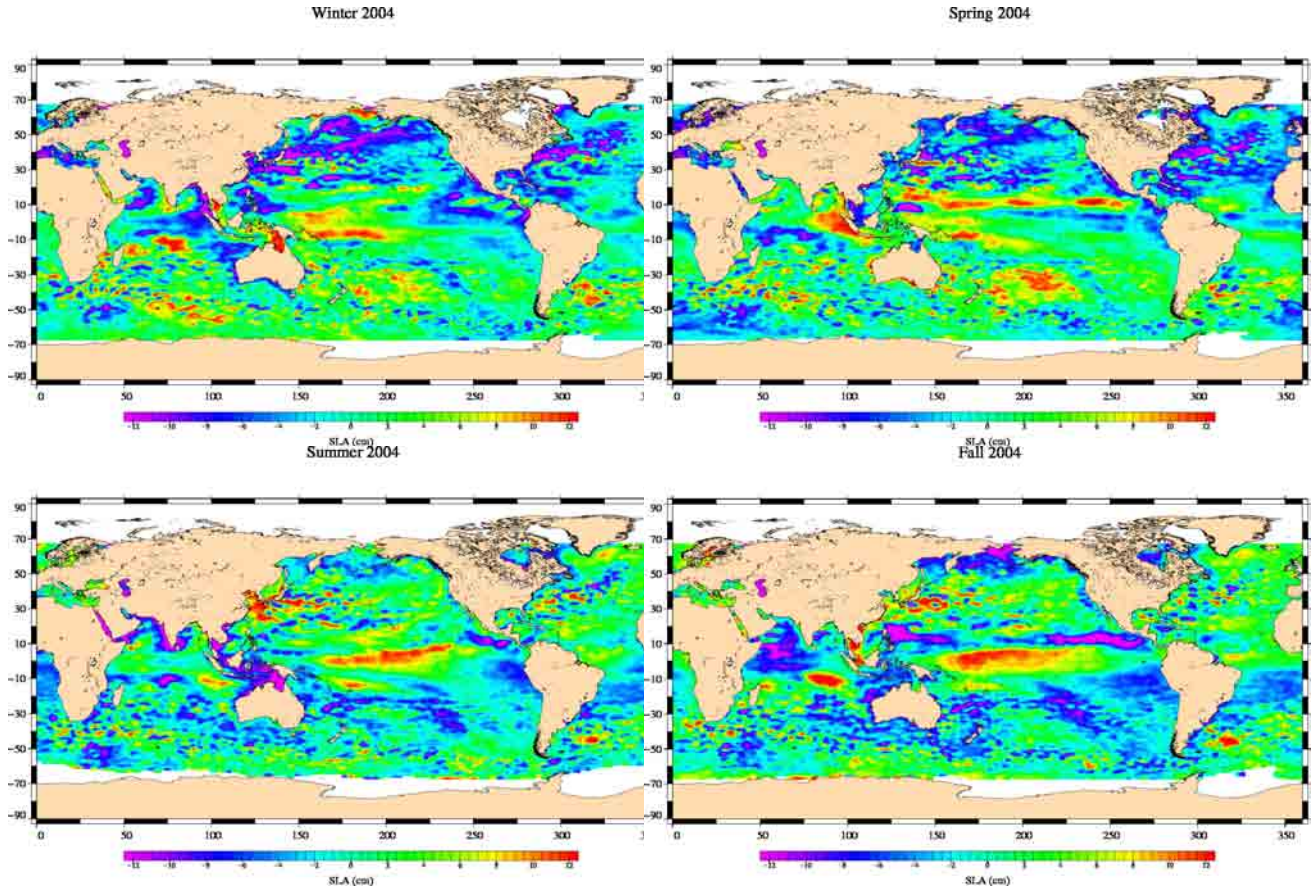

Figure 50: *Seasonal variations of Jason SLA (cm) for year 2004 relative to a MSS CLS 2001*

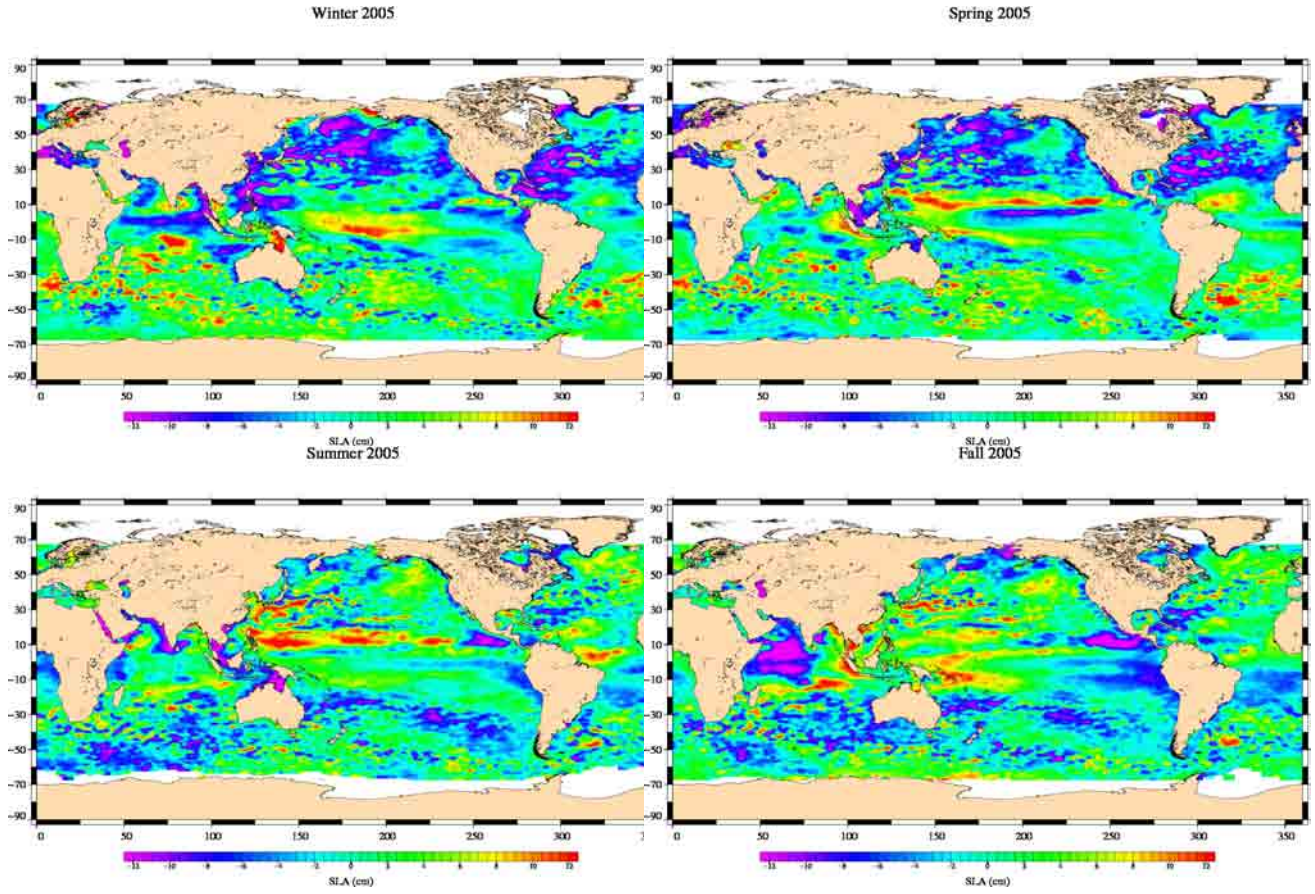

Figure 51: *Seasonal variations of Jason SLA (cm) for year 2005 relative to a MSS CLS 2001*

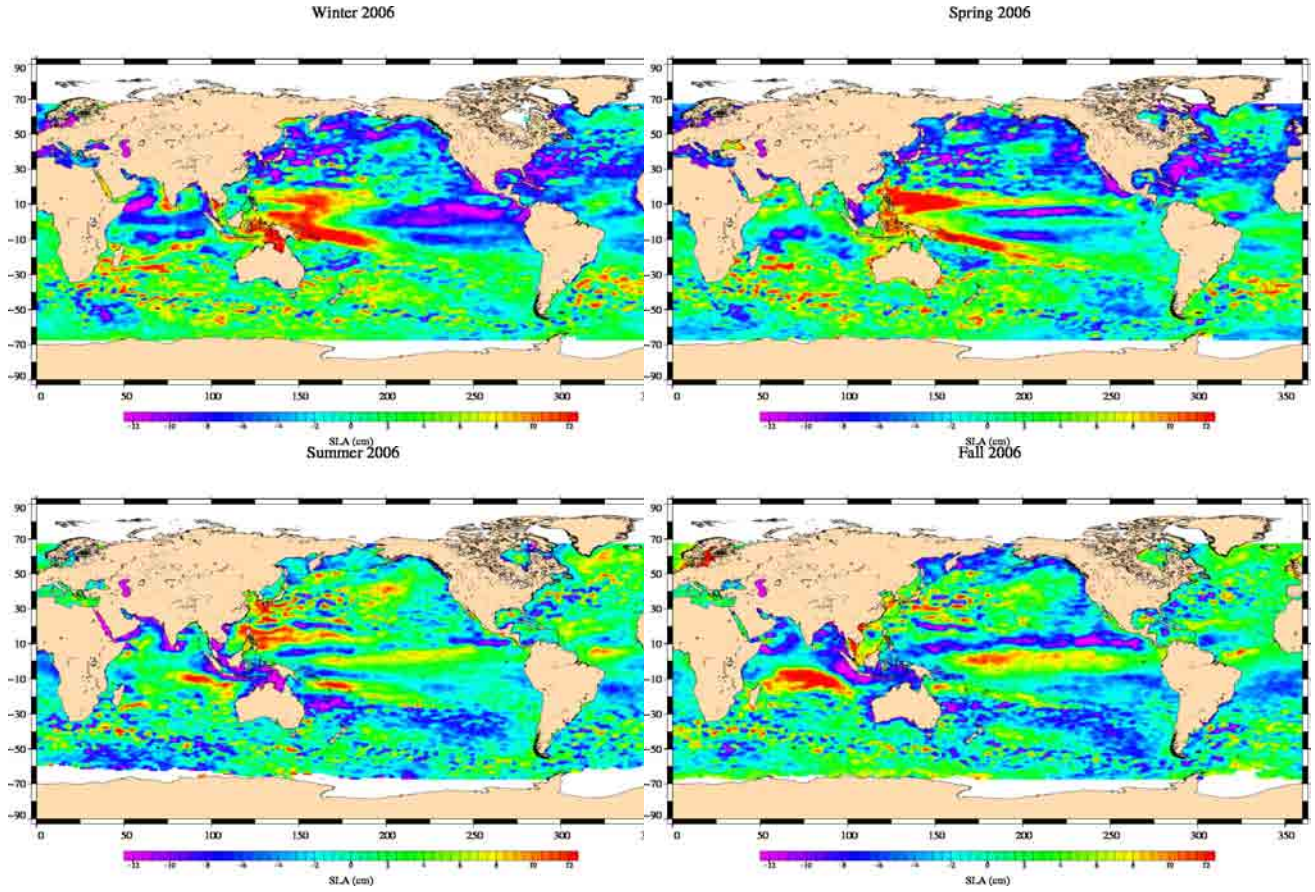

Figure 52: *Seasonal variations of Jason SLA (cm) for year 2006 relative to a MSS CLS 2001*

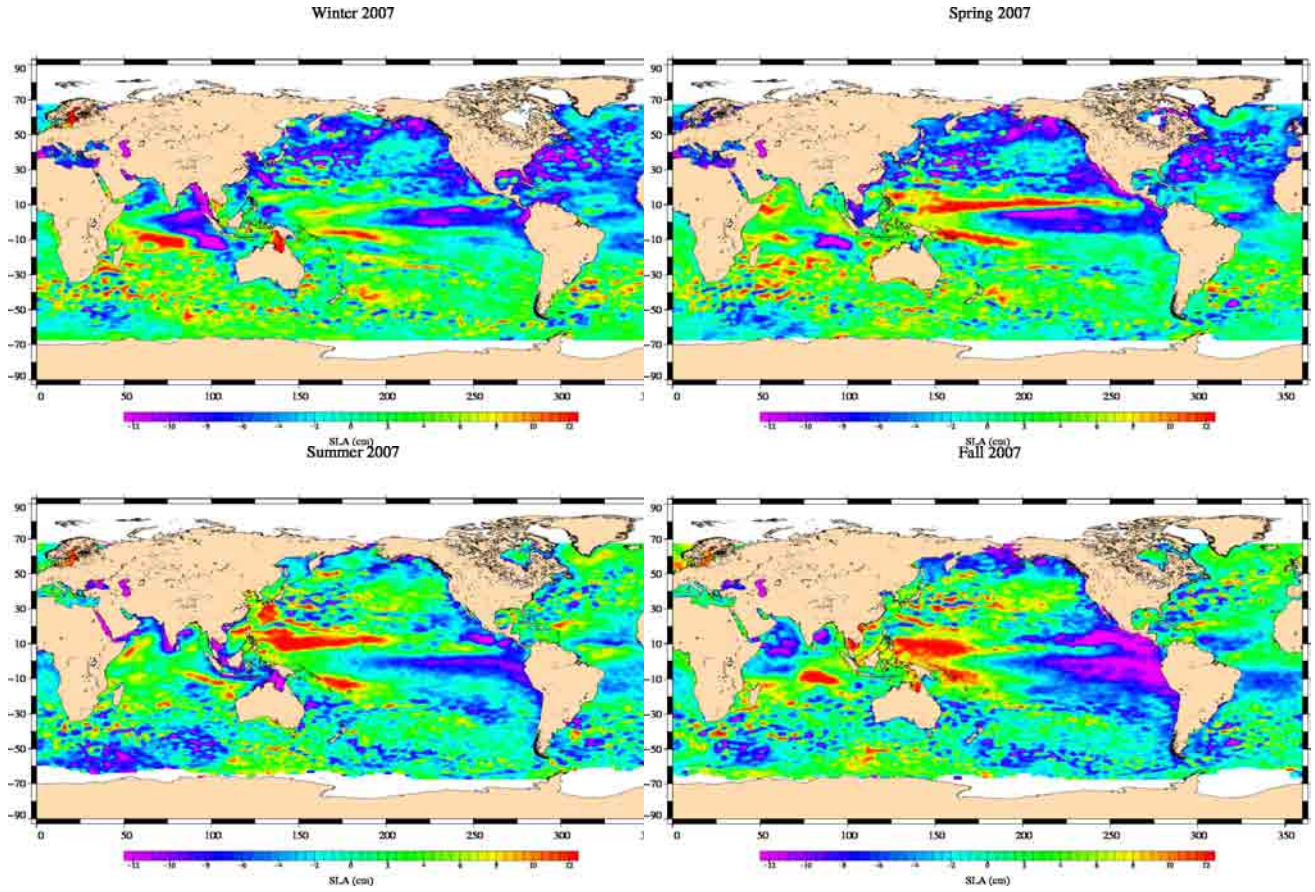

Figure 53: *Seasonal variations of Jason SLA (cm) for year 2007 relative to a MSS CLS 2001*

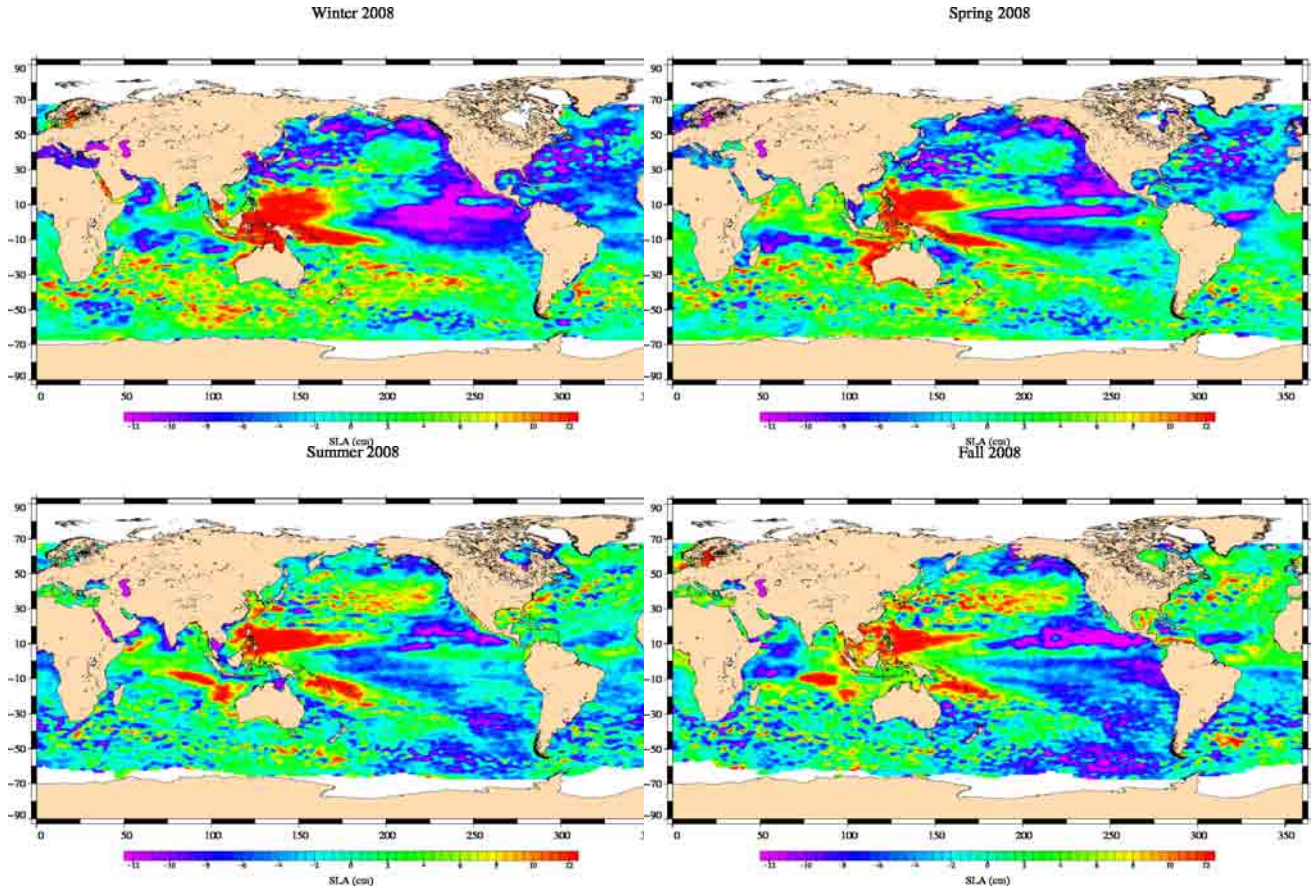

Figure 54: *Seasonal variations of Jason SLA (cm) for year 2008 relative to a MSS CLS 2001*

7. Impact of Reprocessing of Jason-1 data

7.1. Introduction

As described earlier in this report (see section 2.3.), Jason-1 GDRs reprocessing in version "c" has started. Analyzes were conducted on the reprocessed period, from cycle 194 to 232. More cycles have been reprocessed from cycle 151 to 193, as well as cycles 11 and 14 to 16, but regarding the many holes in the series, the period 194-232 is used in the framework of this report. This corresponds to the work presented during the latest OSTST meeting in Nice, France, 9 to 12th November 2008.

The poster is reproduced as Figures 76.

7.2. Reprocessing of Jason-1 data

7.2.1. New features of version "c" and reprocessing status

The main change is the new orbit which uses a new gravity model, new reference frame (ITRF2005 vs ITRF2000 for version b). New correction tables provide better altimetric parameters. The JMR has been recalibrated. Version "c" also provides a new sea state bias, similar to the one presented during the 2006 OSTST in Venice. By then, it had been calculated over a 21 cycles of GDRs version "b", and for version "c", it has been recomputed over 3 years of GDR "b". The dynamical atmospheric correction (DAC) is provided in high-resolution. A pseudo time-tag bias correction is proposed.

Cycles 193 to 227, most cycles between cycles 151 and 193, and cycles 11, 14 to 16, were reprocessed in GDR version "c" by JPL. Cycles 228 to 232 were reprocessed by CNES. The data were processed by Cal/Val by a dedicated processing chain to detect missing and bad measurements (see section 3.2.1.).

After validation of reprocessed data (GDR "c"), valid data of GDR "b" and "c" were compared cycle per cycle for each altimetric parameter, as well as SLA.

Contrary to the first reprocessing, from version "a" to "b", there is no major difference between versions "b" and "c" in terms of quantity of measurements. In the first reprocessing, ground processes were corrected, which allowed to recover many missing passes or portions of passes, and the introduction of the MLE4 retracking algorithm enabled to process waveform that could not be analyzed by MLE3 during high mispointing occurrences. Here, passes and portions of passes that were missing in version "b" are still missing in version "c".

7.2.2. Comparison of altimetric parameters on the reprocessed period

Here, various maps are shown of differences between versions "b" and "c". Altimetric parameters are impacted by the new correction tables that have been applied. The retracking however, is the same, so there is no major change.

7.2.2.1. Sea wave height, Ku-band

The impact of the new correction tables is small for SWH correction. SWH of version "c" are in average 2.8cm higher than in version "b". The main differences between the two product versions are located in coastal zones. Especially, the mean SWH is higher in the Gulf of Guinea, central and south America coasts, north Indian and north of Papua, and lower in closed or semi-closed basins (Black Sea, Gulf of California, Indonesia), where very low SWH are encountered. These are also the regions where standard deviation of the SWH differences is high.

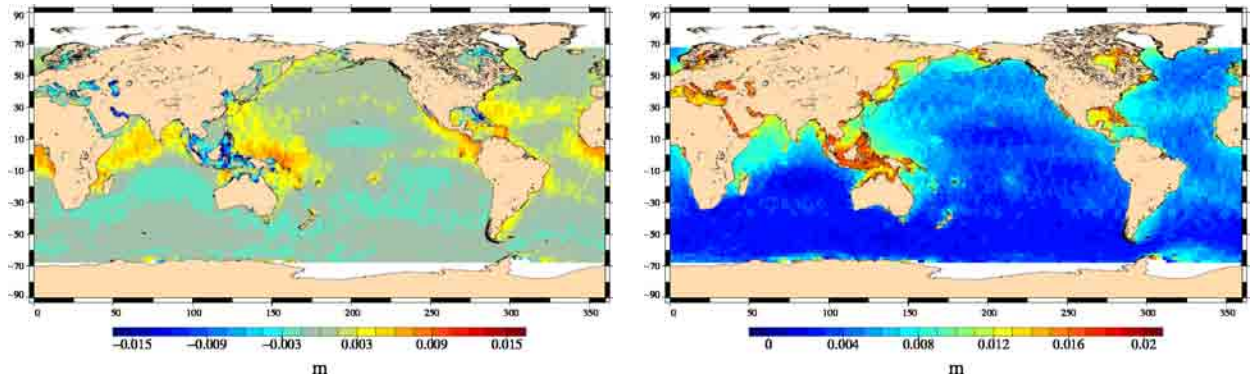

Figure 55: *Cartography of mean and standard deviation of differences between SWH of GDR "c" and GDR "b". Panel showing mean difference is centered on 2.8 cm*

7.2.2.2. Backscattering coefficient

There is a weak mean 0.025dB bias between versions "b" and "c", and a geographical pattern around this mean bias. At high and low latitudes ($\geq$ 40), this mean is higher, especially in the southern hemisphere where it reaches 0.01dB (plus the global 0.025dB bias). It is lower at mid latitudes. The standard deviation of the difference is more homogeneous and shows a increased standard deviation in low and mid-latitudes. The overall impact of the sigma0 change is neglectable.

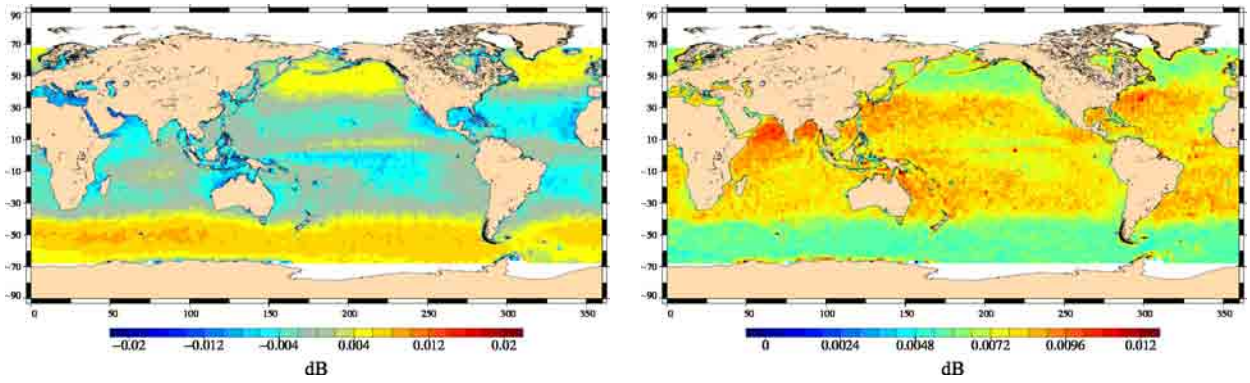

Figure 56: *Cartography of mean and standard deviation of differences between backscattering coefficients of GDR "c" and GDR "b" over 40 cycles. Panel showing mean difference is centered on 0.025 dB*

7.2.3. Comparison of other parameters on the reprocessed period

7.2.3.1. Differences of JMR

Mean bias of radiometer wet troposphere correction between the two product versions is 0.4 cm, with GDR "c" version being wetter. Figure 57 shows that the differences between the two wet troposphere corrections is higher for humid regions (tropics). The impact of JMR provided in GDR "b" overall the Jason-1 mission has been described in section 4.7.

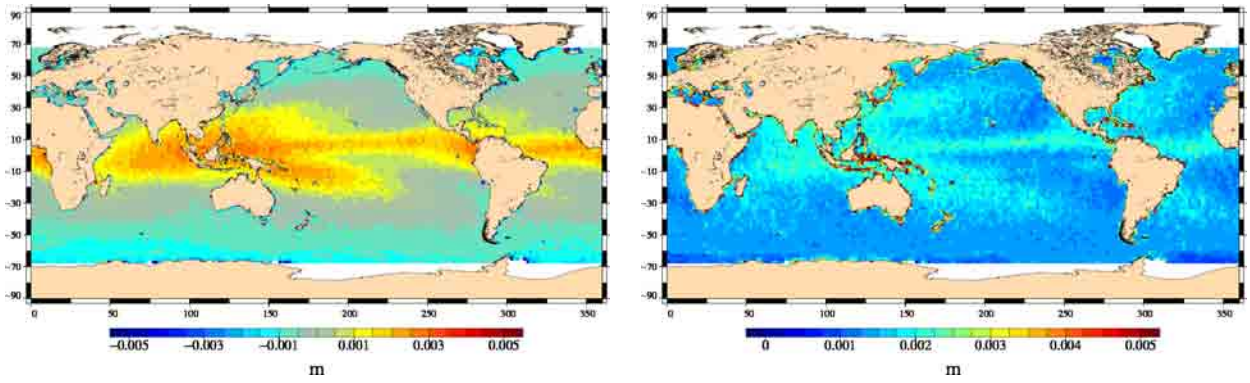

Figure 57: *Cartography of mean and standard deviation of differences between JMR of GDR "c" and GDR "b" over 40 cycles. Panel showing mean difference is centered on 0.39cm*

7.2.3.2. Differences of sea surface bias

Usually, for quality studies in this report, the Venice SSB, computed on 21 cycles, was used. The version "c" SSB was computed on a longer time series. Here, however, the maps presented compare the version "b" SSB that was provided in the product, with the new SSB of version "c". The GDR version "c" SSB is in average 3.2 cm higher than the one of version "b". Figure 58 shows that the differences between the two sea state bias corrections have a geographically correlated pattern, as for average and standard deviation. This has been described by [42] during the Venice OSTST (2006).

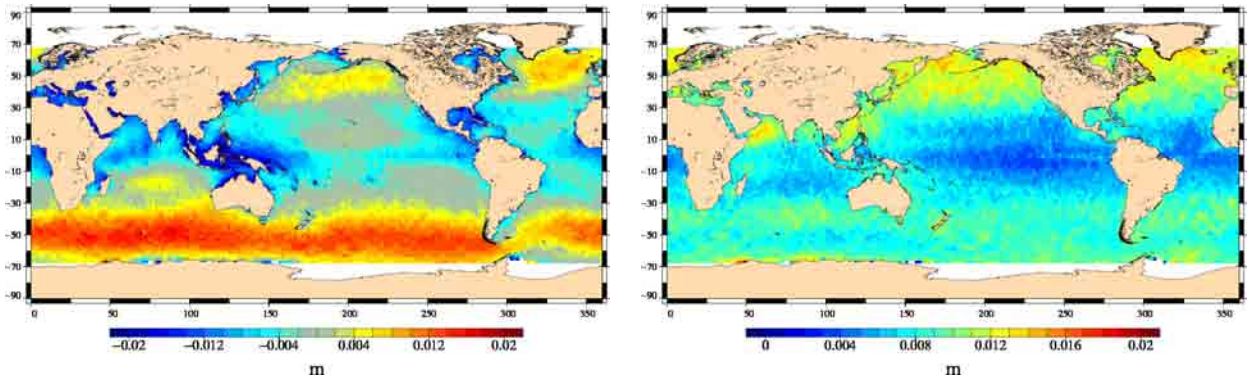

Figure 58: *Cartography of mean and standard deviation of differences between SSB of GDR "c" and GDR "b" over 40 cycles. Panel showing mean difference is centered on 3.2cm*

7.2.3.3. Dynamical atmospheric corrections (DAC)

Figure 59 shows the difference between high and low resolution of DAC. They are very small. The main differences are in coastal areas but also in some parts of the open ocean (north Atlantic and circumpolar current). Differences exist also in several enclosed seas (black sea, baltic sea, ...). This is presented in more details in [43].

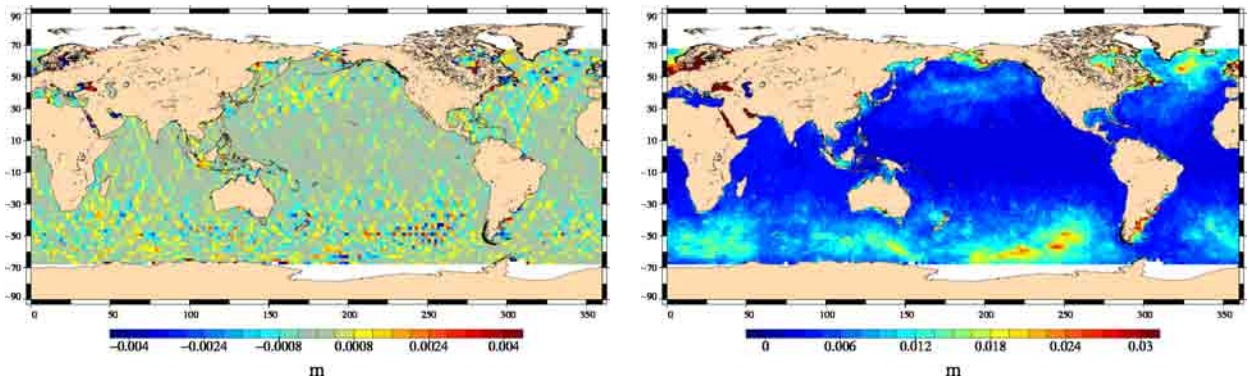

Figure 59: *Cartography of mean and standard deviation of differences between high and low resolution MOG2D of GDR "c" and GDR "b" over 40 cycles.*

7.3. Performances at crossovers

From cycle 193 to 232, version "c" shows better performances at crossovers than version "b", with a variance gain between 0 and $2cm^2$. Note that the gain (blue areas) seems to be higher in the south Pacific, corresponding to the areas were low and high resolution DAC corrections differ most (see figure 59, right).

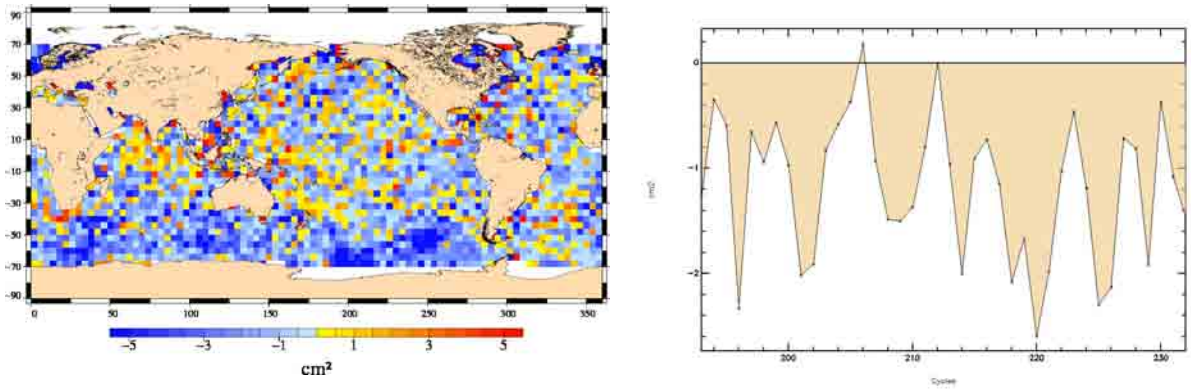

Figure 60: *Cartography (left) and temporal (right) evolution of variance differences at crossovers between version "c" and "b" over 40 cycles.*

7.4. Along-track performances

Along-track variance differences show an annual cycle, with a mean gain up to 7% of the signal variance. The variance difference is positive with top values in September, and minimum values in February. The annual cycle is further investigated in part 7.5.

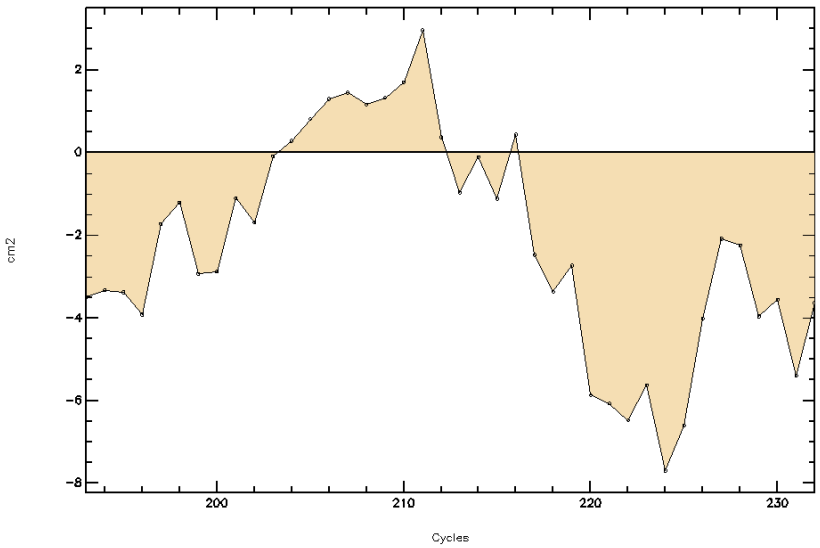

Figure 61: *Mean of orbit differences from GDR version "c" and "b".*

7.5. Comparison of orbit versions "b" and "c"

7.5.1. First version

The main change between versions "b" and "c" is the new orbit. Two versions of the new precise orbit were computed, hereafter called V1 and V2. The first version (V1) had been provided before the beginning of the reprocessing, for quality assessment regarding the sea surface height at crossovers and along-track performances, from cycles 100 to 160, corresponding to the period September 2004 to May 2006.

The average difference of parameters showed an east/west bias (figure 62). Similar performances were observed at crossovers, and the SLA standard deviation decreased down by $3.5cm^2$. A slight annual cycle seemed to appear on the SLA standard deviation differences. These results led to the conclusion that the orbit quality was good enough for the reprocessing to begin.

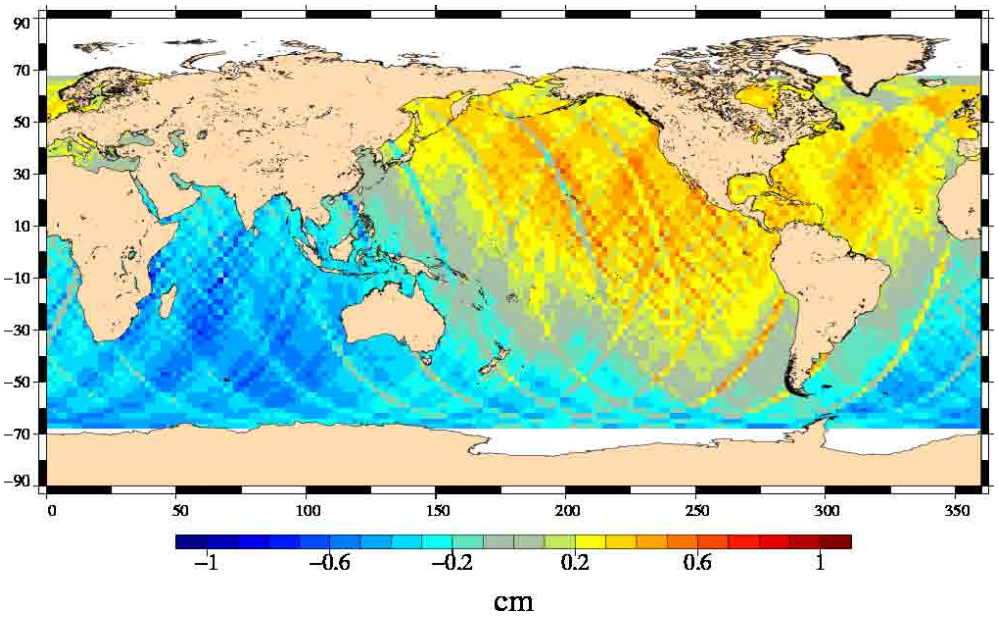

Figure 62: *Mean of orbit differences from GDR version "c" (V1) and "b" from cycle 22 to 232.*

However, after reprocessing cycles 212 to 227, an unexpected behavior of the orbit was observed, with versions "b" and "c" divergences getting high values for the orbits (5cm). This was due to the correction of high degree drifts in the time-varying part of the gravity field that were badly handled with. This feature could not be detected in the previous assessment study, because the corrected drifts had been fitted on the period that had been proposed for the study. Therefore, a new orbit solution was proposed and the already reprocessed cycles were reprocessed again.

In order to perform a better long term monitoring of the orbit impact, the whole orbit dataset was processed before the rest of GDRs were, and a study was led to assess the impact of the new GDR-C orbit.

7.5.2. Final version

This section is a summary of [17]. The study covered the period from cycle 22 to 232. The mean difference of the two orbits does not show an east/west bias like the first version, but a weaker north/south bias, which is more consistent with the expected impact of the reference frame change (ITRF2000 for version "b", ITRF2005 for version "c"), as shown in figure 63.

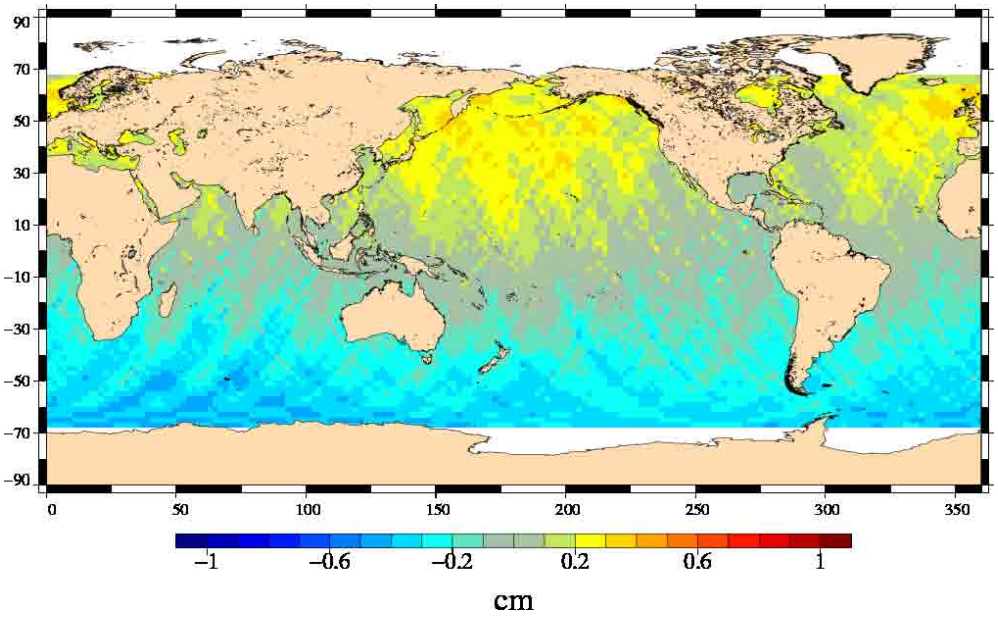

Figure 63: *Mean of orbit differences from GDR version "c" (V2) and "b".*

Mean differences at crossovers are similar, with quite homogeneous maps (not shown). The more geographically homogeneous the differences are, the more consistency exists between ascending and descending tracks. Variance of differences at crossovers shows no significant improvement: the variance of SSH at crossovers decreases slightly (figure 64, right), but a variance reduction lower than $1cm^2$ is not considered as significant. Note, however, that the variance reduction is higher in the warm pool region, while a degradation is observed in the south Pacific and south-west Atlantic oceans (figure 64, left). No improvement is seen either on the temporal variations of variance of differences at crossovers.

A mean variance reduction of $1cm^2$ is observed on along-track SLA. In the case of orbit studies, it can be assumed that a variance reduction along-track is a significant improvement, because wavelengths impacted by orbit changes are far bigger than the mesoscale signal altimetry intends to detect. So the variance reduction is considered, here, not as an erroneous signal absorption, but as an improvement. The most remarkable feature in figure 65 is the annual cycle of the variance difference, which, while remaining negative in average, episodically reaches positive values, with maximum values in September and minimum values in February, maybe linked to the new atmospheric gravity terms in POE standards. Note, however, that there is no hemispheric phasing: both north and south hemisphere behave the same way. Up to $6cm^2$ at the end of the series, the variance reduction can reach 6% of the total variance of the signal.

To confirm these results, SLA calculation with the new POE were compared with tide gauge networks and in situ profiles. Both alternative methods have drawbacks: the tide gauge network has a limited numbers of sensors and, overall, the sensors are located close to the shore, where

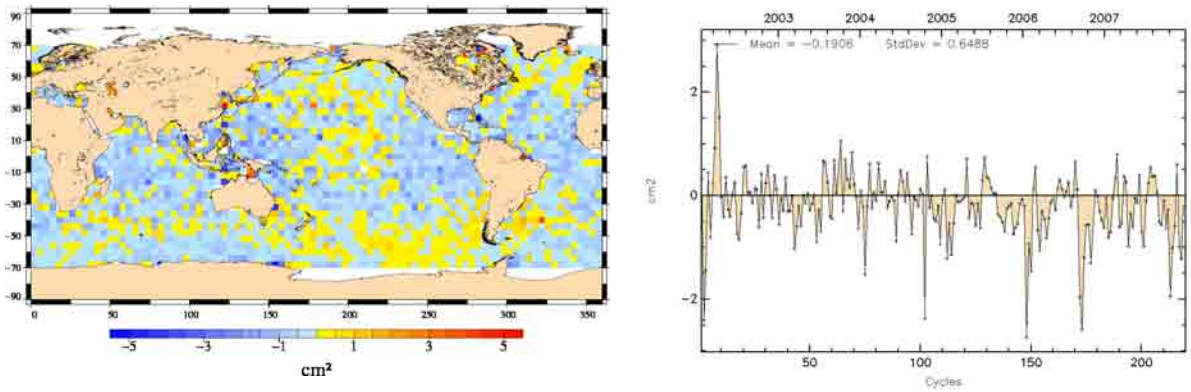

Figure 64: *Cartography (left) and temporal (right) evolution of variance differences at crossovers between version "c" and "b".*

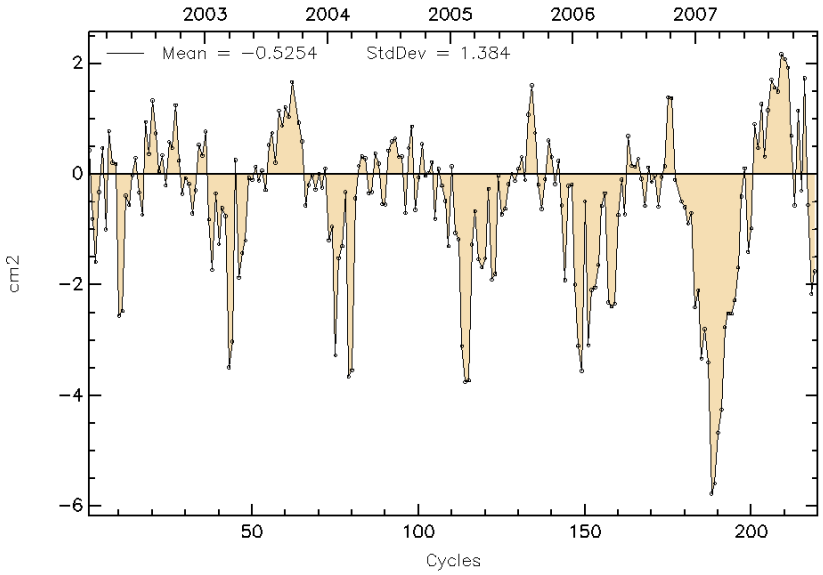

Figure 65: *Along-track SLA variance differences between GDR version "c" (V2) and "b".*

altimetric measurements' quality can be bad ([74]). In situ profiles only provide the steric content of the SSH signal. Therefore, the steric signal has to be extracted from altimetric measurements first, an awkward exercise for which more study is necessary ([75]). Despite these limitations, the comparisons to tide gauges and in situ profiles showed the same annual pattern as mentioned previously, without any significant improvement, although no degradation was observed either. Nevertheless, this comparison showed that the annual pattern is no artifact related to altimetric data (see [17]).

The variance reduction is not geographically homogeneous, as showed on figure 66. The strongest variance reductions are located in north Atlantic, Mediterranean Sea, south Indian and north-east Pacific (blue areas), where it is higher than $3cm^2$. The top reduction is observed in south-east Asia and north of Australia ($\geq 5cm^2$). On the contrary, a degradation up to $4cm^2$ is

observed in the Kuroshio region, north Indian, south Atlantic (orange areas).

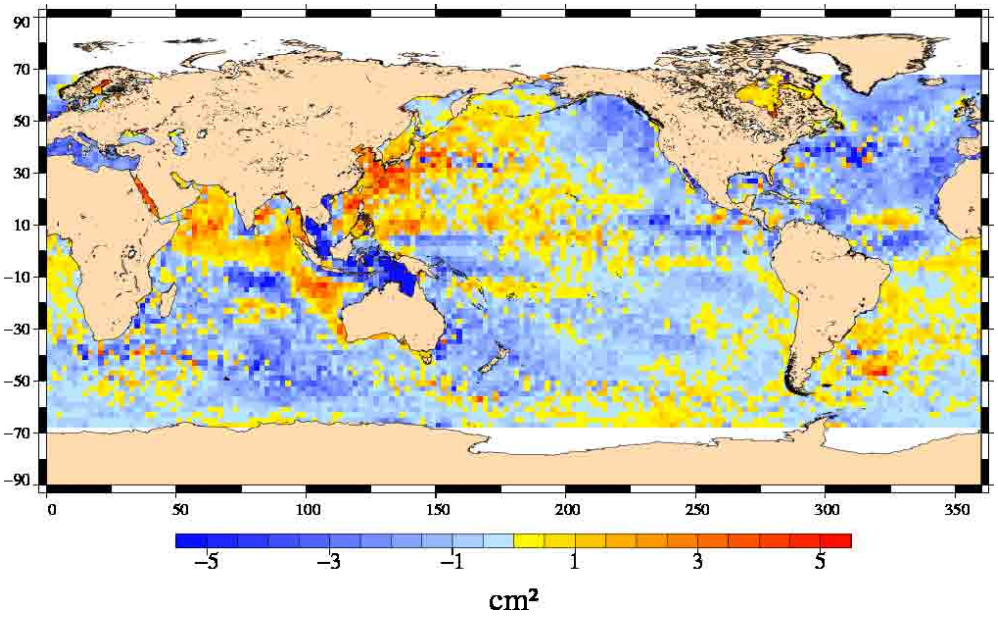

Figure 66: *Along-track SLA variance differences between GDR version "c" (V2) and "b".*

7.6. Impact on mean sea level trends

During the reprocessing period, that is, until mid 2009, the Jason-1 series, as provided to users, is not homogeneous. This can be important for mean sea level applications. Therefore, the impact of orbit and JMR wet tropospheric correction on MSL, has been analyzed. The whole time series POE, JMR and auxillary datasets were provided in advance to perform such investigations.

7.6.1. Impact of the new orbit (V2) on mean sea level trends

The impact of the orbit change on mean sea level trends was then investigated. The new orbit has no impact on global trends, with a slope difference lower than 0.1mm/year. The hemispheric divergence, observed in version "b", is still visible but has been slightly reduced (figure 67).

The impact on local slopes, however, shows north/south differences, correlated to the ITRF change. Thus, a regional bias will be necessary to compute regional MSL studies, while a global bias is sufficient for global studies (figure 68).

7.6.2. Impact of the new JMR calibration on mean sea level trends

The new calibration of JMR has no impact whatsoever on MSL trends and local slopes. Only a global bias should be applied (figure 69).

7.6.3. How to join old and new version

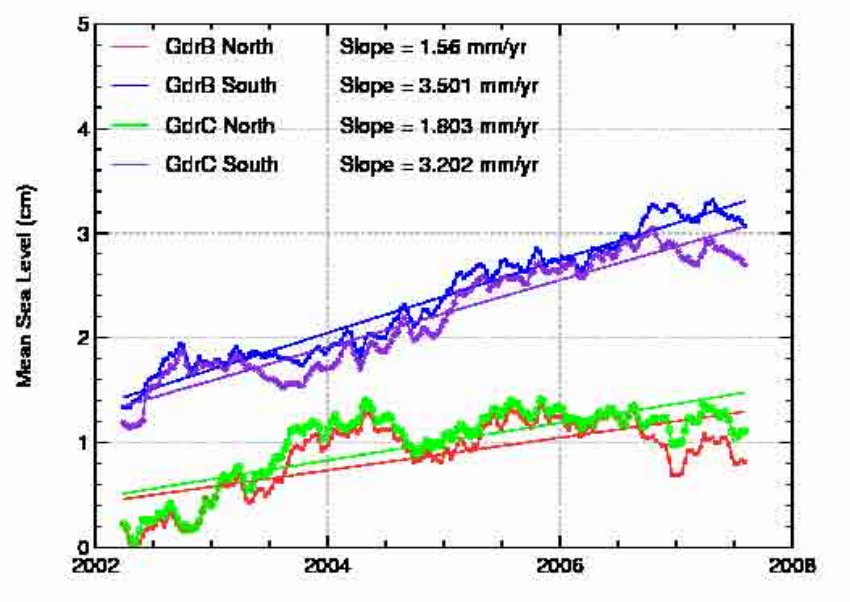

Figure 67: *Hemispheric mean sea level for GDR version "c" (V2) and "b".*

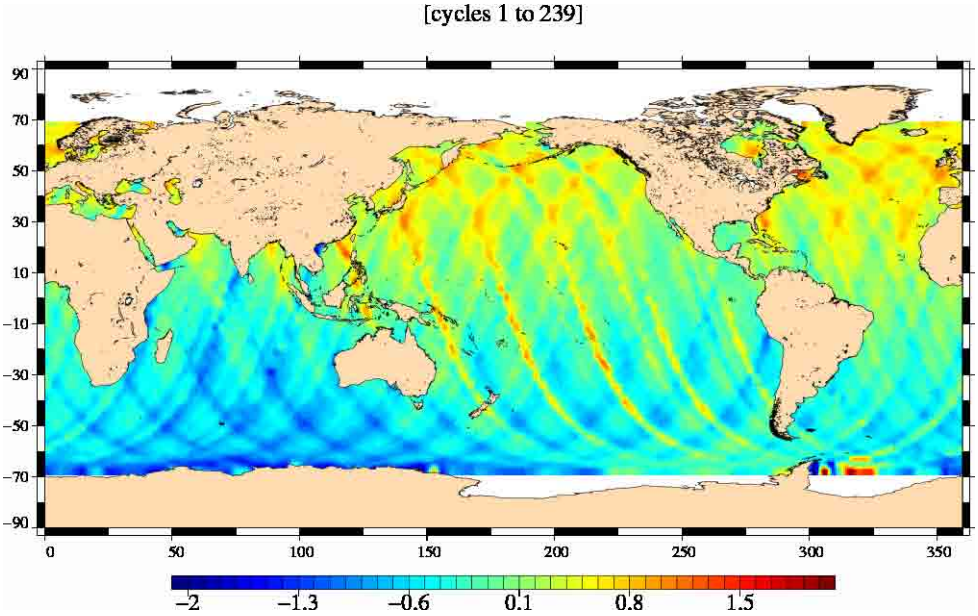

Figure 68: *Regional mean sea level slopes between orbits of GDR version "c" (V2) and "b" (unit:mm/year).*

A method is proposed to join both versions, while the whole dataset is not available in version "c" (which is expected by mid 2009). For global studies, applying a -9.5mm bias correction (when using JMR wet tropospheric correction) or -5.75mm when using model correction is enough to satisfyingly link both series and have a consistent MSL dataset over the whole Jason-1 period. For regional studies, a bias map is proposed (figure 70, left), computed on the last 4 Jason-1 cycles produced in version "b" (229 to 232), which are already available in version "c". This map can

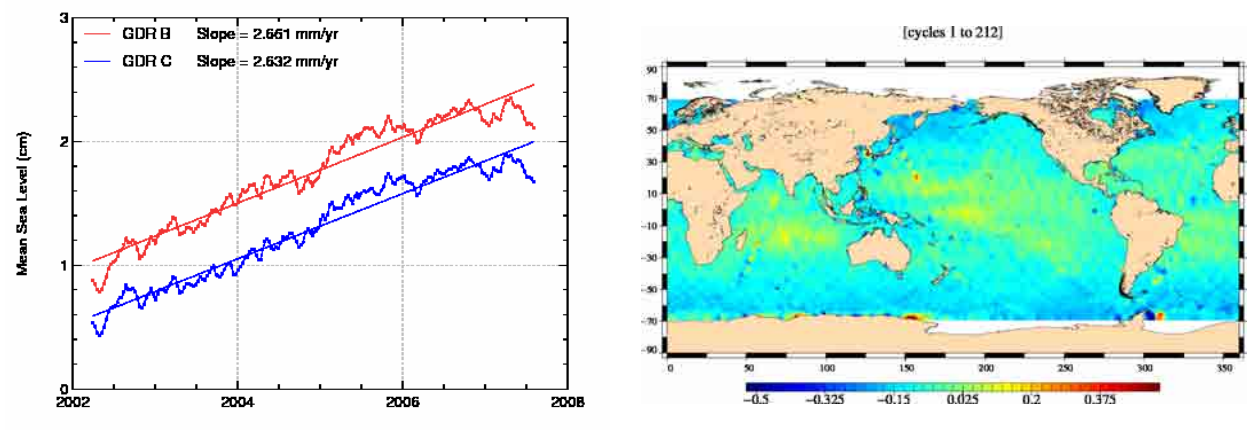

Figure 69: *Mean sea level trends using version b and c JMR (left), difference of local slopes (mm/year) between both versions (right).*

also be used for global purposes (figure 70, right). Note that for this bias calculation, GDR "b" sea state bias was replaced by the Venice sea state bias. This is already quite similar to sea state bias of GDR version "c". Values of biases between GDR version "b" and "c" are likely more important when using sea state bias from products.

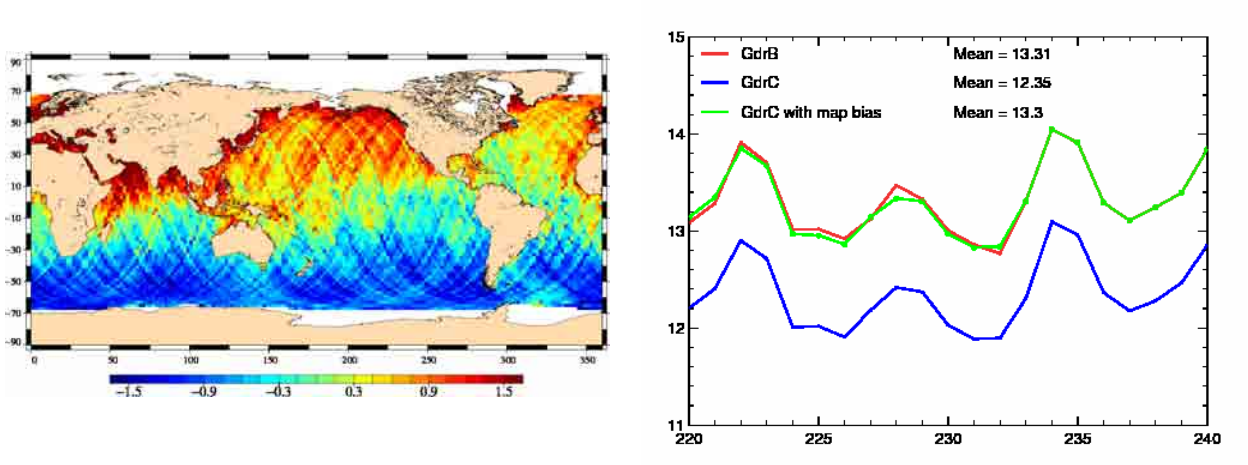

Figure 70: *MSL bias map (left) computed for cycles 229 to 232 and the resulting linked time series (right).*

8. Global and regional Mean Sea Level (MSL) trends

8.1. Overview

Long-term MSL change is a variable of considerable interest in the studies of global climate change. Thus, a lot of works have been performed on the one hand to survey the mean sea level trends and on the other hand to assess the consistency between the MSL derived from all the operational altimeter missions. Besides, external data source have been used to assess the altimetric MSL evolution. The in-situ data provided by tide gauges and temperature/salinity (T/S) profiles have been used to compare the MSL. The main results derived from these works are summarized here (the complete analysis are available in the annual reports [74] and [75]). In addition, the Reynolds SST have been also monitored over the global ocean to analyze the MSL trend.

8.2. SSH applied for the MSL calculation

The SSH formula used to compute the MSL is defined for all the satellites as below :

$$SSH = Orbit - Altimeter\ Range - \sum_{i=1}^{n} Correction_i$$

with :

$$\begin{aligned}
\sum_{i=1}^{n} Correction_i \;=\; & Dry\ troposphere\ correction\ new\ S1\ and S2\ atmospheric\ tides\ applied \\
+\; & Combined\ atmospheric\ correction :\ MOG2D\ and\ inverse\ barometer \\
+\; & Wet\ troposphere\ correction\ (radiometer\ or\ ECMWF\ model) \\
+\; & Filtered\ dual\ frequency\ ionospheric\ correction \\
+\; & Non\ parametric\ sea\ state\ bias\ correction \\
+\; & Geocentric\ ocean\ tide\ height,\ GOT\ 2000 :\ S1\ atmospheric\ tide\ is\ applied \\
+\; & Solid\ earth\ tide\ height \\
+\; & Geocentric\ pole\ tide\ height
\end{aligned}$$

The SSH formula has been modified or updated for each satellite in order to calculate the best MSL. Especially, stability problems of the radiometer wet troposphere correction have been taken into account :

- For Jason-1 : the radiometer wet troposphere correction is used even though 60-days signals are still detected since 2006.
- For Envisat : the ECMWF model wet troposphere correction is used to remove the effects of abnormal changes or trends observed on the radiometer wet troposphere correction, the USO correction has been applied (drift and anomaly (see Envisat yearly report [31])

- For T/P : the radiometer wet troposphere correction drift has been corrected with Scharroo's correction (Scharroo R., 2004 [66]), the relative bias between TOPEX and Poseidon and between TOPEX A and TOPEX B has been taken into account, the drift between the TOPEX and DORIS ionosphere corrections has been corrected for on Poseidon cycles.
- For Geosat Follow-On: the ECMWF model wet troposphere correction is used, the GIM model has been used for the ionospheric correction.

8.3. Analyze of the MSL trend

8.3.1. Global MSL trend derived from Jason-1 and T/P data

The global MSL trend derived from satellite altimetry - TOPEX/Poseidon and Jason-1 - is now used as the reference for climate studies. A SSH bias of 7.5 cm has been applied on Jason-1 data to link both MSL series. This bias has been calculated using the verification phase where Jason-1 and T/P were on the same orbit. This allows us to compute accurately the SSH bias. This MSL plotted on figure 71 highlights a global trend close to 3.05 mm/yr (post glacial rebound not taken into account). The adjustment formal error is low (lower than 0.03 mm/yr) showing a linear evolution of the MSL. However, the MSL rise is lower and very weak from the end of 2005 to 2007. During this period, only Jason-1 measurements are available, thus the comparisons with T/P MSL is not possible to confirm this behavior. But the comparisons with other satellites and in-situ data as described further, do not evidence an abnormal drift on Jason-1 measurements. Besides, a very strong "La Niña" occurred in 2007 and beginning of 2008, and might explain this MSL trend change. Indeed, the MSL started to rise again in 2008.

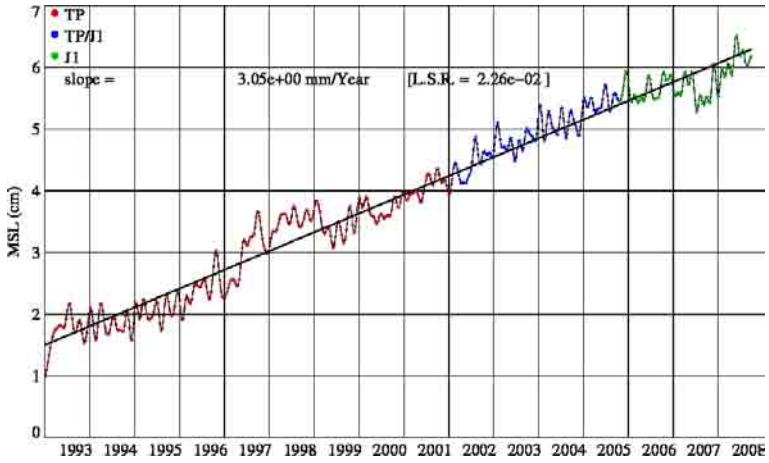

Figure 71: *Global MSL trend derived from Jason-1 and T/P data*

8.3.2. Regional MSL trends derived from AVISO merged products

The AVISO merged products are used to compute the regional MSL trends. Thanks to the high resolution of their grids (0.5 degrees), the MSL regional trends can be calculated with a good

resolution. This allows to very well displayed the variability of regional slopes as plotted on map 72. The local slopes range between ±10mm/yr with large structure in the main oceans, especially in Pacific Ocean. This kind of map brings a lot of information about the regional MSL evolution, which have to be analyzed in details: such as the long term evolution of oceanic circulation, such as the intensity of geostrophic currents, interannual oscillations (decadal, Madden-Julian oscillations for example).

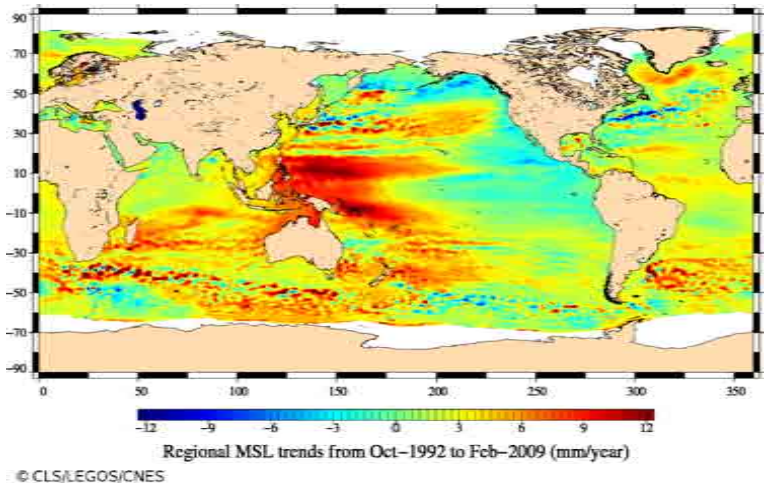

Figure 72: *Regional MSL trends derived from AVISO merged products*

8.4. Multi-mission comparisons of global MSL trends

The MSL has been monitored for each satellite altimeter over global ocean in order to assess the global MSL trend and also to detect any anomalies or any drifts on each MSL series. These different MSL have been plotted in figure 73, after removing annual and semi-annual signals, and filtering out signals lower than 60 days. The T/P and Jason-1 slopes since the beginning of Jason-1 period are very close within 0.2 mm/yr. Even though GFO slope is smaller by 0.7 mm/year over the Jason-1 period, it indicates a similar trend. Finally, only Envisat MSL shows a trend quite different with a global slope close to 1 mm/yr. The estimation of the Envisat MSL seems impacted by an unexpected behavior on the early years. This item is described in detail in the Envisat annual report [52].

8.5. External data comparisons

8.5.1. Tidal gauges and T/S profiles

In order to assess the global MSL trend, comparisons to independent in-situ datasets are of great interest. Two methods have been developed in the frame of in-situ Cal/val and thoroughly described in annual reports ([74] and [75]). First, TOPEX/Poseidon and Jason-1 altimetric data have been compared with tide gauge measurements thanks to a dedicated method which aims at detecting potential drifts in sea surface heights (SSH). The tide gauge network processed is the GLOSS/CLIVAR "fast" sea level database, formerly known as the WOCE network. Secondly, an

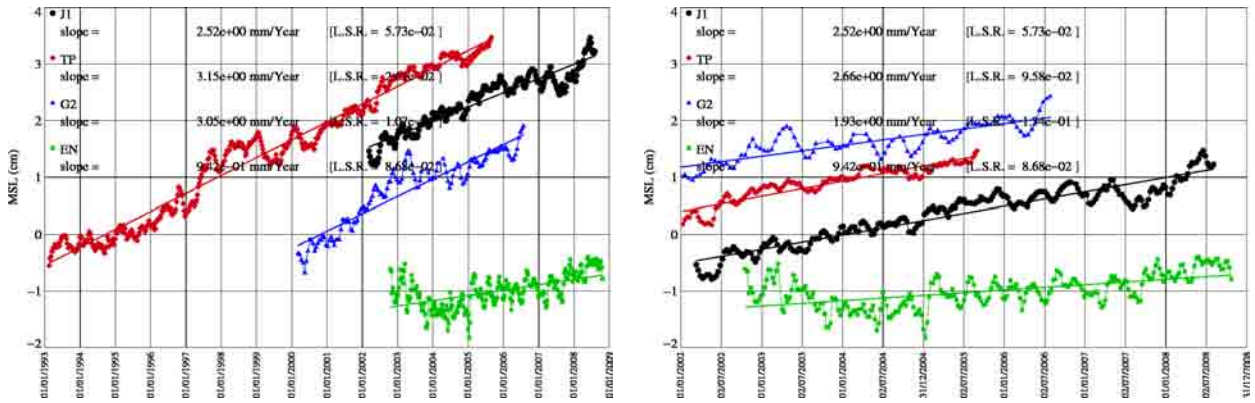

Figure 73: *Multi-mission MSL over global ocean since the beginning of T/P mission on the left and the beginning of Jason-1 mission on the right after removing annual, semi-annual and 60-day signals.*

innovating method with similar objectives has been developed using thousands of free-drifting profiling floats of the ARGO network. Altimetric data have thus been compared to sea level heights computed from these in-situ temperature/salinity profiles. Both methods complement each other since the first one using tide gauges only concerns coastal areas while the second one using T/S profiles is well widespread to get an assessment of the MSL in the open ocean.
From these comparison methods, SSH bias monitorings have been computed and bring out a drift lower than 0.5 mm/year (see figure 74) whatever in-situ data used. This trend results both from the error on datasets and the intrinsic error of the method, partly linked to the colocation of the altimetric and in-situ measurements in space and time. Finally, this study provides an upper bound of the error of the global MSL trend. This error will keep on refining in the future using new in-situ datasets, especially for the T/S profile method.

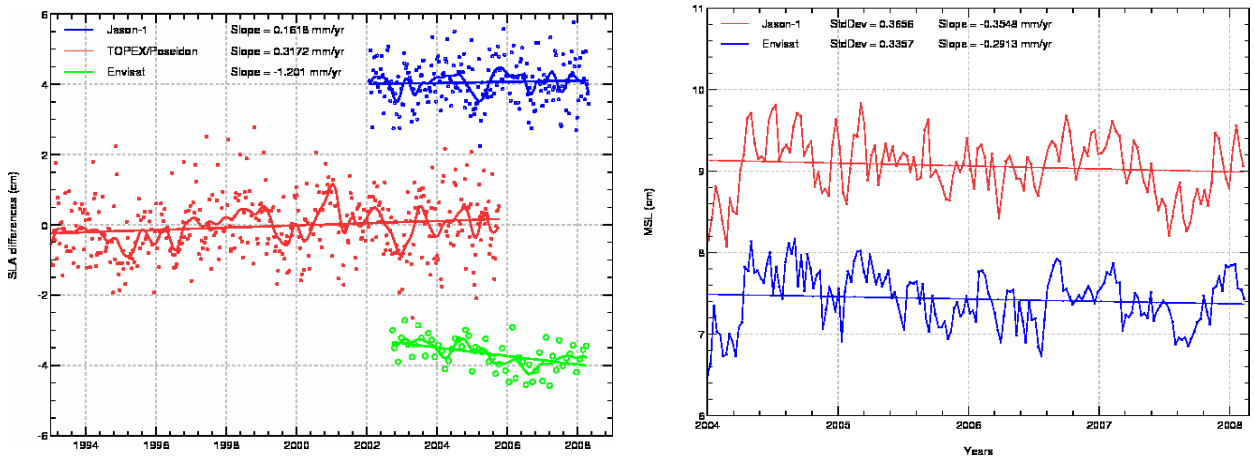

Figure 74: *Altimetric MSL drifts using tide gauges measurements (left) and T/S profiles (right)*

8.5.2. Reynolds's SST

The Reynold's SST has been monitored over the 15 year period from 1993 to 2008 along the T/P and Jason-1 tracks. It is compared with the reference MSL in figure 75, after removing annual signal, semi-annual signal, and signals lower than 60 days. In order to compare the dynamic of the MSL and SST increases, the SST scale has been adjusted on the MSL scale so that the SST trend and the MSL trend are visually the same. The mean SST rises by about 0.013 degree/yr with a dynamic stronger than the MSL. In particular, the signature of "El Niño" is more visible. Besides, the SST curve is relatively flat for 4 or 5 years. It even seems to decrease in 2007, which might be the signature of "La Niña".

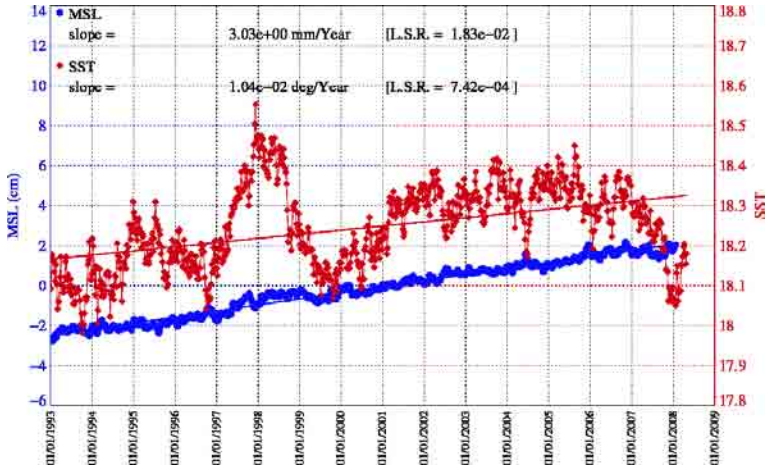

Figure 75: *Comparison of MSL and SST trend over global ocean for the Topex/Jason-1 period*

9. Conclusion

Since the beginning of the Jason-1 mission and until the end of the T/P mission in October 2005, T/P and Jason-1 overflew the ocean over 2 parallel passes except the 21 first cycles, when they were on the same pass. Thanks to this long flight configuration, performances comparisons between both missions have been performed with success during 4 years, proving that the major objective of the Jason-1 mission to continue the T/P high precision has been reached. Almost seven years of Jason-1 data are now available. The good quality of Jason-1 data has been shown in this report : the main altimeter parameters are stable and have the same behaviors as T/P ones, the crossover and along-track performances remain very good.

Moreover, the GDR release (version "b") allowed to impove significantly the Jason-1 data in comparison with the former GDR version, and the version "c" (end of reprocessing in mid-2009) will further improve data quality. The improved geophysical corrections (as high resolution DAC high frequency correction), the new orbit (using ITRF2005), recalibration of JMR, new instrument correction tables and a new sea state bias are the main sources of improvement. Thanks to these improvements, the SSH correlated geographical biases have been reduced and the SSH performances are better. Along-track performances are also improved thanks to the new orbit. However some behaviors remain unexplained, such as the annual cycle observed on along-track SLA variance differences observed between versions "b" and "c". Though version "c" reprocessing (providing a homogeneous time series) will only be completed by mid-2009, mean sea level trend can still be monitored by applying a bias map between version "b" and "c".

End of January 2009, Jason-1 has be moved to an interleaved orbit with Jason-2 (its successor). From there it will continue to gather valuable altimeter data.

10. References

References

[1] Ablain, M., J. Dorandeu, Y. Faugère, F. Mertz, B. Soussi, F. Mercier, P. Vincent, and N. Picot. 2003a. SSALTO/CALVAL Jason-1 data quality assessment and Jason-1 / TOPEX cross-calibration using GDRs. *Paper presented at the Jason-1 and TOPEX/Poseidon Science Working Team Meeting, Arles (France), November.*

[2] Ablain, M., J. Dorandeu, Y. Faugere, F. Mertz, 2004. Jason-1 Validation and Cross-calibration activities Contract No 731/CNES/00/8435/00. Available at: http://www.jason.oceanobs.com/documents/calval/validation_report/j1/annual_report_j1_2004.pdf

[3] Ablain, M. and J. Dorandeu, 2005. TOPEX/Poseidon validation activities, 13 years of T/P data (GDR-Ms), Available at: http://www.jason.oceanobs.com/documents/calval/validation_report/tp/annual_report_tp_2005.pdf

[4] Ablain, M., S. Philipps, P. Thibaut, J. Dorandeu, and N. Picot 2008. Jason-1 GDR Quality Assessment Report. Cycle 250. SALP-RP-P2-EX-21072-CLS250,. http://www.jason.oceanobs.com/fileadmin/documents/calval/validation_report/J1/Bilan_Calval_J1_Cycle_250.pdf

[5] Ablain, M., S. Philipps, S. Labroue, J. Dorandeu, and N. Picot, 2007. SSALTO CALVAL Consistency assessment between Jason-1 and TOPEX. poster presented at OSTST meeting, Hobart, Australia, 12-15 march 2007. Available at: http://www.jason.oceanobs.com/documents/swt/posters2007/ablain_J1TP.pdf

[6] Ablain, M., S. Philipps, J. Dorandeu, and N. Picot, 2007. SSALTO CALVAL Performance assessment Jason-1 data. Poster presented at OSTST meeting, Hobart, Australia, 12-15 march 2007. Available at: http://www.jason.oceanobs.com/documents/swt/posters2007/ablain_J1.pdf

[7] Amarouche, L., P. Thibaut, O.Z. Zanife, P. Vincent, and N. Steunou. 2004. Improving the Jason-1 Ground Retracking to Better Account or Attitude Effects. *Mar. Geod.***27 (1-2): 171-197.**

[8] Arnault, S., N. Chouaib, D. Diverres, S. Jaquin, and O. Coze, 2004. Comparison of TOPEX/Poseidon and JASON Altimetry with ARAMIS In Situ Observations in the Tropical Atlantic Ocean. *Mar. Geod.***27 (1-2): 15-30.**

[9] Brown G.S., "The average impulse response of a rough surface and its application", IEEE Transactions on Antenna and Propagation, Vol. AP 25, N1, pp. 67-74, Jan. 1977.

[10] Callahan, Phil. electronic communication (retrk-gdr-data-rec-r10.062.pdf) send to OSTST on 13 February 2006.

[11] Carayon, G., N. Steunou, J. L. Courrière, and P. Thibaut. 2003. Poseidon 2 radar altimeter design and results of in flight performances. *Mar. Geod.***26(3-4): 159-165.**

[12] Carrère, L., and F. Lyard, Modeling the barotropic response of the global ocean to atmospheric wind and pressure forcing - comparisons with observations. 2003. Geophys. Res. Lett., 30(6), 1275, doi:10.1029/2002GL016473.

[13] Chambers, D. P., S. A. Hayes, J. C. Ries, and T. J. Urban. 2003. New TOPEX sea state bias models and their effect on global mean sea level. J. Geophys. Res. 108(C10): 3305.

[14] Chambers, D., P., J. Ries, T. Urban, and S. Hayes. 2002. Results of global intercomparison between TOPEX and Jason measurements and models. Paper presented at the Jason-1 and TOPEX/Poseidon Science Working Team Meeting, Biarritz (France), 10-12 June.

[15] Chambers, D. P. and B. D. Tapley, 1998: Reduction of Geoid Gradient Error in Ocean Variability from Satellite Altimetry. *Mar. Geod.*, **21, 25-39.**

[16] Choy, K, J. C. Ries, and B. D Tapley, 2004. Jason-1 Precision Orbit Determination by Combining SLR and DORIS with GPS Tracking Data. *Mar. Geod.***27(1-2): 319-331.**

[17] Commien, L., 2009. Différences entre l'orbite des GDR-C et GDR-B Jason-1, NT08.338

[18] Commien, L., S. Philipps, M. Ablain, and N. Picot, 2008. SSALTO CALVAL Performance assessment Jason-1 GDR "C" / GDR "B". Poster presented at OSTST meeting, Nice, France, 09-12 November 2008. Available at: http://www.aviso.oceanobs.com/fileadmin/documents/OSTST/2008/commien.pdf

[19] Desai, S. D., and B. J. Haines, 2004. Monitoring Measurements from the Jason-1 Microwave Radiometer and Independent Validation with GPS. *Mar. Geod.***27(1-2): 221-240.**

[20] Dibarbour, G., Bruit Jason et Analyse spectrale, March 2001, CLS.ED/NT

[21] Dorandeu, J., M. H. De Launay, F. Mertz and J. Stum, 2001. AVISO/CALVAL yearly report. 8 years of TOPEX/Poseidon data (M-GDRs).

[22] Dorandeu, J. and P.Y. Le Traon, 1999: Effects of Global Atmospheric Pressure Variations on Mean Sea Level Changes from TOPEX/Poseidon. *J. Atmos. Technol.,***16, 1279-1283.**

[23] Dorandeu, J, M. Ablain, Y . Faugere, B. Soussi, and J . Stum. 2002a. Global statistical assessment of Jason-1 data and Jason-1/TOPEX/Poseiodn Cross-calibration. Paper presented at the Jason-1 and TOPEX/Poseidon Science Working Team Meeting, Biarritz (France), **10-12 June.**

[24] Dorandeu, J., P. Thibaut, O. Z. Zanife, Y. Faugère, G. Dibarboure, N. Steunou, and P. Vincent. 2002b. Poseidon-1, Poseidon-2 and TOPEX noise analysis. Paper presented at the Jason-1 and TOPEX/Poseidon Science Working Team Meeting, New-Orleans (USA), **October.**

[25] Dorandeu., J., M. Ablain, P. Y. Le Traon, 2003a. Reducing Cross-track Geoid Gradient Errors around TOPEX/Poseidon and Jason-1 Nominal Tracks. Application to Calculation of Sea Level Anomalies. *J. Atmos. Oceanic Technol.,***20, 1826-1838.**

[26] Dorandeu, J., Y. Faugère, and F. Mertz. 2003b. ENVISAT data quality: Particular investigations. Proposal for ENVISAT GDR evolutions. Paper presented at the ENVISAT Ra-2 & MWR Quality Working Group meeting. **October.**

[27] Dorandeu.,J., M. Ablain, Y. Faugère, F. Mertz, 2004 : Jason-1 global statistical evaluation and performance assessment. Calibration and cross-calibration results. *Mar. Geod.***This issue.**

[28] Y.Faugere, J.Dorandeu, F.Lefevre, N.Picot and P.Femenias, 2005: Envisat ocean altimetry performance assessment and cross-calibration. Submitted in the special issue of SENSOR 'Satellite Altimetry: New Sensors and New Applications'

[29] Y.Faugere and J.Dorandeu, 2004: Nouvel algorithme de détection des glaces de mer pour Jason-1. SALP-PR-MA-EA-21235-CLS.

[30] Faugere Y., Estimation du bruit de mesure sur jason-1, December 2002, CLS.ED/NT.

[31] Y.Faugere, N.Granier, and A.Ollivier, 2007: Envisat validation activities. 2007 yearly report, Available at: http://www.jason.oceanobs.com/documents/calval/validation_report/en/annual_report_en_2007.pdf

[32] Förste, C., F. Flechtner, R. Schmidt, U. Meyer, R. Stubenvoll, F. Barthelmes, R. König, K.-H. Neumayer, M. Rothacher, C. Reigber, R. Biancale, S. Bruinsma, J.-M. Lemoine, and J.C. Raimondo. A New Heigh Resolution Global Gravity Field Model Derived From Combination of GRACE and CHAMP Mission and Altimetry/ Gravimetry Surface Gravity Data. *Poster presented at EGU General Assembly 2005, Vienna, Austria, 24-29 April 2005.*

[33] Fu, L. L., 2002. Minutes of the Joint Jason-1 and TOPEX/Poseidon Science Working Team Meeting, Oct. 21-23, JPL Tech. Report. JPL D-25506, edited by L. Fu, USA.

[34] Gaspar, P., S. Labroue, F. Ogor, G. Lafitte, L. Marchal and M. Rafanel, 2002: Improving non parametric estimates of the sea state bias in radar altimeter measurements of sea level. *J. Atmos. Oceanic Technol.,***19, 1690-1707.**

[35] Haines, B., Y. Bar-Sever, W. Bertiger, S. Desai, P. Willis, 2004: One-Centimeter Orbit Determination for Jason-1: New GPS-Based Strategies. *Mar. Geod.***27(1-2): 299-318.**

[36] Hamming, R. W., 1977. Digital Filter. Prentice-Hall Signal Processing Series, edited by A. V. Oppenheim Prentice-Hall, Englewood Cliffs, N. J.

[37] Hernandez, F. and P. Schaeffer, 2000: Altimetric Mean Sea Surfaces and Gravity Anomaly maps inter-comparisons AVI-NT-011-5242-CLS, 48 pp. CLS Ramonville St Agne.

[38] Hirose N., Fukumori I., Zlotnicki V., Ponte R. M. 2001: High-frequency barotropic response to atmospheric disturbances : sensitivity to forcing, topography, and friction, J. Geophys. Res. 106(C12), 30987-30996.

[39] Keihm, S. J., V. Zlotnicki, and C. S. Ruf. 2000. TOPEX Microwave Radiometer performance evaluation, 1992-1998, *IEEE Trans. Geosci. Rem. Sens.,***38(3): 1379-1386.**

[40] Labroue, S. and P. Gaspar, 2002: Comparison of non parametric estimates of the TOPEX A, TOPEX B and JASON 1 sea state bias. Paper presented at the Jason 1 and TOPEX/Poseidon SWT meeting, New-Orleans, 21-12 October.

[41] Labroue, S. P. Gaspar, J. Dorandeu, O.Z. Zanifé, P. Vincent, and D. Choquet. 2004. Non Parametric Estimates of the Sea State Bias for Jason 1 Radar Altimeter. *Mar. Geod.***This issue.**

[42] Labroue, S., Ph. Gaspar, J. Dorandeu, O.Z. Zanife. Latest Results on Jason-1 Sea State Bias with the Non-Parametric Technique. *Talk presented at OSTST meeting, Venice, Italy, 16-18 March 2006.*

[43] Legeais JF. and Carrère L., July 2008, Complément de validation de la DAC_HR par rapport à la DAC , en zone côtière, Technical Note CLS.DOS/08.189.

[44] Lemoine, F. G., S. B. Luthcke, N. P. Zelinsky, D. S. Chinn, T. A. Williams, C. M. Cox, and B. D. Beckley. 2003. An Evaluation of Recent gravity Models Wrt to Altimeter Satellite Missions.*Paper presented at the Jason-1 and TOPEX/Poseidon Science Working Team Meeting,***Arles (France), November.**

[45] Le Traon, P.-Y., J. Stum, J. Dorandeu, P. Gaspar, and P. Vincent, 1994: Global statistical analysis of TOPEX and POSEIDON data. *J. Geophys. Res.,***99, 24619-24631.**

[46] Le Traon, P. Y., and G. Dibarboure, 2004. An Illustration of the Contribution of the TOPEX/Poseidon-Jason-1 Tandem Mission to Mesoscale Variability Studies. *Mar. Geod.***27(1-2) 3-13.**

[47] Luthcke. S. B., N. P. Zelinsky, D. D. Rowlands, F. G. Lemoine, and T. A. Williams. 2003. The 1-Centimeter Orbit: jason-1 Precision Orbit Determination Using GPS, SLR, DORIS, and Altimeter Data. *Mar. Geod.***26(3-4): 399-421.**

[48] Marshall, J. A., N. P. Zelinsky, S. B. Luthcke, K. E., Rachlin, and R. G. Williamson. 1995. The temporal and spatial characterustics of TOPEX/Poseidon radial orbit error. *J. Geophys. Res.* **100(C2):25331-25352.**

[49] Martini A., 2003: Envisat RA-2 Range instrumental correction : USO clock period variation and associated auxiliary file, Technical Note ENVI-GSEG-EOPG-TN-03-0009 Available at http://earth.esa.int/pcs/envisat/ra2/articles/USO_clock_corr_aux_file.pdfhttp://earth.esa.int/pcs/envisat/ra2/auxdata/

[50] Ménard, Y. 2003. Minutes of the Joint TOPEX/Poseidon and Jason-1 Science Working Team Meeting. CNES-SALP-CR-MA-EA-15190-CN.

[51] Obligis, E, N. Tran, and L. Eymard, 2004. An assessment of Jason-1 microwave radiometer measurements and products. *Mar. Geod.***27(1-2) 255-277.**

[52] Ollivier, A., Y.Faugere and N.Granier, 2008: Envisat validation activities. 2008 yearly report, Available at: http://www.jason.oceanobs.com/documents/calval/validation_report/en/annual_report_en_2008.pdf

[53] Picard, B., E. Obligis and S. Philipps, 2008. Monitoring of JMR secondary geophysical products, SALP-NT-MA-EA-21562-CLS.

[54] Phaden Mc.J., April2003 : Evolution of the 2002-03 El Niño, *UCLA Tropical Meteorology and Climate Newsletter,***No57**.

[55] Philipps, S. and M. Ablain,September 2007 : SALP - BC 60453-6-04: Retraitement des GDRs Jason-1 en version 'B' pour les cycles 022 à 127, SALP/BC60453-6-04.

[56] Picot, N., K. Case, S. Desai and P. Vincent, 2003. AVISO and PODAAC User Handbook. IGDR and GDR Jason Products, SMM-MU-M5-OP-13184-CN (AVISO), JPL D-21352 (PODAAC).

[57] Provost., C. Arnault, N. Chouaib, A. Kartavtseff, L. Bunge, and E. Sultan, 2004. TOPEX/Poseidon and Jason Equatorial Sea Surface Slope Anomaly in the Atlantic in 2002: Comparison with Wind and Current Measurements at 23W. *Mar. Geod.***27(1-2) 31-45.**

[58] Quartly, G. D., 2004. Sea State and Rain: A Second Take on Dual-Frequency Altimetry. Mar. Geod. 27(1-2) 133-152

[59] Queffeulou, P. 2004. Long Term Validation of Wave Height Measurements from Altimeters. *Mar. Geod.***This issue.**

[60] Ray, R. (1999). A Global Ocean Tide Model From TOPEX/Poseidon Altimetry/ GOT99.2 - NASA/TM-1999-209478. Greenbelt, MD, Goddard Space Flight Center/NASA: 58

[61] Ray, R. D., and B. D. Beckley, 2003. Simultaneaous Ocean Wave Measurements by the Jason and Topex Satellites, with Buoy and Model Comparisons *Mar. Geod.***26(3-4): 367-382.**

[62] Ray, R. D. 2003. Benefits of the joint T/P−Jason mission for improving knowledge of coastal tides. Paper presented at the Jason-1 and TOPEX/Poseidon Science Working Team Meeting, Arles (France), November.

[63] Ray, R.D. and R.M. Ponte, Barometric tides from ECMWF operational analyses. *Annales G*, **99, 24995-25008**, 1994.

[64] Ruf C., S. Brown, S. Keihm and A. Kitiyakara, 2002a. JASON Microwave Radiometer : On Orbit Calibration, Validation and Performance, *Paper presented at the Jason-1 and TOPEX/Poseidon Science Working Team Meeting, New-Orleans (USA),***21-23 October.**

[65] Ruf. C. S., 2002b. TMR Drift - Correction to 18 GHz Brightness Temperatures, Revisited. Report to TOPEX Project, June.

[66] Scharroo R., J. L. Lillibridge, and W. H. F. Smith, Cross-Calibration and Long-term Monitoring of the Microwave Radiometers of ERS, TOPEX, GFO, Jason-1, and Envisat, **Marine Geodesy, 27:279-297**, 2004.

[67] Tapley, B.D., M.M. Watkins, J.C. Ries, G.W. Davis, R.J. Eanes, S.R. Poole, H.J. Rim, B.E. Schultz, C.K. Shum, R.S. Nerem, F.J. Lerch, J.A. Marshall, S.M. Klosko, N.K. Pavlis, and R.G. Williamson, 1996. The Joint Gravity Model 3. *J. Geophys. Res.***101(B12): 28029-28049.**

[68] Tierney, C., J. Wahr, et al. 2000. Short-period oceanic circulation: implications for satellite altimetry. Geophysical Research Letters 27(9): 1255-1258

[69] Thibaut, P. O.Z. Zanifé, J.P. Dumont, J. Dorandeu, N. Picot, and P. Vincent, 2002. Data editing : The MQE criterion. Paper presented at the Jason-1 and TOPEX/Poseidon Science Working Team Meeting, New-Orleans (USA), 21-23 October.

[70] Thibaut, P. L. Amarouche, O.Z. Zanife, N. Steunou, P. Vincent, and P. Raizonville. 2004. Jason-1 altimeter ground processing look-up tables. *Mar. Geod.***This issue.**

[71] Tournadre, J. 2002. Validation of the rain flag. Paper presented at the Jason-1 and TOPEX/Poseidon Science Working Team Meeting, Biarritz (France), 10-12 June.

[72] Tran, N., D. W. Hancock III, G.S. Hayne. 2002. "Assessment of the cycle-per-cycle noise level of the GEOSAT Follow-On, TOPEX and POSEIDON." *J. Atmos. Oceanic Technol.,***19(12): 2095-2117.**

[73] World Meteorological Organization. 2008. El Niño/ La Niña Update (24 June 2008). Available at http://www.wmo.ch/pages/prog/wcp/wcasp/documents/El_Nino_Jun08_Eng.pdf.

[74] Valladeau, G. and M. Ablain. Validation of altimetric data by comparison with tide gauge measurments for TOPEX/Poseidon, Jason-1 and Envisat. SALP-NT-MA-EA-21589-CLS, CLS.DOS/NT/08-256.

[75] Valladeau, G., and M. Ablain. Validation des données altimétriques par comparaison aux mesures in-situ T/S pour TOPEX/Poseidon, Jason-1 et Envisat. SALP-NT-MA-P2-21635-CLS, CLS.DOS/NT/09-018.

[76] Vincent, P., S. D. Desai, J. Dorandeu, M. Ablain, B. Soussi, P. S. Callahan, and B. J. Haines 2003a. Jason-1 Geophysical Performance Evaluation. *Mar. Geod.***26(3-4): 167-186.**

[77] Vincent, P., S. Desai, J. Dorandeu, M. Ablain, B. Soussi, Y. Faugère, B. Haines, N. Picot, K. Case, A. Badea, 2003b. Summary about Data Production and Quality. Paper presented at the Jason-1 and TOPEX/Poseidon Science Working Team Meeting, Arles (France), November

[78] Vincent, P., J.P. Dumont, N. Steunou, O.Z. Zanife, P. Thibaut, and J. Dorandeu. 2003c. Jason-1 I/GDR science processing: ground retracking improvements. Paper presented at the European Geophysical Society meeting, Nice, April.

[79] Zanife, O. Z., P. Vincent, L. Amarouche, J. P. Dumont, P. Thibaut, and S. Labroue, 2003. Comparison of the Ku-band range noise level and the relative sea-state bias of the Jason-1, TOPEX and Poseidon-1 radar altimeters. *Mar. Geod.***26(3-4): 201-238.**

11. Annex

This annex contains posters presented at OSTST meeting in 2008./

SSALTO CALVAL performance assessment Jason-1 GDR "C"/GDR "B"

L. Commien[1], S. Philipps[1], M.Ablain[1], N.Picot[2]

[1]CLS, Space Oceanography Division, Toulouse, France
[2]CNES, Centre National d'Etudes Spatiales, Toulouse, France

Context

Jason-1 data have been processed in GDR version C from cycle 233 onward. The beginning of the dataset is currently being reprocessed in version C. The present poster analyses the global impact of the new GDR-C version on the system performances for the yet reprocessed cycles (196 to 232), and also focuses on the specific impact of new precise orbit and JMR data on the mean sea level calculation from the whole series.

Three datasets are available. GDRs have been reprocessed from cycle 196 to 232. This first dataset is used to assess the performances of the system (crossover SSH and along-track SLA statistics). New precise orbit, taking into account the time-varying part of the gravity field is available from cycle 1 to 239. Improved calibration of JMR data from cycles 1 to 212 is also used in this study. These are the main evolutions from version B to version C, along with the use of high resolution dynamic atmospheric correction, new SSB calculation and range estimation, introduction of a pseudo time-tag bias correction, and more accurate rain and ice flags.

Global performances of GDR-C

GDR's have been reprocessed from cycle 194 to 232 (except for cycle 195). The performances prove to be very satisfying.

Crossover analysis

The crossover ascending/descending incoherencies are reduced with GDR-C: the map of mean crossover differences is more homogenous than with GDR-B, especially in the Atlantic, This shows a better coherence between ascending and descending tracks (Fig.1), mainly due to new orbit calculation and the introduction of a pseudo time-tag bias correction.

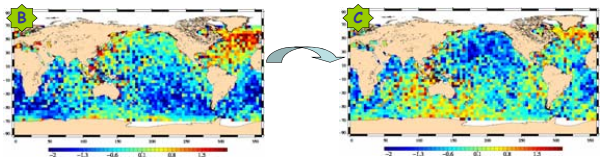

Fig. 1: Mean [cm] of SSH at crossovers, for GDR-B (left) and GDR-C (right).

The variance difference is negative almost everywhere ($var(SSH_{GDRC})$-$var(SSH_{GDRB})$), from 1 to 8cm², which is a clear improvement of GDR-C (Fig.2, left). Temporally, the variance gain is about 1cm², which is low but still an improvement too (right).

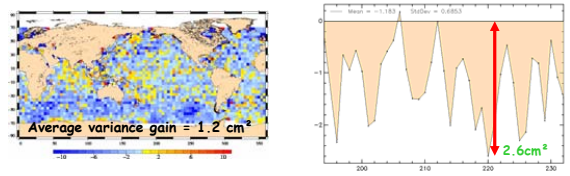

Fig. 2: Variance differences ('C'-'B') of crossover SSH. Spatially (left) and temporally (right), from cycle 194 to 232 [cm²]

Along-track analysis

The variance difference of along-track SLA between both GDR versions, highlights an annual signal (Fig.3). Most of the time, the variance is reduced with GDR-C (~2 cm²), but the variance reduction reaches almost 8 cm². This is mainly related to the orbit change (see below).

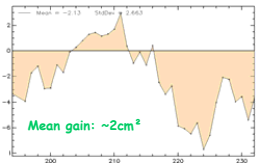

Fig. 3: SLA variance differences "C" – "B" [cm²] from cycles 194 to 232.

Analysis of new orbit over the whole period

GDR-C orbit is a SLR/DORIS/GPS orbit as GDR-B but uses the EIGEN-GL04C gravity field. Contrary to the GDR-B orbit, GDR-C POE takes into account annual and semi-annual time variability and atmospheric contribution of the gravity field, and ocean pole tide effects. The new reference frame used is ITRF2005, contrary to GDR-B (ITRF2000). Figure 4 shows the mean differences between GDR-C and GDR-B orbits for cycles 1 to 239. The main feature is north/south bias, due to the change of reference frame.

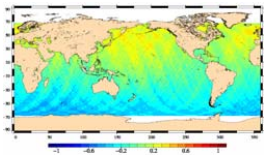

Fig. 4: Mean differences "C" – "B" [cm] of orbits from cycles 1 to 239.

Mean differences at crossovers are geographically more homogeneous, proving a better coherence with version C (not shown). The SSH variance at crossovers decreases slightly. Temporally, a slight improvement is noticed, the quality of both products is equivalent regarding the crossovers performances, with variance reduction similar to the statistics shown on the global performances of GDR-C box (above).

Figure 5 shows a peculiar annual pattern on along-track SLA variance differences. The variance is significantly decreased, reaching 6cm², which approximately corresponds to 7% of the signal's total variance. Note that this improvement enlarges with time. This highlights the add of the time-varying part of the gravity field in the new orbit calculation. This feature has also been observed when comparing the altimetry to in situ measurements (tide gauges and ARGO T/S profiles).

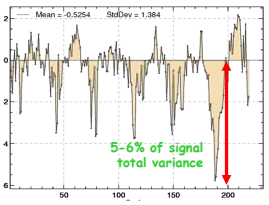

Fig. 5: Cycle per cycle variance differences [cm²] of along-track SLA. ("C" – "B"), with selections on latitude [50°N;50°S] and bathy<1000m.

Impact on MSL

JMR contribution

An improved JMR calibration is used, which corrects for scale error, provides additional reduction of yaw state effects and avoids small shifts that may have occurred after the last two safehold events.

The new radiometer wet troposphere correction has minor effects on mean sea level trends (Fig. 6).

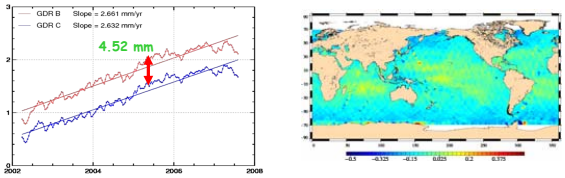

Fig. 6: Filtered MSL trends with "C" and "B" radiometer wet tropospheric correction (left) and local slopes differences (right) [mm/year].

Orbit contribution

The orbit change has geographic impacts on MSL trends, as shown on Figure 7. This north/south difference is due to the ITRF change (2000/2005, see the box about orbit changes). The observed bias usually ranges between -1.5 and 1.5 mm/yr, the positive bias ('C'-'B') being found in the northern hemisphere. There is a 0.066mm/yr decrease of the global slope using GDR-C orbit (2.5% of signal amplitude).

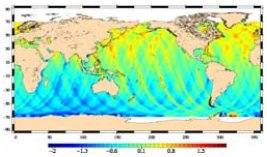

Fig. 7: Differences of MSL trends between "C" and "B" orbits, 2002-2008 [mm/year].

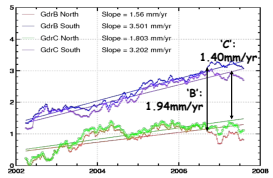

Fig. 8: Cycle per cycle MSL trends [cm] for "B" and "C" by hemisphere.

The slope divergence between north and south, shown on Fig.8, is slightly reduced with GDR-C: in version B, there was a 1.94mm/yr slope difference between north and south, which has cropped to 1.40mm/yr with version C. The impact is significant, since the slope difference corresponds to ~14% of the signal north, and ~9% south. However, the expected N/S slope divergence reduction is low compared to what was observed when using the GSFC ITRF2005 orbit (see Ablain's poster : Error estimation of the global and regional mean sea level trends).

GDR-C/GDR-B linking

A global and hemispheric bias was calculated using the mean of the last 4 GDR-B cycles, 229 to 232. Attention should be paid to the fact that applying a fixed bias is sufficient for global MSL studies but NOT when considering local (hemispheric) MSL evolutions.

The applied bias differs when using radiometer (-9.5 mm) or model wet tropospheric correction (-5.75 mm). The correction, when applied to GDR-C, fits very well with GDR-B MSL.

The map of mean SLA differences from cycle 229 to 232 shows geographically correlated biases (Fig.9, left), related to the change of reference frame (ITRF2000/2005). This map should always be subtracted from the GDR-C-computed MSL maps before watching temporal evolution of MSL trends if local analyses are performed. The same map can also be used for global MSL (Fig.9, right). This has already been taken into account in the AVISO Mean Sea Level products.

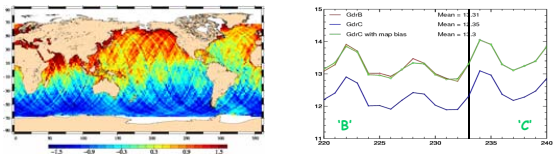

Fig. 9: Mean [cm] along-track differences for cycle 229 to 232 (left) and MSL GDR-C/B linking when subtracting the map (right).

Conclusion

With a year of reprocessed data, the first assessment of GDR-C Jason-1 data is satisfying, showing better SSH performances at crossover and also along-track. Particularly, the CNES POE orbit enables to decrease the SLA variance significantly, mainly thanks to the time-varying part of the gravity field used in its calculation.

The GDR-B/C MSL bias is not homogeneous geographically and should be corrected using a map, a feature already available on the AVISO website. The new JMR correction has almost no impact on mean sea level trends, and the orbit reduces the north/south drift of MSL trends, although a stronger impact could have been expected.

Collecte Localisation Satellites
8-10 rue Hermes
31520 Ramonville Saint-Agne - France

OSTST

Figure 76: *Poster presented at OSTST meeting, Nice 2008*

Assessment of Jason-2 and Jason-1 orbit quality from SSH analysis

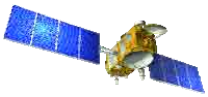

M. Ablain[1], I.Pujol[1],S. Philipps[1], N.Picot[2]

[1]CLS, Space Oceanography Division, Toulouse, France
[2]CNES, Centre National d'Etudes Spatiales, Toulouse, France

Overview

The OSTM/Jason-2 satellite was successfully launched on 20th of June, 2008. Since 4th of July Jason-2 is on the same orbit as Jason-1 spaced out by 55 seconds. The Cal/Val phase allows us to check very accurately the Sea Surface Height (SSH) consistency provided by both satellites. Actually, as the altimeter parameter consistency between both missions seems very good, the Jason-1/Jason-2 SSH cross-calibration directly provides an estimation of the quality of the orbit underlining eventual geographically correlated biases, jumps or drifts. The objectives of this study is then to present the quality of Jason-2 and Jason-1 orbits (DIODE, MOE and preliminary POE orbits) through the SSH calculation. Along-track and crossover analyses are performed from the beginning of the mission to compare the system performances using the different orbits in the SSH calculation provided by Jason-1 and Jason-2. Cross-calibration with Envisat data is also performed to complete these analyses.

Along track SLA analyses / Comparisons with Jason-1

Jason-1 and Jason-2 SLA differences are mapped over all the Jason-2 period using successively MOE orbits (from IGDRs) from cycles 1 to 10 and POE orbit provided by CNES and GSFC from cycles 1 to 7. Jason-2 POE orbits are preliminary since Jason-2 GDRs are not yet available. Note that no correction is applied to the SLA calculation (only Orbit - Range - MSS) since both altimeters are spaced out by 55s.

Mean of J1/J2 SLA differences (cm)

SLA differences with CNES MOE orbits (fig.1) highlight large correlated geographically biases within +/-3 cm in average. These biases vary in space and time (for each cycle) and they can reach +/- 5 cm.

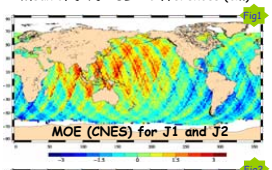

Using CNES POE orbit, Jason-1/Jason-2 SLA consistency (fig.2) are dramatically improved. However, weak hemispheric differences remain close to 1 cm. In addition, this correlated geographically bias is stable in space and time.

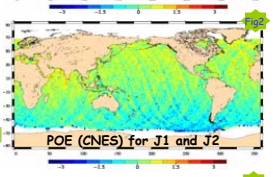

Replacing CNES POE orbit by GSFC orbit only for Jason-2 SLA has no impact on Jason-1/Jason-2 SLA consistency (fig.3) : the weak hemispheric differences are still observed.

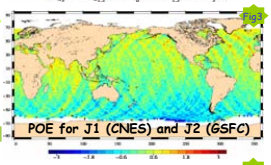

Finally, using GSFC POE orbits provided for both missions, allows us to obtain a more homogenous map. SLA differences are now lower than 0.5 cm and do not show any specific structures (fig.4).

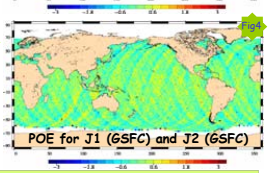

This analysis shows the great impact of the orbit calculation on the SLA consistency between Jason-1 and Jason-2. It highlights that the small residual differences observed on SLA consistencies (with POE) are mainly due to the orbit calculation. However it does not allow us to determine which is the best orbit solution.

Cross-Calibration with Envisat

Using MOE orbit, the SLA consistency is better between Jason-2 and Envisat than between Jason-1 and Envisat.

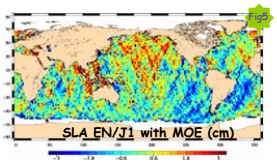

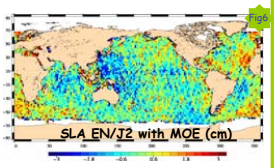

Cross-calibration with Envisat measurements is also performed to check the SLA consistency with Jason-1 and Jason-2. But in this case, both Jason satellites do not measure the same SSH at the same time. Then it is mandatory to cumulate SLA differences over a long enough period to average the oceanic variability discrepancies. Then, we focus here our analysis on SLA differences calculated with MOE orbits, since 11 Jason-2 cycles are available.

SLA consistency is better between Jason-2 and Envisat than with Jason-1 (fig.5 and 6). Correlated geographically biases observed from Envisat/Jason-1 (fig.5) are very well correlated with those detected from Jason-1/Jason-2 (fig.1). This brings out the good consistency of Jason-2 and Envisat MOE orbit. This may indicate also that Jason-1 MOE could be refined.

SSH Crossovers analyses / Comparisons with Jason-1

The monitoring of Jason-1 and Jason-2 SSH statistics at crossovers are performed using successively DIODE, MOE and POE orbits, allowing us to compare the relative performances of each orbit. Thanks to the new Jason-2 DIODE orbit, a dramatic improvement is observed: mean of SSH crossover are more stable and better centered than Jason-1 (fig.2) and standard deviation are significantly lower (fig.4).
Concerning MOE and POE orbits, similar statistics are plotted (fig.1 and 3). A slightly improvement is observed using Jason-2 MOE in comparison with Jason-1 especially for the standard deviation (5.5 cm RMS for J2 instead 5.7 cm RMS for J1 (fig.3)). Results is reversed comparing the GDRs products, but the CNES Jason-2 's POE orbit is preliminary at the moment.

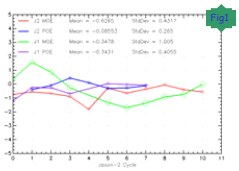

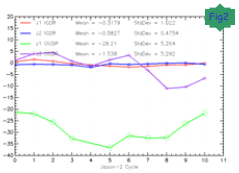

Mean of SSH crossovers (cm)

Impact of MOE and POE orbits for J1 and J2

Impact of DIODE orbits for J1 and J2

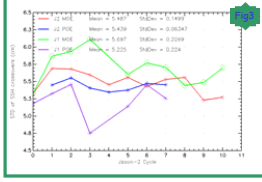

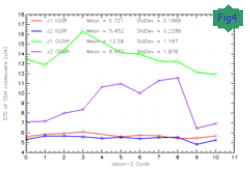

Standard deviation of SSH crossovers (cm)

Performances of New GDR-C Jason-1 orbit over all the Jason-1 period

GDR-C orbit is a SLR/DORIS/GPS orbit as GDR-B but uses the EIGEN-GL04C gravity field, taking into account annual and semi-annual time variability, atmospheric contribution of the gravity field and ocean pole tide effects. In addition, the new reference frame used is ITRF2005.

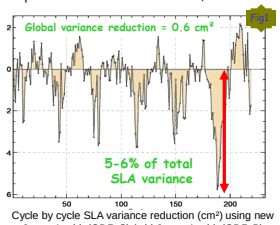

Cycle by cycle SLA variance reduction (cm²) using new Jason-1 orbit (GDR-C) / old Jason-1 orbit (GDR-B)

Mean differences at crossovers are more homogeneous geographically, proving a better coherence with version C (not shown here). A stronger improvement is observed from along-track analyses. Indeed, the SLA variance difference using successively GDR-C and GDR-B POE orbits highlights an annual signal (fig.1) with a strong reduction of variance (until 6 cm²). This feature has also been observed when comparing the altimetry to in situ measurements (Tide gauges and ARGO T/S profiles).

The impact of new GDR-C orbit on global MSL trend is weak (< 0.1 mm/yr). But hemispheric regional trends are impacted by the new ITRF2005 solution within +/-2 mm/yr (fig.2). Hemispheric MSL trend differences are now more homogenous (1.94 mm/yr slope difference with GDR-B orbit instead of 1.40 mm/yr with GDR-C orbit). However, the impact on hemispheric MSL trends is weaker compared to the GSFC ITRF2005 orbit (see Ablain's poster : Error estimation of the global and regional mean sea level trends).

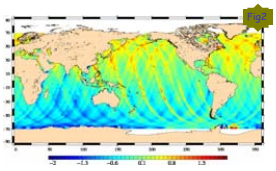

Regional MSL trend differences (mm/yr) using new Jason-1 orbit (GDR-C) / old Jason-1 orbit (GDR-B)

Conclusion

This study aims at underlining the very good quality of Jason-2 orbits. It's especially true for the DIODE orbit which dramatically improves SSH statistics at crossovers in comparisons with Jason-1. Though, MOE and POE orbits show similar performances for both satellites at crossovers, the analysis of SLA consistency highlights a better coherence between Jason-2 and Envisat MOE than with Jason-1 MOE. These not negligible differences (+/- 5 cm) , probably due to the Jason-1 MOE calculation impact directly the quality of multi-mission products using Jason-1 as the main altimeter mission (DUACS product for instance). Finally, the SLA consistency analysis using different POE orbits (CNES, GSFC) is in a good agreement (+/- 1 cm). However it also shows that the POE orbit calculation remains the main source of SLA discrepancies between Jason-1 and Jason-2.

Collecte Localisation Satellites
8-10 rue Hermes
31520 Ramonville Saint-Agne - France

OSTST
Nice, November 2008

Figure 77: *Poster presented at OSTST meeting, Nice 2008*